UNIVERSIDAD AUTÓNOMA DE NUEVO LEÓN
FACULTAD DE CIENCIAS QUÍMICAS

TESIS

ADSORPTION STUDIES OF OCTAMETHYLCYCLOTETRASILOXANE ONTO ELECTROSPUN NANOFIBERS FOR BIOGAS PURIFICATION

Presentada por:
SANDRA PIOQUINTO GARCÍA

Como requisito parcial para obtener el grado de:
DOCTORADO EN CIENCIAS
CON ORIENTACIÓN EN PROCESOS SUSTENTABLES

MONTERREY, N. L., OCTUBRE 2021

Autonomous University of Nuevo León
School of Chemical Science

University of Málaga
Chemical Engineering Department

Doctoral Thesis in Co-tutoring Regime

Doctorado en Ciencias con Orientación en Procesos Sustentables

Folio number: 2-98135-PST-18/207

Doctorado de Química y Tecnologías Químicas. Materiales y Nanotecnología

ADSORPTION STUDIES OF OCTAMETHYLCYCLOTETRASILOXANE ONTO ELECTROSPUN NANOFIBERS FOR BIOGAS PURIFICATION

Author: M. C. Sandra Pioquinto García

Supervisors:

Dra. Nancy Elizabeth Dávila Guzmán

Prof. Dr. D. José Rodríguez Mirasol

Dr. Dña. Juana María Rosas Martínez

Monterrey, N. L., October 2021.

ADSORPTION STUDIES OF OCTAMETHYLCYCLOTETRASILOXANE ONTO ELECTROSPUN NANOFIBERS FOR BIOGAS PURIFICATION

Evaluating Committee

Dr. Nancy Elizabeth Dávila Guzmán.
Thesis Advisor

Dr. José Rodríguez Mirasol.
Thesis Co-advisor

Dr. Margarita Loredo Cancino.
Reviewer

Dr. Eduardo Soto Regalado.
Reviewer

Dr. Sylvain Giraudet.
Reviewer

Dra. María Elena Cantú Cárdenas

Deputy Director of Graduate Studies

Acknowledgments

Obtaining the degree of Doctor of Science has been one of my professional goals that I achieved with the support of many of my teachers and friends. I know that I will be missing names, but I better try to quote them all:

Dra. Nancy E. Dávila Guzmán
Dr. José Rodríguez Mirasol
Dra. Margarita Loredo Cancino
Dra. Juana M. Rosas
Dr. Eduardo Soto Regalado
Dr. Sylvain Giraudet
Dr. Pasiano Rivas García
Dr. Luis Ángel Garza Rodríguez
Dra. Diana Bustos Martínez
Dra. Lina Melva de León Covián
Dr. David A. de Haro del Río
Dr. Gerardo Antonio Flores Escamilla
Dr. Iván Alonso Santos López
Dra. Erika Iveth Cedillo-González
Dra. Anabel Álvarez Méndez
Dra. Shadai Lugo Loredo
Mtra. Norma Tiempos Flores
Dr. Eugenio Hernández
Dr. José Palomo Jiménez
Dra. María José Valero Romero
Dr. Ramiro Ruiz Rosas
Dr. Francisco José García Mateos
Dr. Carlos Javier Lucio Ortiz
Iris Cristina Arvizu
Gloria Azucena Buitimea Cerón
Daniel A. Valdivieso Vera
Alan Antonio Rico Barragán
Carlos Alberto Castillo Candelaria
Melissa Itzel Sánchez Alvarado
Jesús Gerardo Tovar Dimas
Marina M. Atilano Canino
Reyes Benitez Bravo
Santiago Rodríguez V.
Leidy T. Vargas Ibañez
Oscar D. Cárdenas González
Diego A. Casamachin González
Brenda E. Llorente García
María C. Ariza Tarazona
Miguel García Rollán
Miguel Ángel Rodríguez Cano
Javier Torres Liñán
Ayrton Briseño
Behnam Hosseinzaei
Jose Luis Toro Trochez
Naty Ramirez

Thank you Nancy Dávila for sharing your knowledge with me and above all for being a very good advisor. Thank you, Dr. José Rodríguez, for giving me the valuable opportunity to work at the University of Málaga. Thank you, Dra. Margarita, Dr. Eduardo, Dr. Pasiano, and Dr. Sylvain for taking the time for reviews, meetings and for the laboratory materials that you lent me. Nani, thank you for your valuable comments and for your calls from Malaga. Colleagues and friends, thank you for your support to continue with the project. Thanks to the staff of the Faculty and Postgraduate of Chemical Sciences of the Autonomous University of Nuevo León, as well as the staff of CONACYT for the openness to obtain permits, spaces and resources to fulfill my doctoral project. Thank you Yorch (Jorge Luis Robledo) and Quiyos (Esperanza García and Miguel Pioquinto) for supporting me in the decision to continue with my academic training, it is the greatest gift I can have in life, to learn more every day.

This work is dedicated to Valentina Robledo Pioquinto for being my first-born.
One more time...
… We did it!

Table of contents

Summary

Sandra Pioquinto García October 2021

Autonomous University of Nuevo León

Faculty of Chemical Sciences

Study title: ADSORPTION STUDIES OF OCTAMETHYLCYCLOTETRASILOXANE ONTO ELECTROSPUN NANOFIBERS FOR BIOGAS PURIFICATION

Number of pages: 116

Candidate for the degree of Doctor of Science with Orientation in Sustainable Processes

Study area: Engineering, new materials for adsorption processes.

Purpose and Method of Study: The modification of the metal-organic framework (MOF) DUT-4 is studied through the solvent exchange technique to improve its textural properties and favor the adsorption of the octamethylcyclotetrasiloxane (D4) in a gaseous system for biogas purification processes. The life cycle assessment of DUT-4 particles obtained by solvent exchange called DUT-4(DMF), DUT-4(DD), DUT-4(H), and DUT-4(W) are also studied. Likewise, the immobilization of the DUT-4(DMF) particles in electrospun fibers is studied for the adsorption of the D4 siloxane. The environmental impact generated during the adsorbent synthesis process is related to the adsorption capacities of siloxane D4, establishing an environmental impact/adsorption capacity factor. Likewise, the adsorption capacities of the DUT-4 particles and the fibers obtained after immobilizing the MOF particles are compared. A batch adsorption system is used, with a gaseous fluid consisting of a mixture of air and D4 at a concentration of 450 mg/m^3. The continuous adsorption process -under dry conditions and water vapor saturation- of the fibers is studied, at an initial concentration of siloxanes of 2400 mg/m^3, at room temperature and normal atmospheric pressure.

Contributions and Conclusions: The particles of DUT-4(DMF), DUT-4(DD), DUT-4(H), and DUT-4(W) exhibited the same adsorption capacities of siloxane D4 with 9.81 mg/g at an initial concentration of 450 mg/m^3. The fibers with the highest adsorption capacity were 100PD fibers with 8.42 mg/g. According to the life cycle assessment of DUT-4(DMF), DUT-4(DD), DUT-4(H), and DUT-4(W), producing 1 g of DUT-4(W) has a lower environmental impact in all stages of its synthesis with 32 mPt, while producing 1 g of DUT-4(H) generates the highest environmental impact with 269 mPt. But according to the environmental impact/adsorption capacity factor, the production of DUT-4(DMF) is the most convenient since a lower mass of adsorbent is required to remove the siloxane, which reduces the environmental impacts of the adsorption process. Continuous adsorption tests with the fibers showed that in dry and humid conditions, the adsorption efficiency of siloxane D4 is maintained.

_____

Dra. Nancy Elizabeth Dávila Guzmán

Thesis Advisor

Resumen Extendido

El objetivo general de la presente tesis doctoral, que se desarrolla para conseguir el grado de doctora por la Universidad Autónoma de Nuevo León en el programa de "Doctorado en Ciencias con Orientación en Procesos Sustentables" y en régimen de Cotutela con la Universidad de Málaga, en el programa de doctorado de "Química y Tecnologías Químicas. Materiales y nanotecnología" es: obtener una comprensión fundamental de la adsorción de siloxano D4 en fibras electrohiladas con DUT-4. Para cumplirlo, se desprenden 7 objetivos específicos que son:

I. Sintetizar las estructuras metal-orgánicas (MOFs) de DUT-4.
II. Determinar los impactos ambientales de los MOFs de DUT-4.
III. Producir las fibras electrohiladas a partir de los MOFs de DUT-4.
IV. Determinar las propiedades fisicoquímicas de polvos de DUT-4 y fibras electrohiladas con DUT-4.
V. Obtener la cinética de adsorción del siloxano D4 sobre polvos de DUT-4 y fibras electrohiladas con DUT-4.
VI. Evaluar el rendimiento de las fibras electrohiladas con DUT-4 para la adsorción de siloxano D4 en aire mediante un sistema continuo.
VII. Evaluar el desempeño de las fibras electrohiladas con DUT-4 para la adsorción de siloxano D4 en presencia de humedad, utilizando un sistema continuo.

El trabajo que se realizó está organizado en 7 apartados. En el primer apartado se da una introducción al tema donde se abordan los conceptos básicos del tema. En el apartado 2 se dan los antecedentes y los trabajos científicos actuales que conciernen. En los apartados 3 y 4 se describe la contribución científica e hipótesis del proyecto. El apartado 5 está dedicado

a la descripción de materiales y métodos empleados en la parte experimental del proyecto. En el apartado 6 se encuentran las discusiones y resultados del trabajo de investigación y en el apartado 7, se incluyen las conclusiones, así como las áreas de oportunidad encontradas durante el desarrollo de la presente investigación.

1.INTRODUCCIÓN

Debido a la creciente preocupación por los riesgos y los impactos del cambio climático a escala global, se ha promovido el compromiso voluntario a establecer medidas para combatirlo. Una de las estrategias es el uso de fuentes de energía renovables, como la biomasa, hidroelectricidad, eólica, solar y biogás, etc.

El biogás es un tipo de energía formado por la degradación anaeróbica de materia orgánica. Este proceso de degradación consiste en varias etapas que tienen como finalidad convertir las moléculas complejas de proteínas, lípidos e hidratos de carbono en moléculas más sencillas como aminoácidos, ácidos grasos y azúcares. Algunos de los microorganismos involucrados en este proceso son Syntrophothermus lipocalidus y Syntrophobacter fumaroxidans. El biogás se constituye entre un 45-75 % de metano, 20-55 % de dióxido de carbono y pequeñas cantidades (-6 %) de humedad, sulfuro de hidrógeno, compuestos orgánicos volátiles, etc. Dado que el poder calorífico del biogás es similar al de otros combustibles (35-44 $KJ \cdot g^{-1}$), se puede usar como biocombustible en microturbinas, turbinas, motores de combustión y calderas. La producción de biogás ha ido en incremento, principalmente en Europa, Estados Unidos de América y China. El aprovechamiento del biogás depende de las políticas estatales y federales que se desarrollan en estos países, Alemania, por ejemplo lidera la producción de biogás con 1,79 mil millones de Nm^3/año. Para el caso mexicano, la producción de biogás estimada es de 5.110 millones de Nm^3/año.

Siloxanos. Como se mencionó en líneas atrás, el biogás contiene compuestos orgánicos volátiles (COVs) como los siloxanos. Los siloxanos poseen una baja tensión superficial e inflamabilidad, así como alta estabilidad térmica y resistencia a la radiación UV. Actualmente se emplean para fabricar limpiadores, pinturas, productos de cuidado personal, etc. Al final del ciclo de vida de estos productos, los siloxanos pueden llegar a las plantas de tratamiento de aguas residuales (PTAR) o a los rellenos sanitarios (RS), donde se forma el biogás. La concentración de siloxanos en el biogás procedente de PTAR y RS está comprendida entre 10 y 100 mg/m^3. Los siloxanos al tener efectos adversos sobre los sistemas de combustión de biogás se consideran indeseables. Es así que se recomienda una concentración máxima de siloxanos de 15 mg/m^3 en el biogás.

Tecnicas de remoción de siloxanos. Las técnicas de remoción de siloxanos más eficaces son separación criogénica, tratamiento biológico, absorción, separación por membrana y adsorción. De entre ellas, la que presenta un mayor uso es la técnica de adsorción debido a su bajo costo y entre los adsorbentes más usados destacan el carbón activado (CA) y gel de sílice (GS). Sin embargo, recientes estudios se han orientado a la adsorción sobre estructuras metal-orgánicas (MOFs), ya que son materiales con alta selectividad, alta área superficial y alta estabilidad térmica. Otra de las propiedades interesantes de los MOFs, es que se les pueden conferir diferentes propiedades fisicoquímicas mediante el uso de distintos métodos de preparación, como el de plantilla e intercambio de solvente.

MOFs para la remoción de siloxanos. En el 2013, Mito-oka y colaboradores, compararon el MOF de la Universidad Tecnológica de Dresden (DUT-4) con un CA comercial, para la adsorción de siloxano D4. Los investigadores encontraron que el DUT-4 adsorbe un 15% en peso del siloxano D4, mientras que para el CA fue el 20%. Sin embargo, en presencia de humedad, el DUT-4 mostró una alta estabilidad que no mostraba el CA. Uno de los problemas

de la adsorción, es la regeneración del adsorbente. En este sentido, Gargiulo y colaboradores estudiaron en 2019, el MOF MIL-101 para la adsorción de siloxano D4 por termogravimetría. Estos autores consiguieron una regeneración completa del MOF MIL-101, usando vacío a 423 K.

Análisis de ciclo de vida de los MOFs. El análisis del impacto ambiental de la síntesis de los MOFs ha sido poco evaluado. Esta técnica puede ayudar a determinar qué tan verde es un material. Sepúlveda-Cervantes y colaboradores en el año 2018 y Loya-González y colaboradores en el año 2019, analizaron el impacto ambiental de diversos adsorbentes y encontraron que la impregnación, en el proceso de producción de los adsorbentes, es la etapa que más contribuye al daño ambiental. En este mismo sentido, Grande y colaboradores en el año 2017, evaluaron el impacto ambiental del MOF CPO-27-Ni, sintetizado por cuatro rutas diferentes, como adsorbente de captura y almacenamiento de carbono. Ellos concluyeron que las etapas de síntesis y limpieza son las de mayor impacto ambiental.

Inmobilización de MOFs. Los MOFs son partículas del tamaño de micras que para integrarlos es necesario apoyarlos en marcos o estructuras para utilizarlos en procesos a gran escala. Se pueden usar como marcos las membranas, fibras, monolitos y gránulos de mayor tamaño. En este sentido, esta tesis se enfoca principalmente en su inmobilización en fibras. Para elaborar las fibras existen varios métodos como la nanolitografía, el autoensamblaje y el electrohilado. En particular, el electrohilado es un proceso que se basa en el estiramiento de una solución viscoelástica que produce un tejido fibroso.

2.REVISIÓN DE LA LITERATURA

El CA es el adsorbente de mayor uso en la eliminación de siloxanos, sin embargo, al requerir altas temperaturas para la desorción, la regeneración va a encarecer mucho el proceso. Por

otro lado, el GS es el segundo adsorbente de mayor uso para la remoción de siloxanos, la desventaja que presentan estos materiales es que, en presencia de contenidos de humedad elevados, se produce una reducción de hasta 10 veces la capacidad de adsorción de siloxanos en el GS.

Dada las circunstancias expuestas, diversos estudios han sido enfocados en el desarrollo de nuevos materiales para la remoción de siloxanos. Jafari y colaboradores en el año 2015, sintetizaron una nueva clase de adsorbentes poliméricos nanoporosos en condiciones solvotermales, con divinilbenzence (DVB) y 1-divinilimidazol (VI). Las nuevas clases de adsorbentes poliméricos nanoporosos, PDVB y PDVB-IV mostraron capacidades de adsorción de 1951 y 2370 mg/g, respectivamente, y se mantuvieron sin cambios en condiciones de humedad. Cabe destacar que los autores señalan la superhidrofobicidad de los materiales PDVB, para la obtención de estos muy buenos resultados.

Por otro lado, los MOFs inmobilizados en fibras, fueron estudiados por primera vez por Ostermann R y colaboradores (2010), quienes mostraron que las fibras obtenidas poseían elevada área superficial específica y buena accesibilidad. En este sentido, las fibras funcionalizadas con MOF podrían ser una opción para la remoción de siloxanos. Por ello, en esta tesis se propone el estudio de fibras electrohiladas de MOF DUT-4 para la remoción del siloxano D4 en condiciones húmedas, además el estudio de impacto ambiental de las partículas de DUT-4 mediante su análisis de ciclo de vida (ACV).

3.CONTRIBUCIÓN CIENTÍFICA

La contribución científica es el aporte de un estudio sobre la adsorción de siloxano D4 en fibras electrohiladas con DUT-4 para el proceso de purificación del biogás. Asimismo, se proporcionan nuevos adsorbentes con alta área superficial y selectividad hacia los siloxanos

y se ofrece la evaluación de los impactos ambientales de los adsorbentes de DUT-4.

4.HIPÓTESIS

Las fibras electrohiladas con DUT-4 son selectivas hacia la adsorción del siloxano D4 presente en el biogás, en condiciones secas y de humedad.

5.MATERIALES Y MÉTODOS

Para el proyecto, primero se sintetizaron los MOFs de DUT-4 mediante 4 rutas. La primera ruta llamada "síntesis de DUT-4 (DMF)", se realizó con algunas variaciones a lo que describe Senkovska y colaboradores en el año 2009, disolviendo 0.26 g de ácido 2,6-naftaleno dicarboxílico en 30 ml de N, N-dimetilformamida (DMF), luego se añadieron 0.52 g de nitrato de aluminio nonahidratado, la mezcla se colocó en un vaso teflón de 250 mL en el autoclave a 120 ºC por 24 h, posteriormente se enfrió a temperatura ambiente. El producto es centrifugado a 10,000 rpm y 2.5 min, luego se lavó tres veces con DMF y finalmente se secó en estufa a 120 ºC durante 4 h. La segunda ruta llamada "síntesis de DUT-4(DCM)", se llevó a cabo incluyendo una etapa de intercambio de solvente de la síntesis de DUT-4(DMF) que consistió en lavar con 20 mL de diclorometano (DCM), durante una hora (20 min cada lavado), después de lavar con DMF. Posteriormente, el producto se centrifugó a 10,000 rpm durante 2.5 min y se secó en estufa a 120 ºC durante 4 h. La tercera ruta llamada "Síntesis de DUT-4(DH)", incuyó una segunda etapa de intercambio de solvente, es decir, se realizó un tercer lavado con 20 mL de hexano (C_6H_{14}) por una hora (20 min cada lavado), después de haber lavado con DMF y con DCM. De igual manera, el producto se centrifugó y se secó en las mismas condiciones descritas. La cuarta ruta "Síntesis DUT-4(W)", consistió en reproducir la primera ruta, pero utilizando agua desionizada en lugar de DMF, esto a fin de

contribuir a una producción más ecológica.

Concerniente al análisis del ciclo de vida de los MOFs DUT-4 en polvo, la norma en la cual nos basamos fue la norma internacional ISO 14044. También se establecieron las fronteras del sistema para la producción del DUT-4 al incluir cinco etapas: mezcla, síntesis, limpieza, intercambio de solvente y secado. Cabe mencionar que para el análisis, no se consideraron las cargas ambientales asociadas con la construcción del equipo de laboratorio utilizado en la producción de DUT-4, debido a su bajo impacto ambiental asociado. Con base en las rutas de síntesis de los materiales de DUT-4, se formaron los siguientes escenarios a estudiar: Los escenarios DUT-4(DMF) y DUT-4(W), los cuales incluyen las etapas de mezcla, síntesis, limpieza y secado; y los escenarios DUT-4(DCM) y DUT-4(H), los cuales incluyen adicionalmente la etapa de intercambio de solvente. La unidad funcional (UF) usada en todos los escenarios fue de 1 g de DUT-4 producido a escala de laboratorio, de acuerdo con otros estudios de ACV de materiales adsorbentes.

Por otro lado, los datos para el inventario del ciclo de vida (LCI, por sus siglas en inglés) de reactivos químicos y de energía se obtuvieron de los registros de laboratorio, los procedimientos analíticos y los balances material-energía para la síntesis de DUT-4. La producción de energía y reactivos químicos necesarios para sintetizar DUT-4 fueron considerados dentro de los límites del sistema. Para el LCI de estos recursos se usó la base de datos Ecoinvent v3.3. En lo referente a las aguas residuales generadas en la etapa de limpieza, éstas se dispusieron con base al programa de manejo de residuos peligrosos implementado en nuestra universidad. Los impactos ambientales de la disposición final de estos residuos fueron excluidos, como también hicieron Sepúlveda-Cervantes y colaboradores en el 2018 y Loya-González y colaboradores en el 2019. Los requerimientos energéticos de las distintas etapas de síntesis de los diferentes DUT-4 fueron calculados

mediante balances energéticos que se encuentran recogidos en la tesis. Finalmente, este estudio de ciclo de vida tiene un enfoque atribucional, centrado en medir las emisiones y flujos de los recursos originados por la síntesis del DUT-4 (se emplearon datos promedio que representaron los flujos de entrada y salida).

Por otro lado, para la elaboración de las fibras con DUT-4, se empleó un equipo de electrohilado que consistió de 1) una bomba de jeringa, 2) una jeringa de electrohilado (dos en caso de electrohilado coaxial), 3) el colector y 4) la fuente de voltaje. En el electrohilado uniaxial, la solución se conformó de DUT-4, DMF y PAN. En el electrohilado coaxial, la solución para la coraza se conformó de DUT-4, DMF y PAN, este último para conferirle mayor viscosidad y lograr que las partículas de MOF se adhirieran a la superficie de la fibra; la solución para el núcleo se conformó de PAN y DMF. Variando las condiciones experimentales se obtuvieron ocho tipos de fibras: PD, 20DD, 20ED1, 20ED13, 20CD, 70PD, 100PD y 140PD. La primera de estas fibras fueron las fibras sin DUT-4, el número en la nomenclatura representa el porcentaje de DUT-4 con respecto al peso del polímero PAN. Luego, las primeras cuatro fibras se hilaron de forma uniaxial y las otras cuatro coaxial. Las condiciones óptimas para el electrohilado uniaxial fueron: caudal de 2,2 mL/h; distancia aguja- placa de aluminio de 20 cm y voltaje de +10 kV, -10 kV. Por otro lado, las condiciones para el electrohilado coaxial en ambas jeringas fueron: caudal de 0,9 ml/h, distancia aguja-placa de aluminio de 23 cm y voltaje de + 10 kV y -10 kV. Una vez que se estableció que la forma más adecuada de trabajar era en disposición coaxial, el DUT-4 fue sonificado por cuatro horas para disminuir el tamaño de partícula. Todas las fibras se estabilizaron a 120 ºC. La caracterización de los materiales DUT-4 y fibras con DUT-4 se realizó empleando los siguiente equipos:

- Los patrones de difracción de rayos-X (XRD) se obtuvieron en un difractómetro

PANalytical X'Pert PRO MPD, usando radiación Cu-Kα (40 mA y 45 kV). La cristalinidad se determinó mediante el área bajo la curva de los picos cristalinos (después de la corrección de la línea de base).

- El área superficial específica (A_{BET}) del DUT-4 y de las fibras se obtuvo mediante fisisorción de N_2 a 77 K utilizando un Micromeritics ASAP 2020, desgasificando previamente a 150 ºC durante 8 h.
- Las imágenes de microscopía electrónica de barrido (SEM) se obtuvieron con un microscopio JEOL JSM-6490LV, usando un voltaje de aceleración de 0,3 a 30 kV y una pistola de electrones termoiónicos con filamento de W.
- Los espectros FTIR se obtuvieron usando un Bruker Tensor 27 utilizando una celda ATR de diamante de reflexión única, Golden Gate, y una resolución espectral estándar de 4 cm^{-1} en el rango espectral de 4000-500 cm^{-1}.
- Los espectros de RMN de estado sólido ^{27}Al MAS se registraron a temperatura ambiente en un espectrómetro de RMN Bruker AVANCE III HD de 600 MHz a 20 kHz, con un pulso de longitud de 0,27 ms y un retraso de 1 s con desacoplamiento de 1H y sumando 2000 exploraciones (el análisis de RMN solo se llevó a cabo en los polvos DUT-4).

Los experimentos de adsorción en lote se realizaron a una concentración inicial de 450 mg/Nm^3 de D4, con 100 mg de material adsorbente (polvo o fibras de DUT-4), a temperatura ambiente. Los matraces que contenían la fase gaseosa, se agitaron a 700 rpm durante 6-9 h para asegurar el equilibrio, en el interior el material adsorbente estaba colocado en una canasta que pendía de un hilo de alambre. Las muestras se analizaron por cromatografía de gases para determinar la concentración de D4. Así, cada muestra de gas, fue inyectada en un cromatógrafo de gases marca Shimadzu Nexis GC-2030, con un detector de ionización de

llama (FID). La columna capilar utilizada fue una Shimadzu SH-Rxi-5ms. La temperatura del equipo a la entrada, del horno y del analizador fueron de 150, 110 y 250 ºC, respectivamente. Se utilizó helio como gas portador, con un caudal de 1.5 ml/min y una presión de 83,3 kPa. Con split de 5.0, volumen de inyección de 0.5 mL y tiempo de análisis de 1.4 minutos.

Los experimentos de adsorción en continuo se realizaron con una concentración de siloxano a la entrada del lecho de 2429,15 mg/m^3; la columna tuvo un diámetro de 10.0 mm y longitud de 110.4 mm. Los experimentos se llevaron a cabo a temperatura ambiente, a presión atmosférica y con un caudal de 50 mL/min. Durante el experimento en continuo, las muestras de gas se analizaron en el cromatógrafo de gases Shimadzu Nexis GC-2030. El tiempo estimado necesario para una sola ejecución fue de aproximadamente 94.6 min.

6.RESULTADOS Y DISCUSIÓN

El MOF DUT-4 se sintetizó utilizando ácido 2,6-naftaleno dicarboxílico, dimetilformamida (DMF) y nitrato de aluminio nonahidratado, como se detalló previamente. Se obtuvieron 0.46 g de DUT-4, equivalente a un rendimiento del 96.8 %; 0.29 g de DUT-4(DCM) con un rendimiento del 61.1%; 0.27 g de DUT-4 (DH) con un rendimiento del 56.8% y 0.11 g de DUT-4(W) equivalente a un rendimiento del 31.0 %.

En cuanto al Análisis de Ciclo de Vida (ACV) de la producción del DUT-4, se encontró que, para los escenarios DUT-4(DMF), DUT-4(DCM) y DUT-4(H), el mayor impacto ambiental se asoció a los reactivos químicos, empleados durante la síntesis del material adsorbente, obteniendo valores entre 88.6 y 245 milipuntos (mPt). Por otro lado, el consumo de energía tuvo un impacto menor (puntaje entre 2.12 y 24.7 mPt), aunque el escenario DUT-4(W) fue el de mayor impacto ambiental con 31.6 mPt.

En un análisis más profundo, se observó que el escenario DUT-4(H) tuvo el puntaje más alto respecto de los otros escenarios con 269 mPt, esto se debe a la etapa de intercambio de solvente, donde se emplean tres diferentes solventes (DMF, DCM y hexano). La contribución de daño de cada reactivo químico es el siguiente: 61.5 % por el uso de DMF, 33.3 % por DCM y el 5.2 % por el uso de hexano. Con respecto al escenario DUT-4(DCM), éste generó un impacto ambiental de 211.07 mPt, dado que no utiliza hexano. El escenario DUT-4(DMF) generó un puntaje de 112 mPt que es menos de la mitad que el escenario DUT-4(H). Finalmente, el escenario DUT-4(W), en el que se usó únicamente agua desionizada como disolvente, el puntaje fue de 32 mPt. Hasta este punto fue posible visualizar que los disolventes utilizados determinan el perfil de impacto de medio ambiente de los adsorbentes de DUT-4.

Revisando la información energética en México, la producción de electricidad se debe un 87 % al consumo de fuentes fósiles, desglosado de la siguiente forma: 62 % a petróleo crudo, 20% a gas natural, 4% a carbón y el resto a condensado. Cito esto porque el principal indicador de categoría de impacto ambiental en todos los escenarios fue el agotamiento de fósiles que va de 10.71 a 109.14 mPt. La razón es la producción de solventes, ya que el solvente utilizado en cada escenario tiene impactos de $1.86x10^{-4}$, 0.28, 0.53 y 0.75 kg eq de petróleo para los escenarios DUT-4(W), DUT-4(DMF), DUT-4(DCM) y DUT-4(H), respectivamente; y un consumo de electricidad de <0,08 kg eq de petróleo para todos los escenarios. El segundo indicador más representativo del impacto ambiental es el cambio climático y va de 11.34 a 83.10 mPt. Esto se debe a que las emisiones de gases de efecto invernadero (GEI), representaron entre 0.25 y 2.02 kg de CO_2 eq, principalmente por la emisión de dióxido de carbono y metano. Igual que con el indicador anterior, la producción de solventes es la actividad con mayor incidencia en las emisiones de GEI, con $7.23x10^{-4}$,

0.45, 1.50 y 1.83 kg CO_2 eq para los Escenarios DUT-4(W), DUT-4(DMF), DUT-4(DCM) y DUT-4(H), respectivamente, mientras que el consumo de electricidad generó <0.24 kg CO_2 eq. Con lo que respecta al indicador de toxicidad humana, éste generó de 7.48 a 58.70 mPt, que es el equivalente de 0.01 a 0.42 kg 1,4-DB eq. De igual forma, el uso de disolventes es la principal actividad que deriva en este indicador. El indicador de formación de partículas tuvo un puntaje de 2.59 a 16.72 mPt, debido a las emisiones atmosféricas en la producción de disolventes de $PM_{2.5}$, dióxido de azufre y óxidos de nitrógeno.

Finalmente, fue posible observar que mediante la sustitución de DMF por agua en la síntesis del DUT-4(DMF), disminuye el daño ambiental. Por el contrario, se observó que esta sustitución cambió las propiedades fisicoquímicas del MOF original, y por consiguiente, como se describirá más adelante, generó una menor capacidad de adsorción de siloxano. Para determinar cuan importante es el impacto ambiental y el aprovechamiento del adsorbente, se analizó la relación impacto ambiental/capacidad de adsorción, para los cuatro escenarios de producción del DUT-4. Los resultados mostraron que la producción del adsorbente DUT-4(H), tuvo la relación de capacidad de adsorción/impacto ambiental más alta entre los cuatro escenarios de DUT-4. Caso contrario, el escenario de producción de DUT-4(DMF) fue el que mostró la relación de impacto ambiental/capacidad de adsorción más baja.

Los resultados obtenidos para impacto ambiental se pueden explicar, teniendo en cuenta que el DUT-4(DMF) y DUT-4(H) tuvieron la misma capacidad de adsorción (que explicaré más adelante), pero este último tuvo un mayor impacto ambiental provocado por las dos etapas de intercambio de solventes. El escenario de producción de DUT-4(W) empleó un solvente verde, agua desionizada, por lo que tuvo una relación de impacto ambiental/capacidad de adsorción más alta que la de la producción del escenario DUT-4(DMF). El DUT-4(W), tuvo la menor capacidad de adsorción de siloxano, pero para lograr una adsorción similar al resto

(alrededor de 9,80 mg/g), era necesario producir cinco veces más de este material, lo que podría generar ahorros económicos para fomentar una mayor sostenibilidad en la eliminación de siloxanos del biogás. Revisando desde un punto de vista ambiental y técnico, el escenario DUT-4(DMF) fue el mejor escenario para producir el adsorbente de siloxano, ya que la relación obtenida fue 53, 42 y 63 % menor que para el escenario DUT-4(DCM), DUT-4(H) y DUT-4(W), respectivamente.

En cuanto a la caracterización fisicoquímicas de los adsorbentes de DUT-4 (en polvo), el espectro de FTIR de DUT-4(DMF), DUT-4(DCM), DUT-4(H) y DUT-4(W) mostraron bandas de adsorción similares; las bandas características fueron en el rango de 1693-1668 cm^{-1}, correspondientes a la vibración del estiramiento de (ν(C=O)) del grupo carbonilo, que es indicativa de la coordinación del ligante al ion metálico y los picos observados a 989-985 cm^{-1}, que correspondieron a la flexión de los grupos hidroxilo δ(OH), aunado a lo anterior, en el espectro DUT-4(W), se sumaron las bandas a 1294 cm^{-1} correspondiente a la vibración de estiramiento (ν(C-O)), y las bandas entre 921-914 cm^{-1} por enlaces de (δ(O-H)). Por otro lado, los espectros de RMN de estado sólido ^{27}Al MAS demostraron que los MOFs son materiales sexta-coordinados de aluminio, con tres señales superpuestas en el rango de desplazamiento químico entre -20 y 10 ppm. Con base en los resultados de difracción de rayos-X para las muestras sintetizadas de DUT-4 por síntesis solvotermal, se encontraron picos característicos a 6.95º, 13.91º y 21.04º correspondientes a los índices de Miller (101), (110) y (113) respectivamente, y una simetría ortorrómbica. Los porcentajes de cristalinidad calculados fueron de 70.82%, 89.26%, 88.74% y 89.89 % para DUT-4(DMF), DUT-4(DCM), DUT-4(H) y DUT-4(W), respectivamente; este último material resultó ser de cristalinidad no isoestructural al DUT-4. El área superficial específica del DUT-4(DMF),

DUT-4(DCM), DUT-4(H) y DUT-4(W), fue de 1350, 1180, 1330 y 2 m^2/g, respectivamente; el volumen de poro total para DUT-4(DMF), DUT-4(DCM), DUT-4(H) y DUT-4(W) fue de 1.71, 1.48, 1.46 y 0.003 cm^3/g, respectivamente; se observó qué mediante síntesis solvotermal, independientemente del intercambio de disolvente, se obtuvieron elevadas áreas superficiales específicas, pero el MOF a base de agua (DUT-4(W)), tuvo una baja área superficial específica y porosidad en comparación con el resto de MOFs. Con lo que concierne al análisis por SEM, el tamaño de partícula de los materiales obtenidos por síntesis solvotermal fue dependiente del solvente usado en la etapa de secado, ya que el tamaño de partícula de DUT-4(DCM) y DUT-4(H) fue inferior a 500 nm, pero cuando se utilizó un disolvente de alta tensión superficial como DMF o agua, el tamaño de partícula de DUT-4 fue superior a 1 µm, esto se debió a que las fuerzas capilares superaron las fuerzas repulsivas entre las partículas y por lo tanto, las partículas se acercaron entre sí para formar aglomeraciones.

Con el MOF DUT-4(DMF) se produjeron estructuras soportadas sobre fibras electrohiladas, ya que independientemente de la ruta de síntesis, el DUT-4(DMF), DUT-4(DCM) y DUT-4(H) tuvieron la misma capacidad de adsorción de D4 (q=10.9 mg/g a C_0 = 400 mg/m^3 de D4). Para ello se obtuvieron partículas de DUT-4 menores de 100 nm a partir de su sonificación, durante cuatro horas. Esto nos llevó a obtener una mejor distribución de DUT-4 en la superficie de las fibras electrohiladas. La solución polimérica, para la formación de las fibras, fue electrohilada mililitro a mililitro, para evitar que las partículas se precipitaran dentro de la jeringa. Por otro lado, se evaluó el uso de otro solvente distinto al DMF, el dimetilsulfóxido (DMSO), pero las partículas de DUT-4 no se adhirieron a la superficie de la fibra de ninguna manera, por lo que su uso fue descartado. También se probó con etanol, pero no fue compatible con el polímero PAN y también se descartó.

Para los análisis completos de las fibras de DUT-4, se emplearon únicamente las fibras llamadas 70PD, elaboradas de forma coaxial y con 70 % de DUT-4 con respecto al peso del polímero de PAN. Para su elección, se consideraron la microscopía electrónica de barrido (SEM) y pruebas de adsorción-desorción de N_2. Para ello, se revisó cual de todas presentaba mejor distribución de DUT-4 en la superficie de la fibra y por tanto un área de superficie específica (A_{BET}) considerable. Las imágenes SEM de las fibras obtenidas por electrohilado coaxial mostraron un diámetro menor (0.125 μm a 0.5 μm), que las fibras obtenidas por electrohilado uniaxial (0.5 μm a 1.0 μm); además, en las fibras que contenían más del 70 % de DUT-4, las partículas excedían un micrómetro de diámetro, por lo que quedaban atrapadas entre fibras. Las fibras electrohiladas uniaxialmente mostraron una menor A_{BET} que las fibras electrohiladas coaxialmente (20 y 37 m^2/g, respectivamente), además el A_{BET} aumentó a medida que aumentaba la relación de DUT-4 con respecto al PAN (de 37 a 293 m^2/g), para las fibras electrohiladas coaxialmente. El análisis de FT-IR para las fibras 70PD mostró diversas bandas comunes entre las fibras y el DUT-4, donde se hallaron los grupos carboxilos e hidroxilos; también se encontraron bandas comunes entre las fibras 70PD y las fibras sin DUT-4. En cuanto al análisis de DRX, se encontró que las fibras corresponden a estructuras amorfas con un porcentaje de cristalinidad del 31.35%.

Con respecto a los experimentos de adsorción en lote, estos se llevaron a cabo a una concentración inicial de 450 mg/Nm^3 de siloxano D4 a temperatura ambiente. La adsorción fue rápida, alcanzando el equilibrio en aproximadamente 4 h. La capacidad de adsorción al equilibrio de DUT-4(DMF), DUT-4(DCM) y DUT-4(H) fue de 9.80 mg/g, mientras que para el DUT-4(W) fue de 1.80 mg/g a la concentración inicial ya mencionada. Por otro lado, los experimentos de adsorción en las fibras, se llevaron a cabo también a una concentración

inicial de 450 mg/Nm^3 de siloxano D4 a temperatura ambiente. El tiempo al equilibrio varió de 2 h hasta 3.5 h, dependiendo del tipo de fibra, así, las fibras 70PD tuvieron una capacidad de adsorción de 8.42 mg/g a una concentración de equilibrio de 61.26 mg/m^3.

Para los experimentos de adsorción en continuo, se procedió a secar las fibras a 120 ºC por cuatro h; luego, los hilos se enrollaron hasta conseguir un diámetro de 1 cm, que correspondía al diámetro de la columna, y el rollo de fibras fue colocado en la columna verticalmente. Los resultados experimentales que obtuvimos tuvieron altas desviaciones (desviaciones absolutas de aproximadamente 128.92), lo que indicó que no hay reproducibilidad, esto se debió probablemente a la formación de trayectorias preferenciales y/o porque usamos una tasa de flujo muy baja para una altura de lecho tan significativa. Esto nos impidió una discusión de los resultados experimentales debido a la baja reproducibilidad de los datos.

7.CONCLUSIONES

En el presente trabajo se sintetizó la estructura organometálica DUT-4 mediante cuatro rutas diferentes DUT-4(DMF), DUT-4(DCM), DUT-4(H) y DUT-4(W), para mejorar sus características fisicoquímicas y conseguir una mayor adsorción de siloxano D4. También, mediante la metodología de evaluación del ciclo de vida (LCA), los impactos ambientales de las diferentes rutas fueron evaluados. De acuerdo con el análisis FTIR y NMR, los materiales obtenidos por síntesis solvotérmica e hidrotermal mostraron bandas de absorción características de los grupos funcionales del ligante orgánico y los desplazamientos químicos relacionados con el aluminio sexta-coordinado, respectivamente. De acuerdo con el análisis de XRD, los cuatro materiales sintetizados presentaron una cristalinidad con valores entre el 70 y el 90%. Por otro lado, la síntesis solvotermal favorece elevadas áreas superficiales, mientras que la síntesis hidrotermal (DUT-4(W)), generan un área superficial específica baja y un volumen de poro total bajo, debido al solvente utilizado. La tendencia en el tamaño de

partícula fue proporcional a los valores de la tensión superficial de los solventes. Por otro lado, el ACV enfatiza que el uso de DMF, DCM y hexano aumenta el daño ambiental, principalmente en los indicadores de agotamiento de fósiles, cambio climático y toxicidad humana. Por el contrario, la síntesis de DUT-4(W) generó el menor impacto ambiental con 32 mPt por UF. Sin embargo, el DUT-4(W) presentó la capacidad de adsorción de siloxano más baja en comparación con el resto. Finalmente, según la relación impacto ambiental/capacidad de adsorción, la producción del escenario DUT-4(DMF) es la más conveniente porque se requiere una masa de adsorbente menor para eliminar el siloxano, lo que se traduce en una reducción de los impactos ambientales en el proceso de adsorción. En lo referente a la inmovilización de DUT-4 sobre las fibras, se realizó por dos vías para favorecer el menor cambio en sus características fisicoquímicas y lograr una mayor capacidad de adsorción del siloxano D4. Según los análisis de área superficial específica y SEM, las fibras generadas por electrohilado coaxial 70PD fueron las de mejor dispersión en la superficie de la fibra. Según el análisis FTIR, las fibras 70PD mostraron las bandas de adsorción características de las partículas DUT-4. Sin embargo, se demostró que estas fibras eran menos cristalinas que los polvos DUT-4, según el análisis XRD. Las fibras 70PD presentaron una estructura cristalina con un valor de 31.35%. Los resultados muestras que estas fibras se pueden aplicar como material adsorbente para la eliminación de siloxano debido a su alta capacidad de adsorción en equilibrio (8.42 mg/g). Las referencias completas podrán consultarlas al final de la tesis.

List of Tables

List of figures

Products

- S. Pioquinto-García, N. E. Dávila-Guzmán, J. Rodríguez-Mirasol, N. Tiempos-Flores, S. Giraudet, M. Loredo-Cancino, E. Soto-Regalado. **Experimental Study of MOFs for the Removal of Siloxanes in Biogas Purification Processes**. 7th International Conference on Sustainable Development 04-05 September 2019, Rome, Italy. (Oral presentation)
- S. Pioquinto-García, M. Loredo-Cancino, E. Soto-Regalado, S. Giraudet, J. Rodríguez-Mirasol, P. Rivas-García, N. E. Dávila-Guzmán. **Life cycle assessment for the synthesis of metal-organic framework DUT-4.** #LatinXChem Twitter Conference 2020 on Sept 7th 2020. (Poster)
- S. Pioquinto-García, M. Loredo-Cancino, E. Soto-Regalado, S. Giraudet, J. M. Rosas-Martínez, J. Rodríguez-Mirasol, N. E. Dávila-Guzmán. **Efecto de la distribución de tamaño de poro de estructuras organometálicas dut-4 en la adsorción de siloxanos.** 1er Encuentro Nacional Virtual de Investigación en Ingeniería. Presentado en forma Oral en la plataforma Zoom® del 17 al 18 de septiembre del 2020. (Oral presentation)
- S. Pioquinto-García, M. Loredo-Cancino, P. Rivas-García, E. Soto-Regalado, S. Giraudet, J. Rodríguez-Mirasol, N. E. Dávila-Guzmán. **Siloxane Adsorption Over Metal Organic Framework DUT-4 Modified By Solvent Ex-change.** 2do Congreso Internacional de NanoBioIngeniería. Foro Virtual del Centro de Investigación en Biotecnología y Nanotecnología. 24 al 30 de Octubre 2020. (Oral presentation)
- S. Pioquinto-García, M. Loredo-Cancino, E. Soto-Regalado, S. Giraudet, J. Rodríguez-Mirasol, P. Rivas-García, N. E. Dávila-Guzmán. **Analysis of the siloxane adsorption capacity and environmental impact of MOF DUT-4 with substitution of DMF solvent for water.** THE INTERNATIONAL ADSORPTION SOCIETY (IAS) Twitter Conference between the 7th and 11th of December, 2020. (Poster)
- S. Pioquinto-García, M. Loredo-Cancino, P. Rivas-García, E. Soto-Regalado, S. Giraudet , J. Rodríguez-Mirasol, N. E. Dávila Guzmán. **Limpieza del biogás a través de la adsorción: Remoción de siloxanos.** 3er. Ciclo de conferencias del Club Eco Smart. “Aprendiendo a ser sostenibles”. Universidad Autónoma de Baja California. 14 de Abril 2021. (Oral presentation)
- S. Pioquinto-García, L. A. Garza-Rodríguez, D. Bustos-Martínez, F. de J. Cerino-Córdova, E. Soto-Regalado, S. Giraudet, N. E. Dávila-Guzmán. **«Siloxane removal for biogas purification by low cost mineral adsorbent»**, J. Clean. Prod., p. 124940, nov. 2020, **doi: 10.1016/j.jclepro.2020.124940**. https://www.sciencedirect.com/science/article/pii/S0959652620349842
- S. Pioquinto-García, N. Tiempos-Flores, A. A. Rico-Barragan, N. E. Dávila-Guzmán. **«Metal-organic frameworks as adsorbents for impurities of biogas»**, Mater. Today Proc., p. S2214785321018460, abr. 2021, **doi:**

10.1016/j.matpr.2021.02.693. https://www.sciencedirect.com/science/article/pii/S2214785321018460

- S. Pioquinto-García, J. M. Rosas-Martínez, M. Loredo-Cancino, S. Giraudet, E. Soto-Regalado, P. Rivas-García, N. E. Dávila-Guzmán. “Environmental assessment of metal-organic framework DUT-4 synthesis and its application for siloxane removal”, J. Environ. Chem. Eng., p. 106601, oct. 2021, **doi: 10.1016/j.jece.2021.106601**. https://www.sciencedirect.com/science/article/pii/S2213343721015785

1 Introduction

The global negotiations to reduce the risks and the impacts of climate change began in 1992. Nowadays, each country determines voluntarily what measures are willing to take against climate change and announces them to the rest of the world on the Conference of the Parties (COP). According to the United States Energy Information Administration (EIA) definition, renewable energy comes from sources that are replenished but have a limited flow per unit of time. This having been said, the main types of renewable energy are biomass (including wood, municipal solid waste, landfill gas and biogas, ethanol, and biodiesel), hydroelectricity, geothermal, wind, and solar [1].

1.1 Biogas

One type of renewable energy widely spread is biogas, which can be generated for the anaerobic degradation of residual organic materials by the activity of microorganisms [2]. The process of anaerobic degradation of residual organic materials is divided into four stages [3]: (1) hydrolysis, (2) fermentative or acidogenic, (3) acetogenic, and (4) methanogenic stage. Throughout these stages, complex molecules of proteins, carbohydrates, and lipids are converted into simpler compounds such as amino acids, sugars, and long-chain fatty acids (1). Then it gives way to the formation of short-chain fatty acids, alcohols, hydrogen, carbon dioxide, among others (2). The short-chain fatty acids are then converted into acetic acid, hydrogen and carbon dioxide (3), which in turn are transformed into a variable amount of methane (4). Some of the microorganisms involved in anaerobic

fermentation are *Syntrophothermus lipocalidus*, which acts in the first stage of organic matter degradation and helps regulate the pH of the medium [4], and *Syntrophobacter fumaroxidans* (Figure 1), which participates in the conversion of propionate to CO_2, H_2 and, acetate [5].

The biogas is a mixture of methane (45-75 %) and carbon dioxide (20-55 %). moisture, hydrogen sulfide, and volatile organic compounds (VOCs) which may be present in small amounts [6]. The calorific value for biogas is between 35-44 KJg^{-1} which is similar to diesel (45 KJg^{-1}), liquid purified gas (LPG, 34 KJg^{-1}) and is still higher than coal (34 KJg^{-1}), and wood (20 KJg^{-1}) [7], [8]. Biogas can be used directly for cooking, but biogas needs to be purified to remove the minor compounds using several purification stages for other uses. Then, the biogas can be used as biofuel in microturbines, turbines, combustion engines, and boilers.

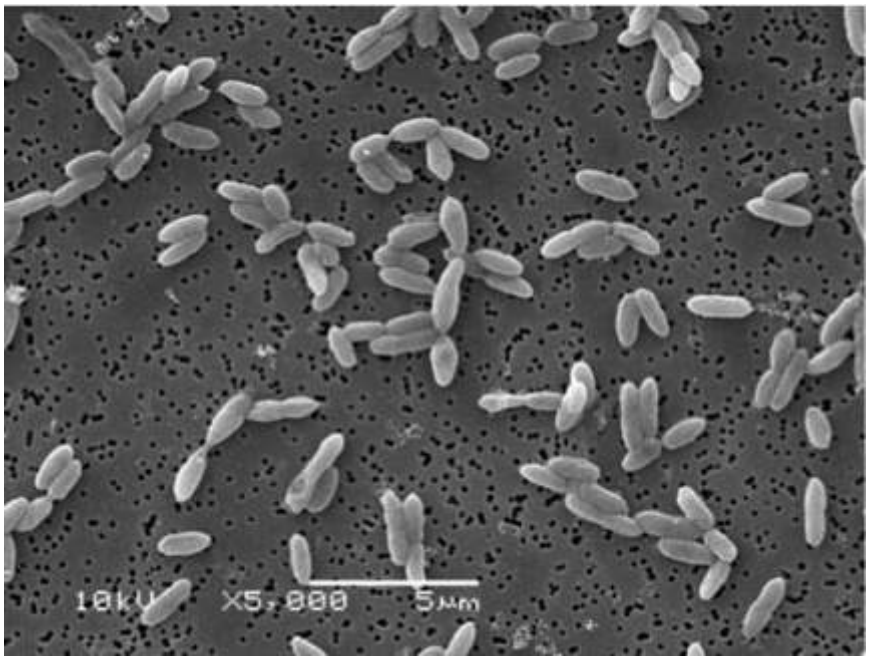

Figure 1: SEM image of Syntrophobacter fumaroxidans [5].

Around the world , the production of biogas/biomethane was approximately 35 million tons of oil equivalent (Mtoe) in 2018, while for the same year, the biomethane and biogas potential were 730 and 570 Mtoe, respectively. It is worth mentioning that biomethane is near-pure methane obtained by upgrading biogas. Europe, China, and the United States are the leaders in global biogas production, mainly for the state and federal policies shifted towards installing biogas co-generation plants and supporting the use of biogas in the transport sector [9]. Germany leads Europe in biogas production, with 1.79 billion Nm^3/year of upgrading capacity derived from biogas plants and biogas upgrading plants. Biogas output from Waste Water Treatment Plants (WWTP) and Landfill Plants in México is estimated to be 5.11 billion Nm^3/year [10].

1.2 Siloxanes

Siloxanes have a low surface tension, low flammability, high thermal stability, high resistance to UV radiation, and good waterproof behavior, these are the reason why they are widely required to manufacture products such as cleaners, paints, products for personal care, fuel additives, and adhesives. At the end of the life cycle of these products, the siloxanes reach wastewater treatment plants and landfills. During the anaerobic fermentation of sewage sludge and organic waste, it is difficult for siloxanes to disintegrate, thus they do volatilize and form part of the biogas [11]. Siloxanes do not have a greenhouse effect, but currently their accumulation in the air, soil, and water continues to be studied [12].

Silicon, oxygen, and carbon atoms bind silicon-oxygen bonds (Si – O) with organic groups bound to form siloxanes. The siloxanes are classified into linear and cyclic structures (Figure 2) [13]. Hexamethyldisiloxane (L2), Octamethyltrisiloxane (L3), and Octamethylcyclotetrasiloxane (D4) are the most abundant siloxanes in biogas [13].

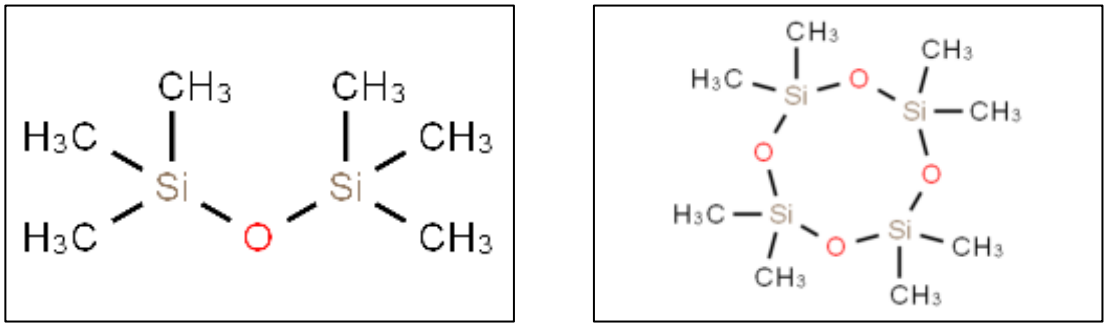

Figure 2: Linear and cycle siloxane L2 and D4, respectively [14].

The concentration of siloxanes in biogas from Landfill and WWTP is between 10 and 100 mg/m^3 [13]. Siloxanes have adverse effects on biogas combustion systems; therefore they are considered essential pollutants to remove from biogas [7]. The siloxane is converted during the combustion process mainly in formaldehyde (CH_2O) and orthosilicic acid (H_4SiO_4) [14], both chemical reagents contribute to abrasion, metal friction, and failure of other mechanical elements of the combustion system (Figure 3), which leads to suspension of service [15]. There is no standard specifying the maximum concentration of siloxanes in biogas, but an acceptable general limit of 15 mg/m^3 is recommended [16]. Jenbacher, Deutz, Caterpillar, and Waukesha manufacturers recommend a maximum siloxane concentration (C_{max}) for biogas internal combustion engines of 10, 5, 28, and 25 mg/m^3, respectively. While Capstone, and Ingersoll-Rand manufacturers recommend a C_{max} for biogas

microturbines of 0.03 and 0.06 mg/m^3, and Solar manufacturer recommend a C_{max} for biogas turbines of 0.1 mg/m^3 [12].

Figure 3: Exhaust valve and wheel of the turbocharger turbine damaged by siloxanes [18].

The necessity of siloxane removal from biogas is also a priority for advancing biogas' energy recovery potential. Current technologies for siloxane removal from biogas include adsorption, absorption, cryogenics, separation by membranes, biological processes, among others [17].

1.3 Siloxanes cleaning techniques

1.3.1 Cryogenic separation

The cryogenic system includes the cooling chamber with a coil that transports the freezing agent and allows condensation formation [18]. Temperatures of up to -70 ºC are used to remove the most significant number of siloxanes, and in other cases, low temperatures are used to reduce energy consumption and, in turn, reduce costs. Generally, a temperature of -29 to 5 ºC is used; therefore, this siloxane removal technique is combined with some other techniques such as adsorption, absorption, biological treatment, among others [19]–[21].

Schweigkofler and Niessner (2001) observed that cooling at 5ºC of biogas samples from a waste disposal site and a sewage treatment plant resulted in the removal of siloxanes by 11 % and 9 %, respectively, when the siloxanes concentration in biogas before treatment was L2 (~0.8 mg/m^3), hexamethylcyclotrisiloxane (D3) (~0.42 mg/m^3), D4 (4.95 mg/m^3), and decamethylcyclopentasiloxane (D5) (~0.63 mg/m^3). In this same work, the adsorption and cryogenic techniques were combined using a packed bed of silica gel and a temperature of -50ºC; the results demonstrated a 98 % siloxane removal efficiency, when the initial siloxanes concentration was L2 (<0.05 mg/m^3), D3 (~0.25 mg/m^3), D4 (6.45 mg/m^3), and D5 (~9.65 mg/m^3) [21].

On the other hand, Wheless and Pierce (2004) reported that Los Angeles County Sanitation Districts removed 50 % of the siloxanes present in the biogas through a cooling system, at 4.4 ºC and a pressure of 25.17 bar, when the siloxane inlet concentration was 2 mg/m^3. Also, on bench-scale research, they removed 95 % of the total siloxanes at a temperature of -28.9 ºC. They also mentioned that the operable elimination mechanism consists of the dissolution of gaseous siloxanes in the condensate formed and that one of the problems to deal with this type of technology is icing [22].

Ajhar *et al.* (2010) theoretically determined the concentrations of siloxanes D4, D5, L2, D3, L3, and L4 of an ideal gas at different temperatures (-70ºC to 0ºC) and a pressure of 1 bar. As can be seen in Figure 4, at lower temperatures, siloxanes D4, D5, and L4 condensed to a greater extent than siloxanes L2, D3, and L3. In this sense, it is noted that siloxanes with a lower boiling point are more difficult to condense. They also mentioned that using pressures greater than 1 bar during condensation would favor removing a more significant amount of siloxanes [17].

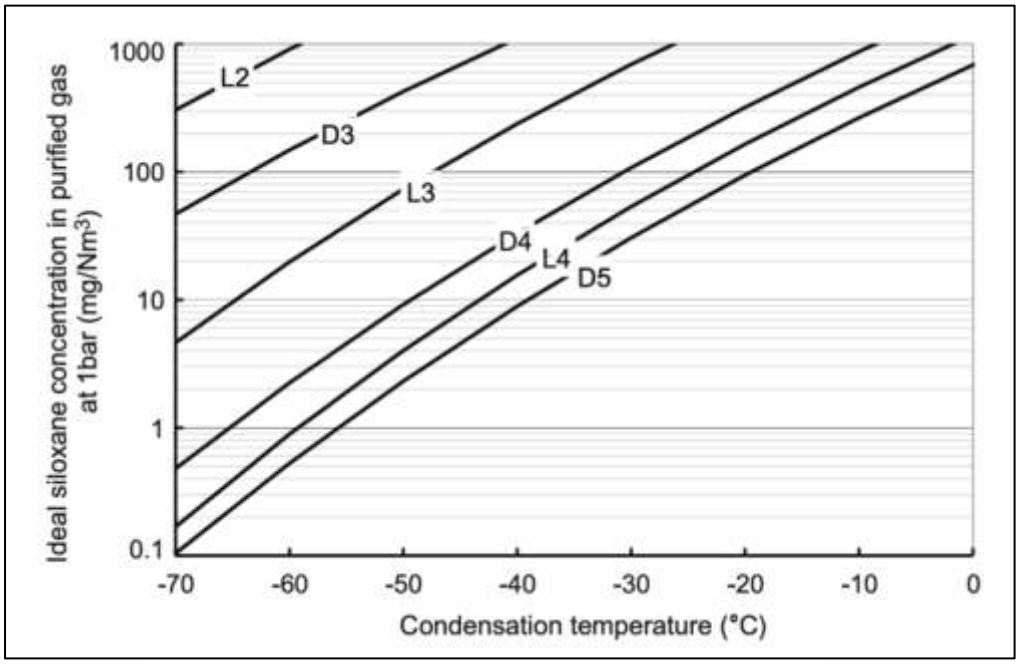

Figure 4: Theoretical concentration of siloxanes at different cooling temperatures and 1 bar [25].

The cryogenic technique requires high investment and operating costs, so it is recommended to treat of biogas with a high siloxane load. In addition, another challenge is the formation of ice and the difficult task of cleaning the cooling chamber [18], [22]–[24].

1.3.2 Biological treatment

A siloxane removal technique that is economical, simplicity and ecological is biological removal [12]. It consists of using filters constructed of organic materials that contain microorganisms capable of taking siloxanes as a carbon source [19]. It can be biotrickling, bio-scrubbers or stage biodegradation filters [12].

Accettola *et al*. (2008) studied the biodegradation of siloxane D4 in batch cultures using inoculation with P. *putida* and activated sludge from two Waste Water

Treatment Plant (WWTP) from Austria and WWTP of a silicones company. Only batch cultures with activated sludge showed changes in turbidity and optical density. They identified in the cultures γ-proteobacteria, of which *Pseudomonas* dominated. They also looked at the biodegradation of siloxane D3 in a biotrickling filter (height of inert packing material 0.5 m, diameter 0.07 m) for 35 days with an initial siloxane concentration of 77 mg/m^3 (gas flow rate, 0.5 L/min). They found removal efficiencies of 10-20 percent with four changes of a medium, subsequently they changed the siloxane concentration at 45 mg/m^3 (0.9 L/min^{-1}) and, then, at 59 mg/m^3 (0.7 L/min^{-1}), with only a change of medium on days 57 and 64, respectively. The removal efficiency obtained for both cases was approximately 10 % [25].

Popat and Deshusses (2008) used siloxane D4 as the sole source of carbon and energy for enrichment crops in a batch inoculated with activated sludge from a WWTP in Riverside, CA. They observed the slow growth of biomass and aerobic biodegradation. Later, they used aerobic and anaerobic biotrickling filter systems (height 45.0 cm x diameter 3.8 cm) (Figure 5), with cattle bone porcelite (CBP) and lava rocks as packing materials. The siloxanes concentration was approximately 45 mg/m^3. The results showed efficiency removal of 10-15 % of siloxanes with an empty bed residence time (EBRT) of around to 4 min. They also achieved 43 % removal of siloxanes in the aerobic biotrickling filter with an EBRT of 19.5 min. This result demonstrated the mass transfer limitations as key to explain the low siloxane removal in biotrickling filters [26].

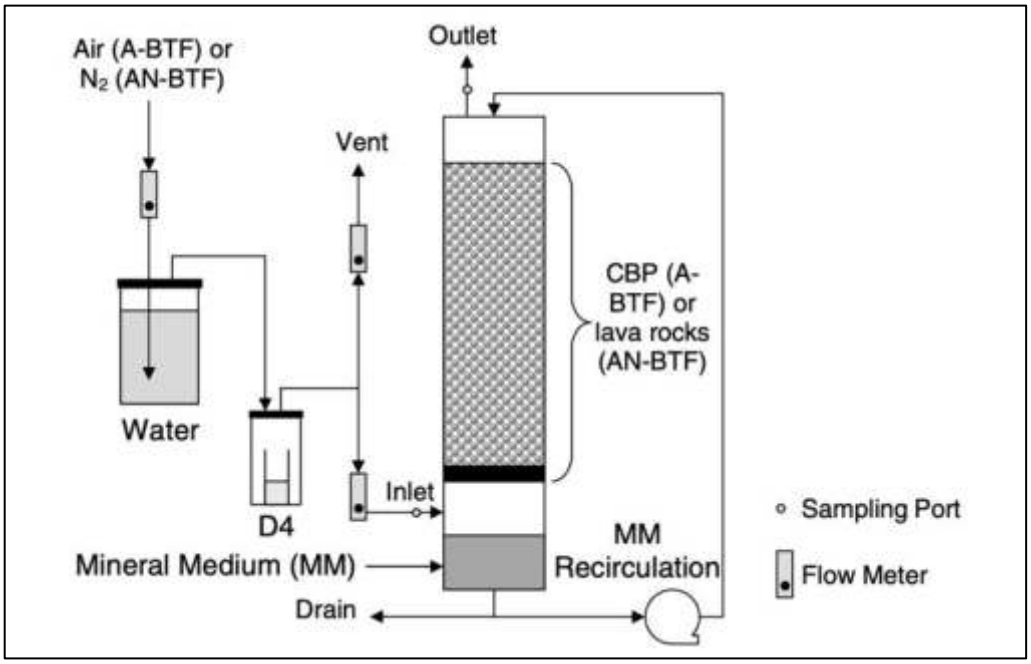

Figure 5: Aerobic and anaerobic biotrickling filters systems for removal of D4 [29]. A=Aerobic, AN=anaerobic.

In addition to the low availability of substrate and of microorganisms, the biodegradability and hydrophobic nature of siloxanes generates a low mass transfer of siloxanes in the liquid phase increasing contact time, for which enzymes or biosurfactants can be used [18], [25]. The final products of the biodegradation of siloxanes are silicic acid, carbon dioxide, dimethylsilanediol (DMSD) and water [19]. On the other hand, the biological system with bioscrubbers has been used to remove volatile compounds with low molecular weight and high solubility in water, for example methanol, isopropyl alcohol, acetone and heptane, but there are no studies on the removal of siloxanes [27].

1.3.3 Absorption

The absorption process for removing siloxane can be a physical or chemical way using strong basis/acids at high/low pH values [17] and high boiling point [28]. The

siloxanes will be transferred by diffusion and dissolution in the absorbent liquid [11]. For physical absorption have been used water [20], dodecane, hexadecane [21], sodium hydroxide; and for chemical absorption mineral oil [11]; nitric acid, sulphuric acid, and phosphoric acid have been studied [21]. The use of absorbents will depend on their physicochemical properties, toxicity, price [13], safety, degree of corrosion, and carbonate formation that could trigger [29], since siloxanes react and form, carbonates, which precipitate in the equipment, use bases can be ineffective [13].

Ghorbel et al. (2014) analyzed silicone oil 47V20, Seriola 1510, and Polyalphaolefin as absorbents for siloxanes using a small column glass wetted-wall (height 0.66 m x diameter 0.02 m), flow rate of 0.1 m^3/h, room temperature and inlet gas concentration between 500-1500 mg/m^3. It was determined that the most efficient absorbent was silicone oil 47V20 with a 60 to 98 % efficiency [13]. In adittion, Rojas Devia & Subrenat (2014) studied motor oil, cutting oil, and a water-cutting oil mixture for absorbing hexamildisiloxane (L2) and octamethylcyclotetrasiloxane (D4) using a bubble column (height 0.4 m x diameter 0.05 m) at an initial concentration between 800 – 4800 mg/m^3, residence time between 0.1-8.2 s and temperatures of 25, 50, and 90 ºC. The results showed that the motor oil had a removal efficiency of 80 % for D4 and 60 % for the L2 at room temperature.

Charry Prada *et al.* (2020) studied the Superacid 9/1 solvent formed for sulfuric acid and acetic acid glacial (9:1 mole ratio) for removing impurities from biogas that include H_2S, CO_2, volatile organic compounds and precisely five ppmv siloxanes. The system consisted of a bubble column reactor with a liquid height (H_L) of 3.2 m and H_L/D ratio of 3.37 (Figure 6). The results showed that the superacid solvent

removed 100 % of the siloxanes at 288.15 K, 861.26 kPa, and a solvent flow rate of 10.23 L/s [30]. The disadvantage of the absorption technique is the regeneration of the solvent; this is the reason why new "green solvents" have been sought. Slupek *et al.* (2021) studied deep eutectic solvents (DESs) of tetrapropylammonium bromide (TPABr) and tetraethylene glycol (TEG) as absorbents of L2, L3, and D4 siloxanes (C_0= 50 mg/dm^3) in a model biogas stream. The results showed that the highest solubility of siloxanes was obtained in the DES composed TPABr: TEG (1: 3) molar ratio. At 50 mL of DES TPABr: TEG (1:3), 50 mL/min flow rate and room temperature, the siloxanes were removed with high efficiency (375-5300 min), and the absorbent DES TPABr: TEG was completely regenerable [31].

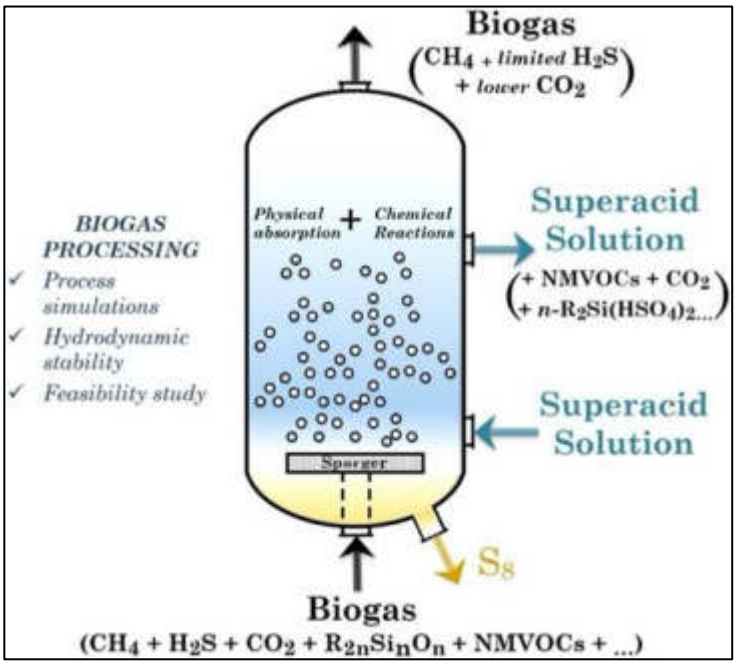

Figure 6: Bubble column reactor using the Superacid 9/1 for biogas purification process [33].

1.3.4 Membranes

The membranes are polymeric or inorganic materials simple with large surface area and small size. The permeability and selectivity of the membranes and pore size and molecular interactions can determine their effectiveness in removing siloxanes from biogas [12]. The minor compounds from biogas such as hydrogen sulfide, toluene, and dichloromethane can damage the membrane; therefore, it is necessary to pre-clean the biogas and reduce the acidic conditions mechanical destruction and fouling membrane. The accumulation of siloxanes on the membrane surface could reduce its efficiency due to the pore blocking. The membrane technique could be combined, for example, with pressure swing adsorption (TSA), in order to reduce operating and investment costs [7].

Ajhar & Melin (2006) conducted simulations using IVT user-added subroutines for AspenPlusTM to evaluate a membrane in energy consumption and material flow. The analytical method included chromatography/mass spectrometry (GC-MS) to analyze the loaded siloxanes. The authors found that the polydimethylsiloxane (PMDS) had selectivity towards siloxane D4, and they identified, for the first time, that the permeation was a useful method of removing siloxane from biogas [32]. At other times, Ajhar et al. (2012) investigated a commercial silicone-rubber membrane (*PermSelect XA1M-10 cm*^{2}) (Figure 7) for removal of L2, L3, L4, D3, D4, and D5 siloxanes of a carbon dioxide feed. The results showed that the permeability ranged from 9000 to 50 000 barrer at 20 ºC, depending on the type of siloxane. Also, they observed that the more volatile siloxane (L2) showed a substantial decrease in permeability after increasing the temperature (50ºC) compared to the rest [33].

Figure 7: PermSelect XA1M-10 cm^2 for removal siloxane test [36].

Santos-Clotas *et al.* (2020) explorer the diffusion of D4, D5 siloxanes, and other impurities from biogas using a PDMS hollow-fiber membrane bioreactor. The initial concentration of D4 and D5 siloxanes were 54±3 and 102±4 mg/m^3, and the inoculum of the membrane bioreactor was the anaerobic sludge from the WWTP of Girona Spain. They discovered that removal efficiencies for D4 and D5 were 4 to 14 percent and 2 to 23 percent, respectively, for 0 to 36 days, with a gas residence time (GRT) of 18 seconds. From days 37 to 64 and a GRT of 31.5 s, siloxane removal increased to 17 and 21 % for D4 and D5 siloxanes, respectively [34].

1.3.5 Adsorption

The adsorption process is the most used siloxane removal technique [29], [33] due to its relatively low cost and high efficiency. Thus, over the years, the most widely used adsorbent materials have been activated carbon (AC) and silica gel (SG) [35]. However, these two materials require a high energy requirement for their regeneration process, therefore those materials are not regenerated [29], [33] and present low adsorption capacity when wet biogas is used [36].

Oshita et al. (2010) worked with ten adsorbents, 6 were AC to evaluate the adsorption capacity of siloxanes. They used a 17 mm x 250 mm column and filled it with 0.5 g of AC and sealed it with 0.1 g of glass wool. The initial concentrations of siloxane D4 and D5 were 46 ppm (552 mg/m^3) and 21 ppm (252 mg/m^3). The highest adsorption capacities were 404 mg/g for D4 and 531 mg/g for D5. In turn, they established a relationship between adsorption capacity and surface area and concluded that adsorbents with large BET specific surface areas, especially those with high external surface area and relatively large diameter micropores, are desirable for siloxane removal. Yu et al. (2013) investigated D4 adsorption on 11 commercial ACs and discovered that wide micropores and narrow mesopores with a diameter of 1.7-3.0 nm are the best for D4 adsorption.

The acidic and basic sites in AC adsorption have also been studied, in addition to the unique surface area in siloxane adsorption. The chemical reagents generally used for the modification of ACs are nitric acid (HNO_3), sulfuric acid (H_2SO_4), sodium hypochlorite (NaClO), potassium permanganate ($KMnO_4$), potassium dichromate ($K_2Cr_2O_7$), peroxide hydrogen (H_2O_2), and ozone (O_3) [37]. In addition, ammonium persulfate ((NH_4)$2S_2O_8$), perchloric acid ($HClO_4$), hydrogen peroxide (H_2O_2), and nitric acid (HNO_3) can be used to introduce oxygenated groups to the surface of AC [38]. Gong et al. (2015) investigated the removal of D4 in an anthracite-based AC that had been pretreated with an NH_3 and HCl solution. Ammonia (NH_3) treatment increased the concentration of the basic groups, which improved the adsorption potential of D4. On the other hand, the treatment with HCl introduced acidic functional groups such as phenolic, lactonic, and carboxylic groups, which exhibited different behaviors in D4 adsorption. According to scientific literature, carboxylic

groups inhibit siloxane adsorption, while phenolic groups promote siloxane adsorption [39].

The formation of other siloxanes in the desorption stage of AC can be associated with the loss of siloxane adsorption capacity of the carbons after regeneration. Tran et al. (2019) studied the AC called STIX, AP4, and 207C to know the renewability of siloxane adsorbents after thermo-desorption treatment. They found that the greater the number of alkali metals on the surface of the AC, the more significant the fraction of polymerized siloxane D4. They also proposed the formation of polymeric species such as polysiloxanolate, polydimethylsiloxane (PDMS), or α–ω-silanodiols by transforming adsorbed D4 into the porosity of adsorbents during the adsorption and thermodesorption steps [40]. In Figure 8, the bands at 1265, 1092, and 816 cm $^{-1}$ were for D4, but the new bands correspond to the formation of siloxane D3.

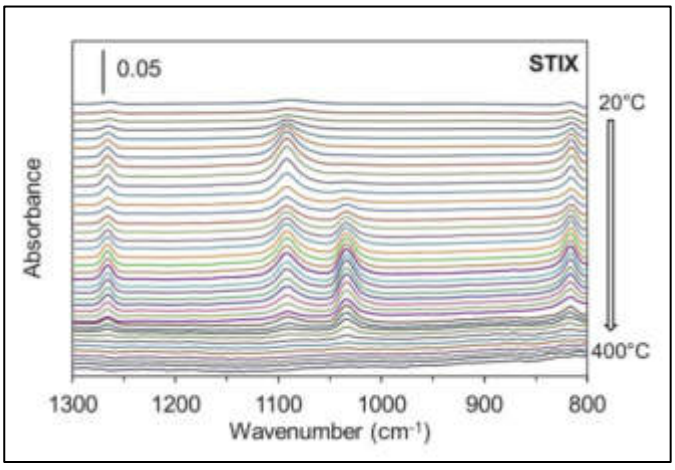

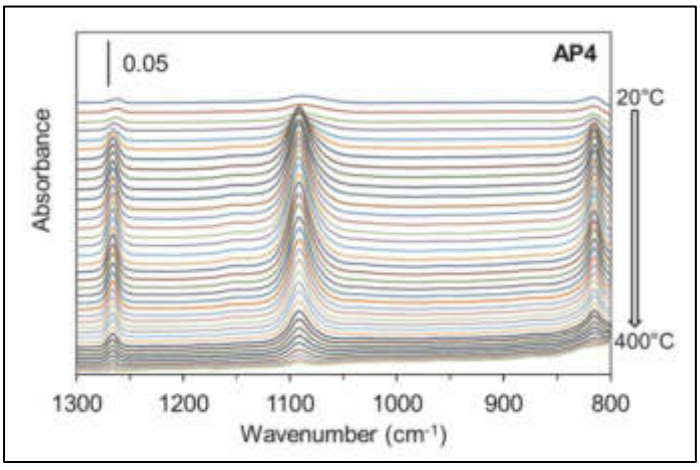

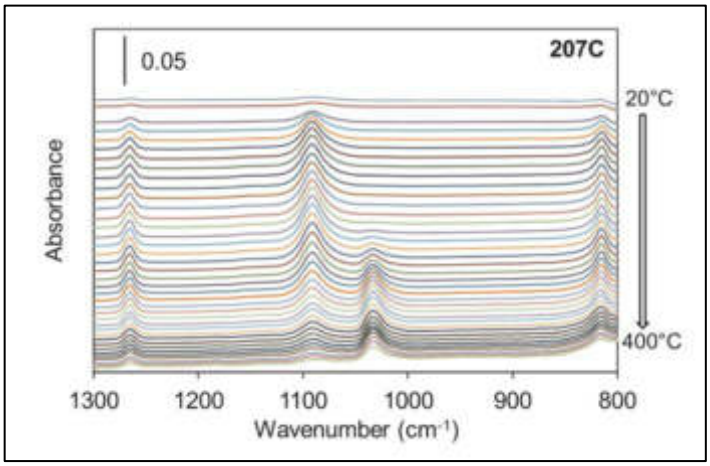

Figure 8: Thermodesorption of D4 on AC STIX, AP4 and 207C [39].

1.4 Metal-organic Frameworks (MOFs)

Metal-organic frameworks (MOFs) and other porous coordination polymers (PCP) have also been investigated as adsorbents for biogas impurities [41]. MOFs are porous materials with high selectivity and feasible regeneration, mainly due to their large surface area, pore volumes [42] and, thermo-mechanical stability [43]. MOFs are porous crystalline structures made up of metal groups joined together by organic ligands [44]. The type of permanent pore and cavity are strongly influenced by the geometric characteristics of the metallic units and the organic ligands of the MOF. Due to high porosity and surface area, easy modification, thermal stability, and regeneration [45], MOF has been widely used in catalysis, gas adsorption [46], [47], optics, magnetism [45], and chemical sensors [48].

1.4.1 Enhance the properties of MOFs

MOFs can be modulated in size, shape, and properties to suit a specific application. Therefore, different methods have been studied to achieve it, such as solvent

adjustment, templating method, acid-based adjustment route, sonochemical process, and others [49].

The templating method consists of utilizing an agent to form a desirable open framework at specific condition and crystallization. Bajpe et al. (2010) reported a templating mechanism on a specific molecular level using Kegging-type heteropolyacids (HPAs) for the $Cu_3(BTC)_2$ MOF (Figure 9). An aqueous solution of $Cu(NO_3)_2 \cdot 3H_2O$ (10 mL) was prepared with HPA (6.4 mL) at pH ~1.6, then BTC (0.1 M) in ethanol (13.3 mL) was added, and finally, the precipitate was dried at 40 ºC. The results showed that the order in the preparation sequence was an indication that HPA was prearranging the Cu^{+2} ions. In this scenario, the organic linker rule was to connect the structured Cu^{+2}/HPA units [50].

Figure 9: Preparation sequence during formation of $Cu_3(BTC)_2$ MOF using a HPA templating [53].

The acid-based adjustment influences the nucleation and crystal growth process during the fabrication of MOFs. Guo et al. (2011) worked with $Dy(BTC)(H_2O)$ MOF crystals using sodium acetate as the coordination modulator. $Dy(NO_3)_3 \cdot xH_2O$ (60 mg), BTC (20 mg), DMF (8 mL) and deionized water (2 mL) were dissolved, next was added sodium acetate (0-5 equivalent), was kept the solution at 60 ºC for 0-48 h, then washed with dimethylformamide and finally dried at room temperature. The

authors discovered that increasing the sodium acetate concentration accelerated particle formation (Figure 10). In addition, they observed that the size of the particles increased from 3.5 equivalent of a modulator and associated it with the aggregation of nanoparticles that were formed very quickly [51].

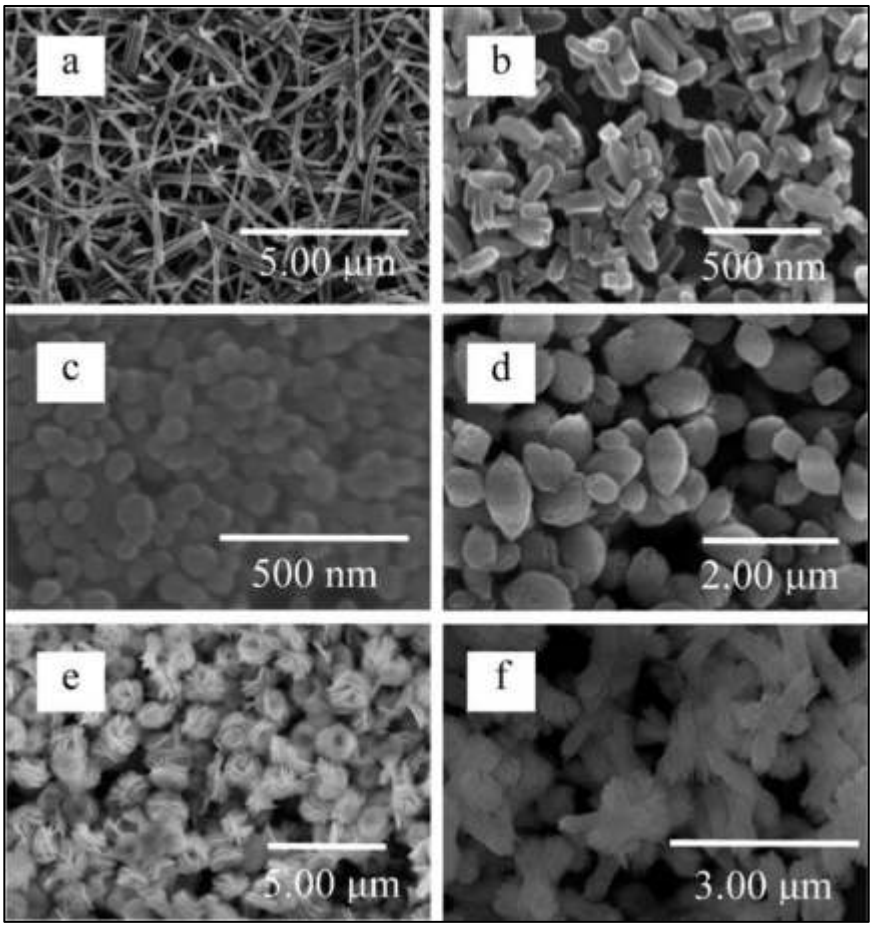

Figure 10: SEM images for Dy(BTC)(H_2O) using at a) 1 (pH 4.4), b) 2 (pH not specified), c) 3 (pH 5.8), d) 3.5 (pH 6.5), e) 4 (pH 7.2) and f) 5 (pH 7.9) equiv. sodium acetate [54].

The sonochemical process involves acoustic cavitation that begins with the formation, growth, and collapse of a bubble, generating high temperature and pressure. Son et al. (2008) employed the sonochemical process for the synthesis of MOF-5. $Zn(NO_3)_2 \cdot 6H_2O$ (1.34 g) was mixed with H_2BDC (0.25 g) in 1-methyl-2-

pyrrolidone (40 mL). Next to stirred under nitrogen, the solution was transferred in a 50 mL transparent horn-type tube reactor for ultrasonic processes between 10 to 50 % of the maximum power and temperature between 129 – 164 ºC. The results were compared with the MOF-5 crystals prepared by convective heating using an oven at 105 ºC for 24 h, next to putting the crystals in chloroform (2 days) and vacuum dried at 150 ºC for 24 h (Figure 11). The authors concluded that the sonochemical method reduced the cubic crystal size from 900 µm to 5-20 µm, while physicochemical properties were similar [52].

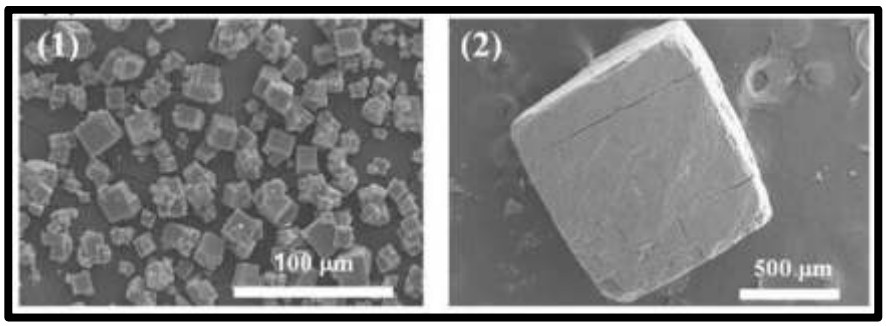

Figure 11: SEM images for MOF-5 synthetized by (1) sonochemical and (2) conventional method [55].

Solvent adjustment is the most convenient method to modulate the properties of MOFs. Zhang et al. (2012) worked with the synthesis hydrothermal of $Cu_3(BTC)_2$ MOF (Figure 10). H_3BTC (2.5 mol) and $Cu(OAc)_2 \cdot H_2O$ (2.5 mol) were dissolved in water/ethanol mixture (60 mL, ethanol volume ratios of 0, 25, 33, 50, 67, 75, and 100 %), stirred for six hours at room temperature, then washed with water/ethanol and finally vacuum-dried at 60 ºC for 24 h. The authors found that the MOF cannot form in the absence of ethanol or small ethanol in water. From 33% vol. of ethanol, the structure of the MOF with particle sizes from 20 to 300 nm was obtained (Figure 12).

It was observed that using 50% vol. of ethanol, the specific surface area (A_s) of the MOF remained in a range of 724-1067 m^2/g, exceeding the reported A_s of 692 m^2/g [53].

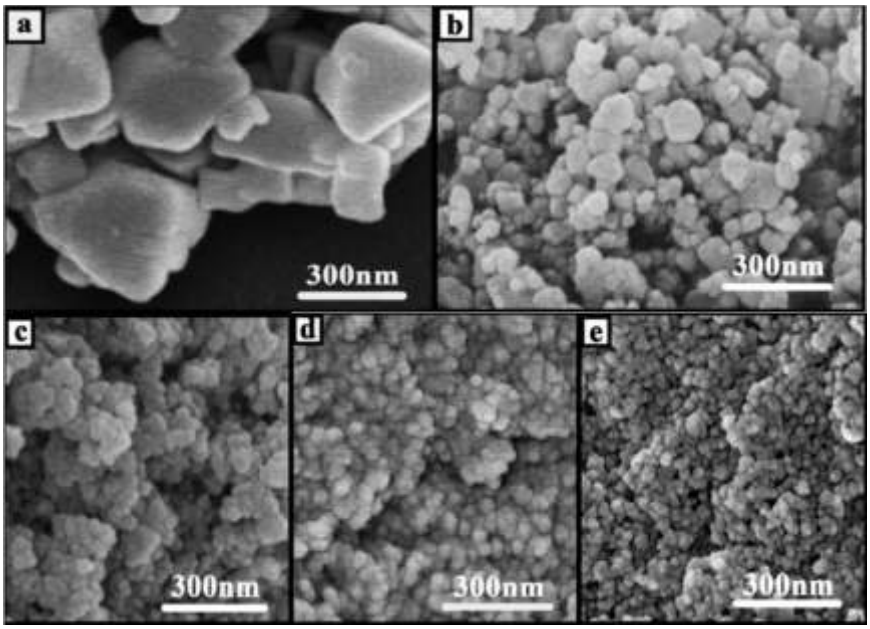

Figure 12: SEM images of $Cu_3(BTC)_2$ using water/ethanol mixtures at a) 33, b) 50, c) 67, d) 75 and e) 100 % volume ratios [57].

1.4.2 Exchange solvent for MOFs

The improvement of the properties of the MOFs can be achieved through a correct activation of the adsorbent. Activation consists of eliminating the guest molecules from the interior of the MOF pores, comprising two stages: exchange of the host molecule and evaluation of the guest molecule (Figure 13) [54].

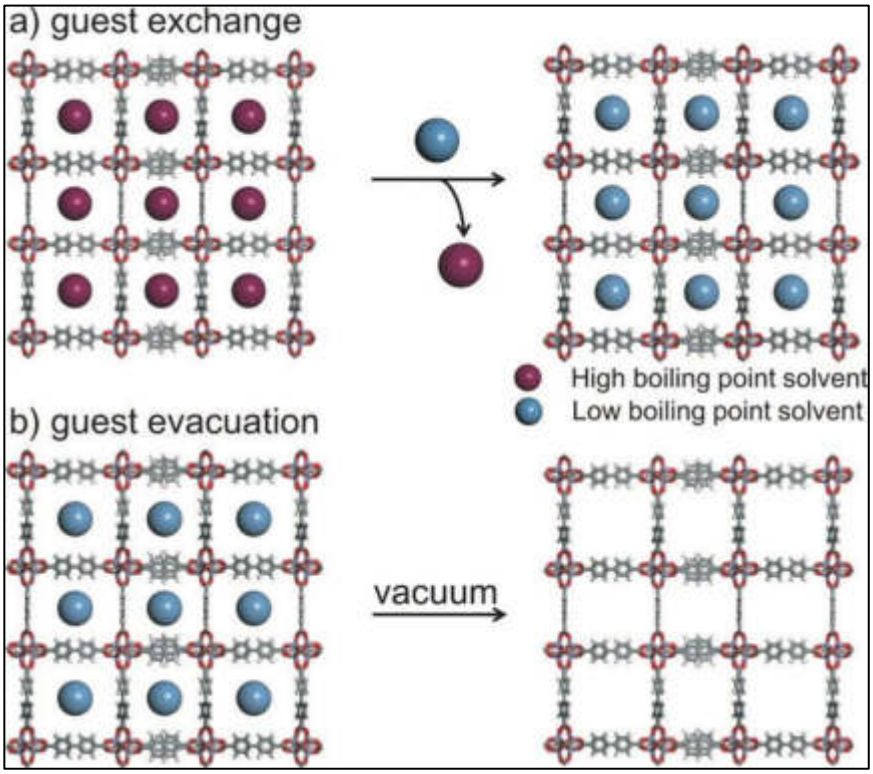

Figure 13: Scheme of exchange solvent for activation of MOF.

The exchange solvent involves washing the MOFs with low boiling point solvents such as alcohols, dichloromethane, trichloromethane, and hexane, replacing the solvent several times before drying under vacuum. Ma et al. (2012) worked with the exchange solvent for the activation step for UMCM-9 MOF. 40 mg of UMCM-9 was washed three times with dimethylformamide (DMF, 20 mL), next the precipitated was washed three times with dichloromethane (CH_2Cl_2, 20 mL), then, the crystals were washed three times with *n*-hexane (C_6H_{14},20 mL), and finally, the crystals were evacuated under vacuum at 0.05 torr for two hours at room temperature. The results showed that the MOF with the washing with CH_2Cl_2 had a specific surface area of 1330 m^2/g and after washing it with C_6H_{14}, the surface area obtained was 4980±50 m^2/g.

1.5 MOFs for siloxane removal

Mito-oka and coworkers (2013) employed the MOF from Dresden University of Technology (DUT-4) and conventional AC for siloxane adsorption. The results showed that DUT-4 adsorb 15 wt% of siloxane D4 while AC adsorbs approximately 20 wt %. However, under humid conditions, the authors mentioned that the DUT-4 has a high level of selectivity attributed to its strong hydrophobicity and optimal chemical interactions with siloxane D4 leading to high uptake, compared with AC [55]. Furthermore, Gargiulo et al. (2019) explored the MOF MIL-101 on siloxane D4 adsorption by thermogravimetry at 298, 318, and 338 K. The results showed that the adsorption capacity of MIL-101 decreased with increasing temperature, from 3.2 mol/kg to 298 K at 2.7 mol/kg to 338 K. Also, they confirmed a complete regeneration of MOF under vacuum at 423 K [56].

1.6 Life Cycle Assessment for MOFs

Although MOF have been pointed out as "green materials" for sustainable processes, the environmental impact of their synthesis has been barely evaluated. The life cycle assessment (LCA) is a methodology that can determine how green a material is [57]. LCA has been used by Loya-González et al (2019) [58] and Sepúlveda-Cervantes et al (2018) [59] to determine the impacts of adsorbents materials such as AC synthesized from biomass waste. In these works, the impregnation stage of the AC production was found to be the largest contributor to environmental damage, owing to the high-energy consumption of this stage and the use of chemicals such as $ZnCl_2$ and KOH.

To the best of our knowledge, there is not any study in the literature about using LCA for the synthesis of MOF for biogas application. Grande et al (2017) [60] evaluated the environmental impact of the MOF CPO-27-Ni synthesized by four different routes as a carbon capture and storage adsorbent. They found that the main contributors to the environmental impact of CPO-27-Ni were the synthesis and cleaning stages, mainly associated with the toxicity of tetrahydrofuran and dimethylformamide. When water was used in the synthesis or cleaning stage, the environmental impact was reduced from 1136.2 to 12.3 kg CO_2 eq per kg of MOF.

1.7 MOFs immobilization

MOFs are ideal particles to integrate/support them in frameworks or structures that allow to development of large-scale or industrial processes. Integration into other structures includes the use of membranes, fibers, monoliths, and pellets.

1.7.1 MOFs Membranes

A *membrane* is a thin-film composite made up of various components that incorporates all of their properties to achieve a specific goal (adsorption, catalysis, gas separation, etcetera) [61]. MOF membranes can be of two types: supported MOF membranes and mixed-matrix membranes (MMM) (Figure 14). The former, in most cases, are films formed on porous oxide substrates such as silica, alumina, titania, and zinc oxide. On the other hand, MMMs are obtained by mixing MOF with polymeric matrices (these ones can be commercial as Pebax®, @Matrimmid) on a glass substrate [62], [63]. In general, the permeability and selectivity of membranes

can be improved by increasing the amount of MOF. However, this increases their fragility, and they can break [64].

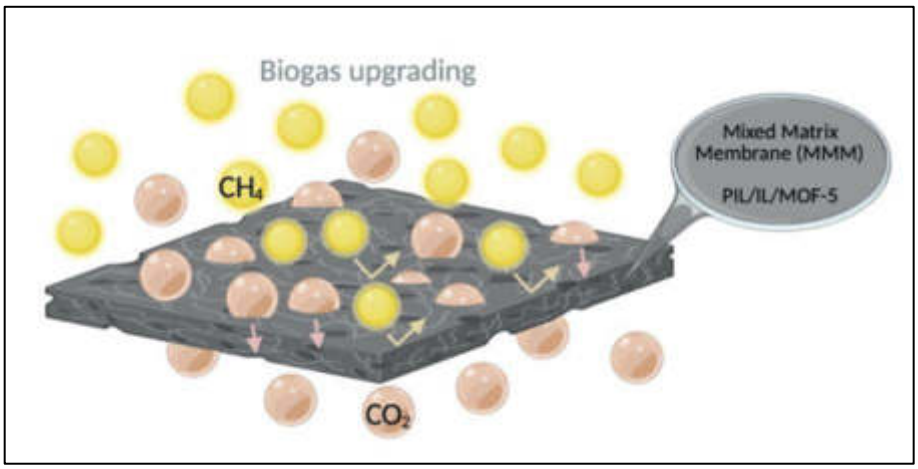

Figure 14: Scheme of MMM used for separation of CO_2 in biogas upgrading [69].

1.7.2 MOFs monoliths

A *monolith* is a structure that has a specific shape with the same channel dimension. These structures have the advantage that their channels facilitate a lower pressure drop. In addition to their thin walls, they present both better mass and heat transfer [64], [65]. The conventional way to obtain monoliths with MOFs can be by wash coating to deposit MOFs on monolithic supports, consisting of metallic support introduced into a MOF-polymer solution. Moreover, the fabrication of monolithic MOFs by extrusion approach consists of the extrusion of a plasticizer/binder close to the MOF. One of the disadvantages of monoliths is that if the amount of MOF is increased (> 50%), the mechanical stability of the monolithic structure may collapse, in addition to the fact that there may be a heterogeneous MOF distribution. A recent methodology (after the year 2016) to obtain monoliths with MOF is conducted by 3D

printing (Figure 15), in which two solutions are started, one of them contains the MOF + binder, while the other solution contains a plasticizer [65].

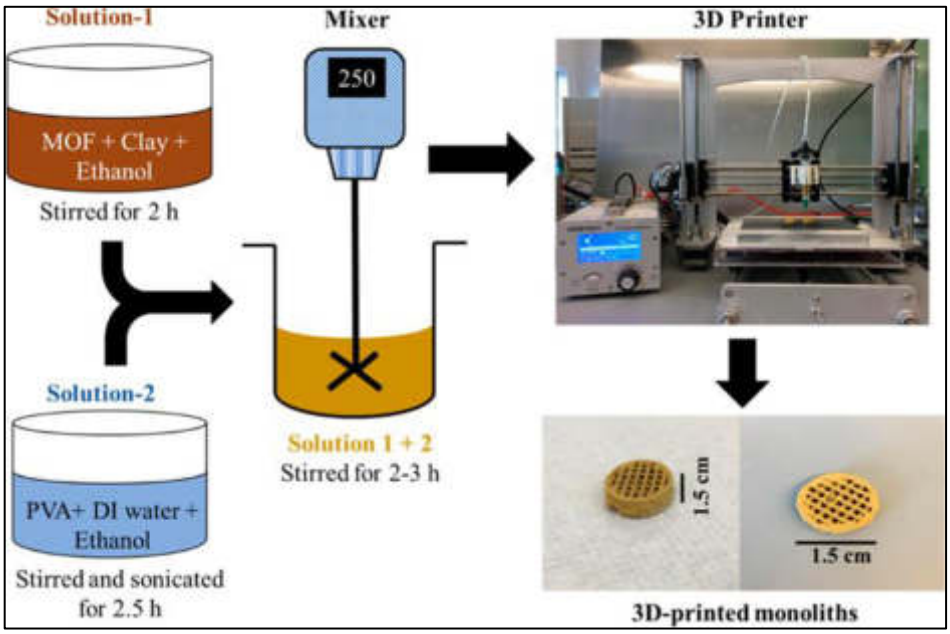

Figure 15: Procedure for preparing MOF monolith by 3D printing [70].

1.7.3 MOFs pellets

MOF pellets can be made with a manual press without using binders and at pressures of hundreds of MPa (Figure 16). The applied pressure will depend on the physicochemical characteristics of the material, since the textural properties of the MOF could be affected [66]. In this sense, it is recommended to carry out a measurement control of a specific surface area and XRD patterns [64]. On the other hand, pellets can also be formed using binders and solvents to achieve greater volume and mechanical stability; in this case, a weight ratio ≤ 30% of the MOF can be used. Silica, bentonite, kaolinite, cellulose-acetate, methylcellulose, polystyrene is used for the pellets and solvents like dimethylformamide, dimethylacetamide, tetrahydrofuran, water are used [67].

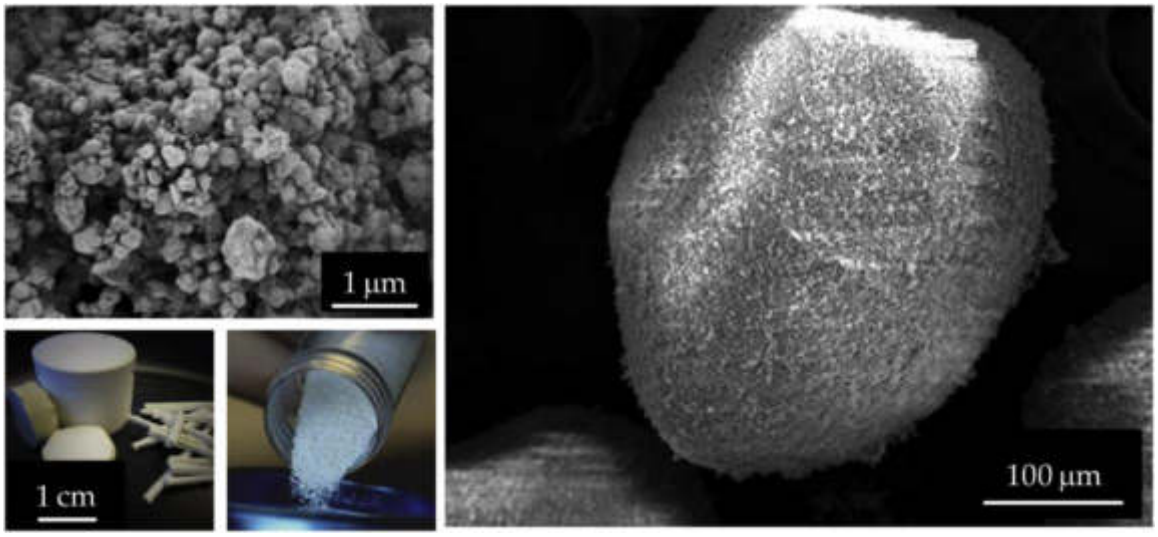

Figure 16: Images of ZIF-8 crystals (left), and pellets (right) [72].

1.7.4 MOFs fibers

Fibers are polymers with diameters between tens to hundreds of nanometers with both high specific surface area and volume ratio [68]. These materials have demonstrated high potential in solar cells and hydrogen storage [68][69]. In water treatment and environmental remediation, MOFs fibers materials have been actively prepared for removing or separating contaminants from liquid and gas environments based on various physical and chemical techniques, notably adsorption and ultrafiltration [70],[71], [72].

1.8 Electrospinning

There are several methods for producing fibers; from high-volume production methods such as melt fibrillation, island-in–sea and gas jet techniques, and exact methods like nanolithography, and self–assembly. However, their usefulness is limited by high production costs and low production rates. Hence, the electrospinning

technique is advantageous for producing nanofibers due to its low operating costs and relatively high production rate [68].

Electrospinning is a process based upon the uniaxial stretching of a viscoelastic solution, thus producing a nonwoven fabric of nanofibers. The electrospinning process is performed by driving a liquid solution through the tip of a metal needle that is attached to a syringe, and in the presence of the electric field, the jet migrates to the lower region of lower potential, which is a plate where fibers are collected (Figure 17) [73]. Electrospun fibers could be considered suitable supporting materials for nano-crystallites with active sites for gas adsorption, such as MOFs.

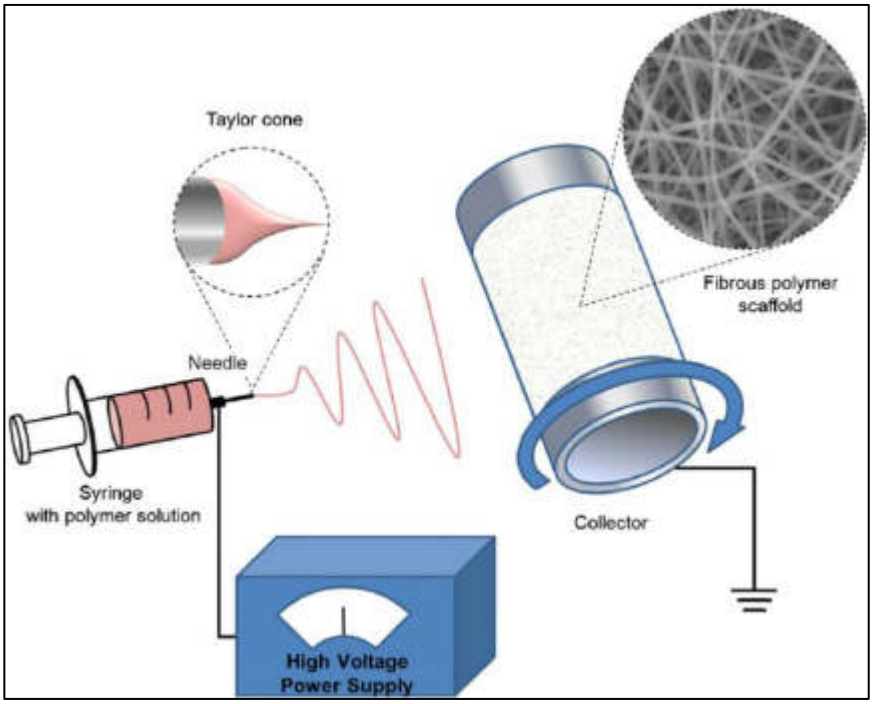

Figure 17: Electrospinning system (ResearchGate, Heungsoo Shin) [80].

With the electrospinning technique, two routes can be achieved to immobilize the MOF, direct electrospinning, and surface decoration.

In direct electrospinning (Figure 18 a), b) c)), a composite fiber is prepared by combining MOF particles with a polymer solution, resulting in the MOF particles being embedded in the polymer matrix. This route has three steps: 1) MOF powder particle synthesis, 2) MOF-polymer slurry preparation, and 3) direct electrospinning slurry. Polystyrene (PS)-tetrahydrofuran (THF), PVP-ethanol (EtOH), and polyacrylonitrile (PAN)-dimethylformamide (DMF) is the primary polymer-solvent systems used in this technique. One of the disadvantages is that the internal pores of the MOFs can be covered with the polymer, which reduces its textural properties. In this sense, solvents with high volatility can be used, for example, polylactic acid (PLA)-dichloromethane (CH_2Cl_2) solvent-polymer systems can also be tested. On the other hand, spin the MOF with more than one polymer and washing with methanol or another solvent with a lower boiling point can be studied.

The growth of MOF particles on the surface of the fibers is the surface decoration path (Figure 18 d), e) f)). The benefit of this approach is that textural properties like unique surface area and internal pores are preserved, and they are not covered, therefore, they are available for any application. In addition, the other physicochemical properties do not change. However, the nature of the polymer must be considered, since it will have to withstand the use of solvents, temperatures, and pressures necessary for the formation of the MOF (hydrothermal and solvothermal synthesis) [74].

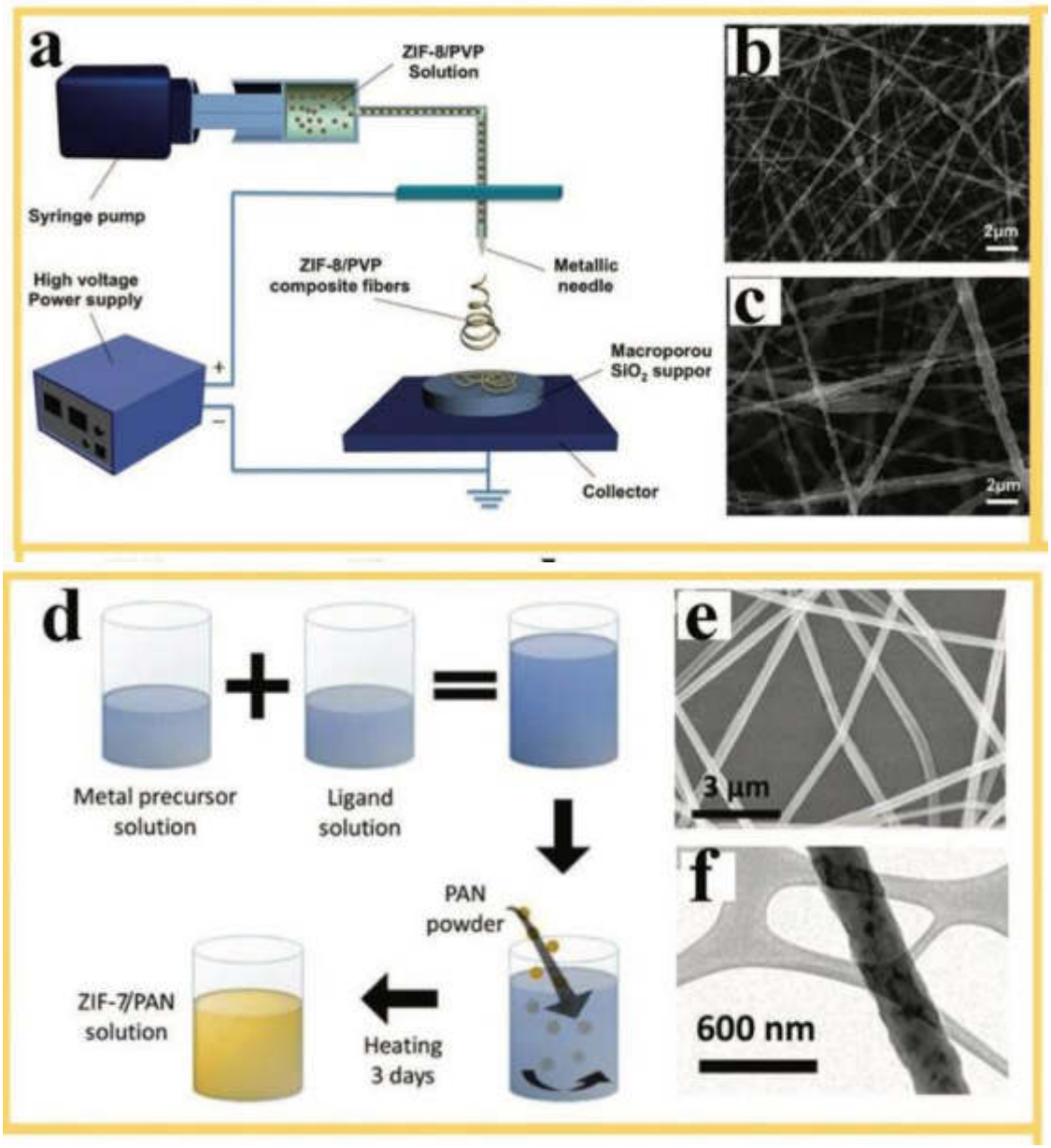

Figure 18: a), b), c) route and images of fibers obtained by direct electrospinning using ZIF-8 and PVP solution. d), e), f) route and images from fibers obtained by surface decoration.

2 Literature review

The most popular adsorbent used in siloxane removal is activated carbon (AC), nevertheless it requires high desorption temperatures and high regeneration costs. [28]. Ricaurte et al. (2009) studied the adsorption-desorption cycles for AC cloth to remove siloxane L2 and D4; they observed a reduction in the adsorption capacities of 65 mg/g to 25 mg/g after three cycles. In other studies, Finocchio and coworkers (2009) studied AC after exposure to a mixture of CO_2/CH_4 with siloxane D3 and water vapor and observed that D3 was partially polymerized to non-volatile compounds such as polydimethylsiloxane. The polymerization to non-volatile compounds could explain the limited thermal regeneration of AC after siloxane adsorption [75], [76].

On the other hand, silica gel (SG) is the second adsorbent material employed for siloxane removal. The adsorption mechanisms of SG and siloxanes are described as hydrogen bonding [77], which is a weak interaction leading to low desorption temperatures (<300°C) [78]. However, when wet biogas is used, the adsorption capacity of SG is approximately ten times lower than studies performed in the absence of water [79].

For this reason, several studies have been studied about the performance of new advanced materials in the removal of siloxane. Jafari and coworkers (2015) synthesized a new class of nanoporous polymeric adsorbents under solvothermal conditions, where imidazole groups were introduced into the samples by copolymerization of divinylbenzence (DVB) with 1-divinylimidazol (VI). The new classes of nanoporous polymeric adsorbents (PDVB and PDVB-IV) were evaluated

under different adsorption conditions, including humidity on D4 removal efficiency. The adsorption capacity of PDVB and PDVB-IV was 1951 and 2370 mg/g, respectively, which remained unchanged under moisture conditions, these adsorption capacities of D4 have been the highest reported, including AC. The authors indicated that high adsorption capacities were obtained due to the super-hydrophobicity of PDVB materials.

Metal-organic frameworks (MOFs) are a class of crystalline materials formed by the linkage of metal atoms or clusters through organic molecules [80]. MOFs materials show good performance in gas storage, gas separation, catalysis, optoelectronics, immobilization, and sensing. The high degree of porosity that MOFs can develop is without doubt the feature that has attracted the most interest in these materials. Additionally, MOFs currently holds the record of the crystalline compound with the highest specific surface area (MOF-210 exhibits a specific surface area value of 6240 m^2/g). Hence, MOFs can be used to adsorb, selectively, polluting or noxious gases. The adsorption of CO_2 is one of the most critical concerns, at present, due to its environmental implications.

Although MOFs are promising materials for adsorption processes [81], several studies have pointed out that MOFs materials had poor thermal and mechanical stability, and both can cause high-pressure drops when used in fixed bed columns, due to their small particle size [82][83]. Senkovska et al. (2009) found that the DUT-4 lost 34.6 percent of its weight over a temperature range of 50 to 250°C, while the DUT-5 lost 40.6 percent over the same temperature range [84], demonstrating the poor thermal stability of these materials. Several supports have been employed to

immobilize powder adsorbents materials with small particle size [85]–[87], among which nanofibers have stood out, due to their remarkable properties.

Ostermann R. and coworkers (2010) prepared nanofibers of MOF for the first time by electrospinning; the authors obtained a hierarchical MOF nanofiber with high specific surface areas and good accessibility. The increasing thermal decomposition temperature of Cr-MOF after incorporating the electrospun nanofibers from 230ºC to 450ºC (for a weight loss of 40%) was demonstrated [88].

In this sense, functionalized fibers with MOF could be a viable option to remove siloxanes, because they have the advantage of being selective for siloxanes, in wet conditions, contrary to activated carbon. In addition, functionalized nanofibers can be regenerated at low temperatures (< 300ºC) and can be reused.

To our best knowledge, we have not found studies of electrospun fiber for applications in biogas purification processes using MOF. As a result, new materials with functional groups that can serve as active sites for removing siloxane D4 for biogas purification processes are being investigated. DUT-4 (MOF) electrospun fibers prepared by dissolution methods are proposed to improve their adsorption properties of siloxane D4.

In the literature, a study of the environmental impact of the MOF DUT-4 has not been found, and this is important because DUT-4 is a promising material for cleaner biogas production. This work also aims to evaluate the environmental impact of the DUT-4 with the LCA methodology, proposing alternatives to reduce its environmental impact.

3 Scientific Contribution

The results of this research will offer a study of siloxane D4 adsorption onto electrospun fibers for biogas purification. In addition, new adsorbents with high surface area and high selectivity towards siloxanes will be provided for the biogas purification process, as well as the assessment of their environmental impacts.

4 Hypothesis

The electrospun fibers with DUT-4 are selective towards the adsorption of siloxane D4, present in biogas, under dry and humid conditions.

5 General Objective

This thesis aims to gain a fundamental understanding of the adsorption of siloxane D4 in electrospun fibers with DUT-4.

5.1 Specific objectives

I. To synthesize metal-organic structures (MOF) DUT-4.
II. To determine the environmental impacts of MOF DUT-4.
III. To produce electrospun fibers from DUT-4.
IV. To determine the physicochemical properties of DUT-4 powders and DUT-4 electrospun fibers.
V. To obtain the adsorption kinetics of siloxane D4 on DUT-4 powders and electrospun fibers of DUT-4.
VI. To evaluate the performance of DUT-4 electrospun fibers for the adsorption of D4 siloxane in the air using a continuous system.
VII. To evaluate the performance of DUT-4 electrospun fibers for the adsorption

of D4 siloxane in the presence of humidity, using a continuous system.

6 Materials and methods

6.1 Materials

In Table 1 the materials, reagents, and equipment to be used to develop the doctoral thesis project are shown.

Table 1: Reagents, materials, and equipment.

Chemical reagents	
Octamethylcyclotetrasiloxane, 98 %	Sigma Aldrich
2,6-naphthalene dicarboxylic acid, 95 %	Sigma Aldrich
DMF	Sigma Aldrich
$Al(NO_3)_3$ $9H_2O$, 98+%	Sigma Aldrich
Dimethyl sulfoxide (DMSO), 99.9 %	Sigma Aldrich
methyl alcohol	Sigma Aldrich
deionized water	Control Técnico y Representaciones, CTR
Equipment and location	
Gas chromatograph	Water laboratory 1 (WL1), Autonomous University of Nuevo Leon (UANL)

Nitrogen physisorption	Institute of Civil, UANL. Central Research Support Services (SCAI), University of Malaga (UMA)
Scanning Electronic Microscope	SCAI-UMA
Infrared spectroscope	SCAI-UMA
X-ray diffractometer	SCAI-UMA
Analytical balance	WL1-UANL
Continuous adsorption system	WL1-UANL
Immersion thermostat	WL1-UANL
Magnetic stirrer	WL1-UANL
Stove	UANL UMA
Heating blanket	WL1/UMA
Autoclave	WL1-UANL UMA
Centrifuge	WL1-UANL
Vacuum drying oven	WL1-UANL
Electrospinning system	UMA

6.1.1 DUT-4(DMF) synthesis

The synthesis of DUT-4(DMF) was performed with some variations as described by Senkovska et al. [89] 0.26 g of 2,6-naphthalene dicarboxylic acid was dissolved in 30 mL of N,N-dimethylformamide (DMF); subsequently, 0.52 g of nonahydrate aluminum nitrate was added and mixed. The mixture was put into a 250 mL teflon liner in an autoclave at 120 ºC for 24 h. At the end of this time, it was cooled to room temperature. The product was centrifuged at 10,000 rpm and 2.5 min, then washed three times with DMF, and finally dried in an oven at 120 ºC for four h.

6.1.2 DUT-4(DCM) synthesis

The synthesis of DUT-4(DCM) was carried out by including a solvent exchange step in the synthesis of DUT-4(DMF), adding 20 mL of dichloromethane (DCM) for one h (20 min each wash). The product was then centrifuged at 10,000 rpm for 2.5 min and dried in an oven at 120 ºC for 4 h.

6.1.3 DUT-4(DH) synthesis

In the synthesis of DUT-4(H), a second solvent exchange stage was included, consisting of three washes with 20 mL of hexane (C_6H_{14}) per one h (20 min each wash). The product was centrifuged and dried in the same way as in the previous synthesis.

6.1.4 DUT-4(W) synthesis

This synthesis was carried out using deionized water instead of DMF to contribute to a greener production.

6.2 Life Cycle Assessment for DUT-4 powders

Goal and scope definition of the product system. The LCA of the DUT-4 production process in laboratory-scale was carried out according to ISO 14044 [90]. The system boundary for DUT-4 includes five stages: mixing, synthesis, cleaning, solvent exchange, and drying (Figure 19). In this analysis, the environmental burdens associated with the laboratory equipment construction used in the production of DUT-4 were not considered. Each of the different DUT-4 synthesis strategies was considered as study scenarios:

- Scenarios DUT-4(DMF) and DUT-4(W): include the stages of mixing, synthesis, cleaning, and drying.
- Scenarios DUT-4(DCM) and DUT-4(H): include additionally the solvent exchange stage due to exchanges with different solvents.

Such scenarios are represented in the boundaries system as shown in Figure 19. The functional unit (FU) was defined as the production of 1 g of DUT-4 produced on a laboratory scale. According to other LCA studies of adsorbents materials, the FU unit was established on a mass basis, such as activated carbon and MOF-74 [59], [60].

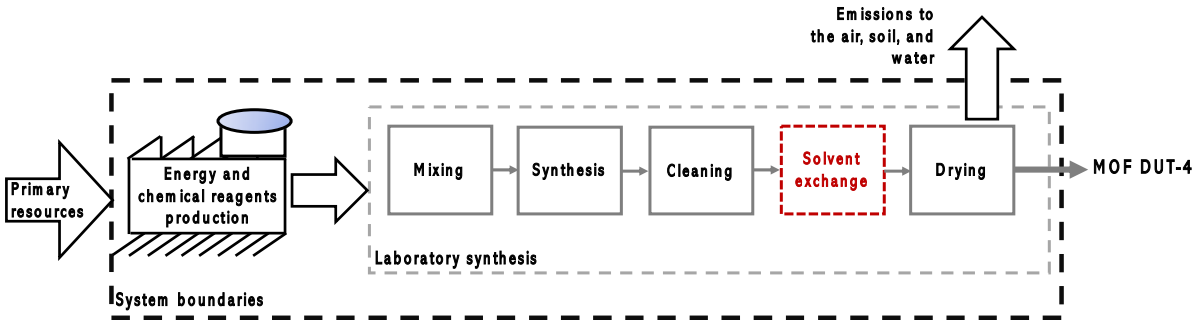

Figure 19: System boundaries to produce DUT-4.

Life cycle inventory analysis. The data for the life cycle inventory (LCI) of chemical reagents and energy used in the scenarios for DUT-4 synthesis were obtained from the laboratory logs, analytical procedures, and material-energy balances. The production of energy and chemical reagents needed to synthesize DUT-4 was considered inside the system boundaries (Figure 19). The LCI for these resources was taken from the Ecoinvent v3.3 database [91]. The wastewater generated in the cleaning stage was disposed of according to the hazardous waste management program implemented in our university [92]. Therefore, the environmental impacts of the final disposal of this waste were not considered in the LCI, as reported by Loya-González et al. [58] and Sepúlveda-Cervantes et al [59].

The life cycle stages of DUT-4 production that demand energy were synthesis, cleaning, solvent exchange, and drying. The energy requirement in the synthesis stage was calculated by an energy balance. The energy balance in the autoclave

was performed considering the following scheme:

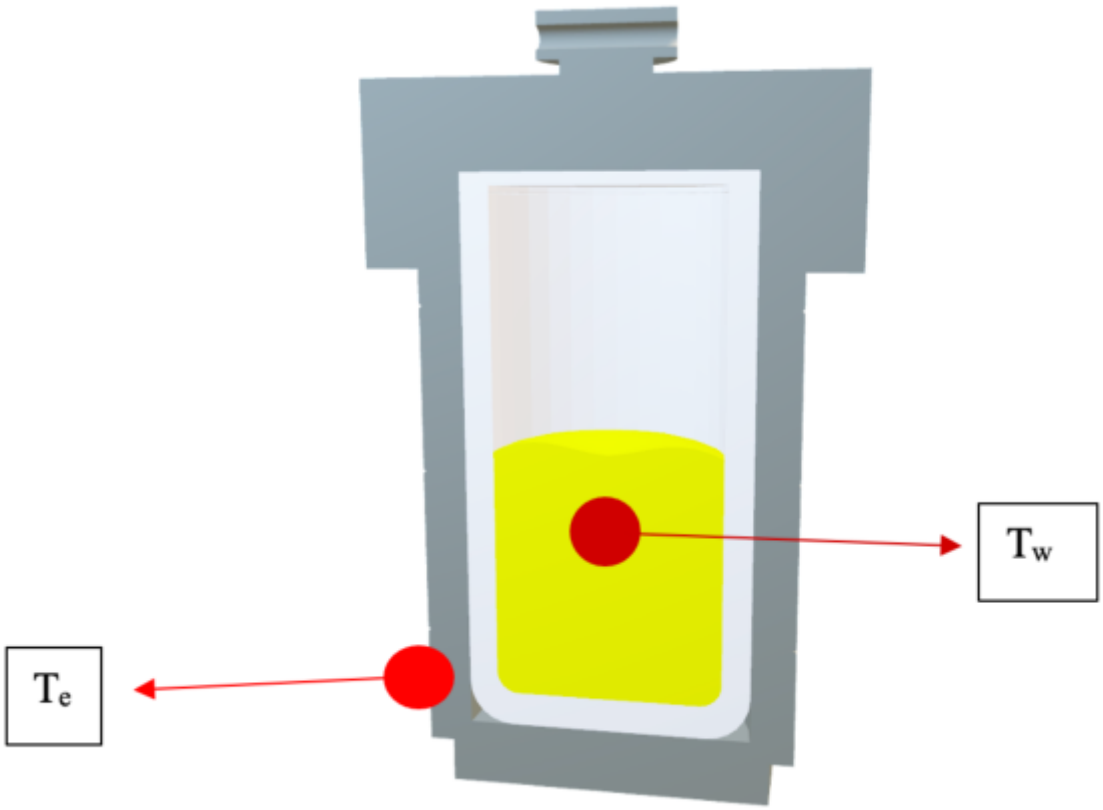

Figure 20: Diagram for energy balance into the solvothermal reactor.

The energy balance into the solvothermal reactor (Figure 20) is shown in Eq. (1). The first term $(\mathrm{m}_1 \int_{\mathrm{Te}}^{\mathrm{Tw}} \mathrm{Cp}_{mix}\mathrm{dT})$ corresponding to sensible heat was calculated based on the specific heat capacity, boiling point, and mass fraction of each chemical species in the solution. The second $(\mathrm{m}_2 \int_{\mathrm{Te}}^{\mathrm{Tw}} \mathrm{Cp}_{\mathrm{tf}}\,\mathrm{dT})$ and third term $(\mathrm{m}_3 \int_{\mathrm{Te}}^{\mathrm{Tw}} \mathrm{Cp}_{\mathrm{ss}}\,\mathrm{dT})$ corresponded to Teflon and stainless steel (autoclave) heating, respectively, were calculated based on their specific heat capacity. Table 2 lists the variables and values used in the energy balance of the hydrothermal and solvothermal reaction of DUT-4.

$$E = m_1 \int_{Te}^{Tw} Cp_{mix} dT + m_2 \int_{Te}^{Tw} Cp_{tf}\, dT + \; m_3 \int_{Te}^{Tw} Cp_{ss}\, dT \qquad \text{Eq. (1)}$$

Table 2: Value of each variable and parameters used for the energy balance into the solvothermal reactor.

Variable	Description/unit	Value
m_1	Fluid mass (g)	60
m_2	Stainless steel mass of autoclave (g)	4600
m_3	Teflon liner mass of autoclave (g)	403
T_w	Work temperature (ºC)	120
T_e	Environmental temperature (ºC)	120
Cp_{mix}	Fluid specific heat (J/g·K)	4.1
Cp_{ss}	Stainless steel specific heat (J/g·K)	0.5
Cp_{tf}	Teflon liner specific heat (J/g·K)	1.0

The cleaning and solvent exchange stages include the separation of the solvent by centrifugation. The energy consumption in these stages was calculated by the rotational kinetic energy equation Eq. (2).

$$E_{cr} = \frac{1}{2} * m * r^2 * (2\pi f)^2 * f_r \qquad \textbf{Eq. (2)}$$

Where *r* is the rotor radius (0.068 m), *f* is the frequency (166.67 s^{-1}), *m* is the mass to centrifuge (0.69-0.161 Kg), and f_r is the friction factor (1.45).

The energy required in the drying stage was obtained by calculating the heat energy required to remove the solvent per unit mass of DUT-4. The energy balance for this

stage was taken from Sepúlveda-Cervantes et al. [59]; the parameters used are specified in Eq. (3) and Table 3:

$$\frac{q_T}{m_s} = C_{ps}(T_{sb} - T_{sa}) + X_a C_{pL}(T_v - T_{sa}) + (X_a - X_b)\lambda + X_b C_{pL}(T_{sb} - T_v) + (X_a - X_b)C_{pV}(T_{va} - T_v) \quad \textbf{Eq. (3)}$$

Where q_T/m_s is the amount of heat transferred per unit mass of solids (J/g), C_{ps}, C_{pL}, and C_{pV} are the solid specific heat, the liquid specific heat, and the steam specific heat, respectively (J/g·K). T_{sb} and T_{sa} are the final temperature of the solids and the feed temperature, respectively (K). X_a and X_b are the initial and final mass per unit mass of dry solids, respectively. T_v y T_{va} is the vaporization temperature and the final vapor temperature (K), respectively. λ is the latent heat of vaporization (J/g).

Table 3: Parameters and variables for determining the energy consumption in the dry stage of DUT-4(DMF), DUT-4(DCM), DUT-4(H), and DUT-4 (W).

Parameter	DUT-4(DMF)	DUT-4(DCM)	DUT-4(H)	DUT-4(W)
T_{sa} (K)	298	298	298	298
T_v (K)	426	312	341	373
T_{sb} (K)	393	393	393	393
T_{va} (K)	393	393	393	393
I (J/g)	639.476	329.517	335.000	2260.872
Cp_s (J/g·K)	4.105	1.003	2.167	4.105
Cp_l (J/g·K)	4.181	1.000	2.206	4.181
Cp_v (J/g·K)	1.610	1.804	1.419	1.825

X_a	2.691	9.768	4.501	4.029
X_b	0.000	0.000	0.000	0.000

During the drying stage of study scenarios, DMF, DCM, hexane, and water are released into the atmosphere. Gravimetric analysis was carried out to estimate the mass of these emissions. The DUT-4 sample was weighed before and after being dried in an oven, at 120 °C for 4 h. The weight difference was related to the emission of the solvent from the DUT-4.

The LCI was carried out following an attributional approach. This viewpoint attempts to measure the environmental consequences of the manufacturing process. It is focused on assessing the emission of products and resource flows as it passes through its life cycle, using representative average data, for all processes and input and output flows [93].

Life cycle impact assessment. The SimaPro 7.3.3 LCA software was used to create the life cycle impact assessment (LCIA) model (PRe-Consultants, Amersfoort, the Netherlands). The LCIA was performed according to the ReCiPe 2016 method [94], considering midpoint and endpoint indicators.

6.3 Fabrication of DUT-4 fibers

The manufacturing process of the fibers with DUT-4 was carried out using seven different routes (20DD, 20ED1, 20ED13, 20CD, 70PD, 100PD,140PD) and one route (PD) for fibers without DUT-4 with the equipment in Figure 21. The

electrospinning equipment consists of 1) syringe pump, 2) electrospinning syringe, 3) the collector and, 4) the voltage source (Figure 21). Four routes were for uniaxial electrospinning and the rest for coaxial electrospinning. The amounts of DMF, PAN, and DUT-4 used are listed below for each type of electrospinning solution (Table 4). For specific routes, ultrasound was used for four h to decrease the particle size of DUT-4.

Table 4: Specifications of each electrospinning solution.

Uniaxial electrospinning						
Name	**Solution A**		**Solution B**		**DUT-4 size particle**	
	PAN, g	**DMF, g**	**DUT-4, g**	**DMF**		
PD	0.3	3.0	0.0	0.0	Without particle	
20DD	0.5	2.0	0.1	3.0	ultrasound	
20ED1	0.5	2.0	0.1	3.0	<100 μm	
20ED13	0.5	2.0	0.1	3.0	100-300 μm	
Coaxial electrospinning						
Name	**Solution C**		**Solution D**			
	PAN, g	**DMF, g**	**PAN, g**	**DMF, g**	**DUT-4, g**	**DUT-4 size particle**
20CD	0.4	2.5	0.1	2.5	0.1	ultrasound
70PD	0.25	3.0	0.1	3.0	0.25	ultrasound
100PD	0.25	3.0	0.1	3.0	0.35	ultrasound
140PD	0.25	3.0	0.1	3.0	0.50	ultrasound

The homogeneous suspension for uniaxial electrospinning was composed of a mixture of solutions A and B (Table 4). Solution A reagents were mixed at 350 rpm and 80 ° C for one hour, while solution B reagents were mixed at 350 rpm and room temperature for 1 hour. The spinning solution for the fibers, without DUT-4 (PD), was obtained only from the mixture of the reagents PAN and DMF to obtain solution A. In addition, in the solution for 20DD fibers, solution B was put in ultrasound for four hours at 50 ºC. Subsequently, solutions A and B were mixed at 350 rpm for 15 min

and room temperature. The uniaxial conditions were: a flow rate of 2.2 mL/h; the needle was set at a distance of 20 cm from the aluminum plate. The applied electrical potential difference to produce fibers was 20 kV (tips at+10 kV and collector potential at -10 kV).

The conditions to obtain solutions A and B separately for coaxial electrospinning were the same for the solutions for uniaxial electrospinning, considering that solution B was placed in ultrasound. Solution A was put into the syringe that will form the core of the fibers, and Solution B was put into the syringe that will form the shell of the electrospun fibers. The conditions of the coaxial electrospinning technique for both syringes were a flow rate at 0.9 mL/h, a distance at 23 cm, and the electrical potential difference was 20 kV. The fibers were stabilized at 120 ºC and were studied in collaboration with the University of Malaga, Spain.

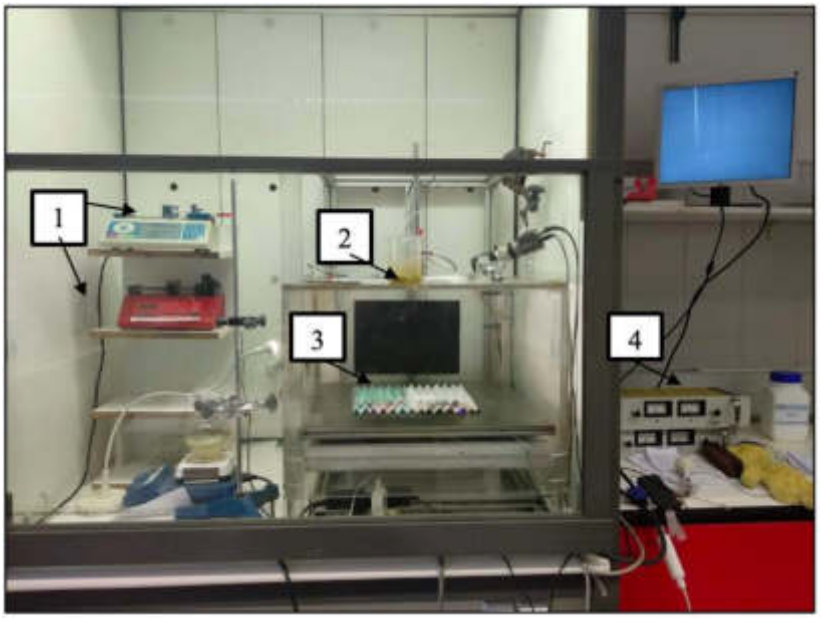

Figure 21: Uniaxial and Coaxial Electrospinning Equipment.

6.4 Characterization of DUT-4 powders and fibers

X-ray diffraction patterns (XRD) were recorded on a PANalytical X'Pert PRO MPD diffractometer using Cu-Kα radiation (40 mA and 45 kV); the relative crystallinity was determined by the area under the curve of the crystalline peaks (after baseline correction). The specific surface area (A_s) of DUT-4 and fibers were obtained by N_2 physisorption at 77 K using a Micromeritics ASAP 2020 after out-gassing the DUT-4 and fibers at 150 ºC for 8 h. Scanning electron microscopy (SEM) images were obtained using a JEOL JSM-6490LV microscope with acceleration voltage from 0.3 to 30 kV and thermionic electron gun with W filament. FTIR spectra were obtained from a Bruker Tensor 27 using a Golden Gate Single Reflection diamond ATR cell and a standard spectral resolution of 4 cm^{-1} in the spectral range of 4000–500 cm^{-1}. Solid-state ^{27}Al MAS NMR spectra were recorded at room temperature in a Bruker AVANCE III HD 600 MHz NMR spectrometer at 20 kHz, with a length pulse of 0.27 ms and a 1 s delay with 1H decoupling and summing up 2000 scans. NMR analysis was for DUT-4 powders only.

6.5 Batch adsorption test

The adsorption experiments were carried out at 450 mg/Nm^3 of initial concentration of D4, 100 mg of adsorbent material (DUT-4 powder or fibers), and room temperature. Flasks were stirred at 700 rpm for 6–9 h to ensure equilibrium. The samples were tested for D4 concentration using gas chromatography during the adsorption experiments. To test the concentration of siloxane D4, each sample was injected into a Shimadzu Nexis GC-2030 gas chromatograph with a flame ionization detector (FID). The capillary column used was a Shimadzu SH-Rxi-5ms (15 m x 0.25

mm inner diameter x 0.25 m film thickness). The inlet oven, detector, and inlet oven temperature were set to 150, 110, and 250 degrees Celsius, respectively. Helium was used as the carrier gas, with a flow rate of 1.5 mL/min and a pressure of 83.3 kPa. With split radio 5.0, the injection volume was 0.5 mL, and the process took 1.4 minutes. The adsorption capacity was calculated using mass balance in the following way:

$$q = \frac{(\mathrm{C_o} - C)\mathrm{V}}{\mathrm{m}} \qquad \text{Eq. (2)}$$

where q represents the adsorption capacity (mg/g), Co represents the D4 initial concentration (mg/Nm^3), C represents the D4 concentration over time (mg/Nm^3), V represents the volume (m^3), and m represents the adsorbent mass (g).

6.6 Continuous adsorption test

The inlet siloxane concentration in the continuous system was 2429.15 mg/m^3; the shape of the adsorber is the cylinder with a diameter of 10.0 mm and the length of the cylinder was 110.4 mm. The experiments were carried out at room temperature, at atmospheric pressure, and with a 50 mL/min flow rate. During the dynamic process, gas samples will be analyzed with a Shimadzu Nexis GC-2030 gas chromatograph. The estimated time required for a single run was approximately 94.6 min.

6.7 Disposal of the generated waste

Wastes generated during the development of this project were disposed based on the current Safety and Environment Regulations of the Faculty of Chemical Sciences of the UANL.

7 Results and discussion

7.1 Synthesis of DUT-4, DUT-4(D), DUT-4(DH) and DUT-4(W)

The DUT-4 metal-organic framework was synthesized using 2,6-naphthalene dicarboxylic acid, dimethylformamide, and aluminum nitrate nonahydrate, as previously detailed in the work plan (section 12.1). The autoclave (Figure 22) was placed in an oven at 120ºC for 24 h; then, it was allowed to cool at room temperature. The solution was extracted and poured into 2 mm microtubes for centrifugation. Once centrifuged, 1.0 ml of DMF was added to each microtube to wash the precipitate. The washing consisted of vigorously shaking the microtubes for 10 minutes and then centrifuging. It was repeated three times. In this way, 0.46 g of DUT-4 was obtained (yield 96.8%). Following the methodology described in the work plan (section 12.1.2 and 12.1.3), with the washing with dichloromethane, were obtained 0.29 g (yield 61.1%) of DUT-4(D), and washing with dichloromethane and hexane we obtained 0.27 g (yield 56.8%) of material DUT-4 (DH). The metal-organic frameworks DUT-4, DUT-4(D) and DUT-4(DH) were obtained (Figure 23).

Figure 22: Teflon liner with DUT-4 solution after 24 h at 120 ºC.

Figure 23: From right to left, DUT-4, DUT-4 (D) and DUT-4 (DH) after the DMF, DMF-DCM and DMF-DCM-hexane washes.

The metal-organic framework DUT-4 was synthesized by hydrothermal synthesis, using 2,6-dicarboxylic naphthalene, deionized water, and nonahydrate aluminum nitrate, as detailed in the work plan (12.1.4). Subsequently, it was washed three times with deionized water and centrifuged after each wash, obtaining 0.11 g.

7.2 Life Cycle Assessment

Life cycle inventory of DUT-4 production. The inputs and outputs flow in the production of DUT-4 are detailed in Table 5. According to these data, the use of chemical reagents to produce DUT-4 generated the highest environmental impact with a single score between 88.6 and 245 mPt, while the electrical energy consumption generated a single score between 2.12 and 24.7 mPt, except for scenario DUT-4(W), where the electricity consumption generated 31.6 mPt while the use of chemical reagents caused 0.66 mPt.

Table 5: Inventory data for DUT-4 production.

FLOW	VALUE	UNITS/FU
Inputs		
Electricity		
Synthesis stage (for all scenarios)	211	W-h
Cleaning and solvent exchange stage		
Scenario DUT-4(DMF)	70	W-h
Scenario DUT-4(DCM)	90	W-h
Scenario DUT-4(H)	80	Wh
Scenario DUT-4(W)	160	Wh
Drying		
Scenario DUT-4(DFM)	2	Wh
Scenario DUT-4(DCM)	4	Wh
Scenario DUT-4(H)	2	Wh
Scenario DUT-4(W)	9	Wh
Chemical reagents		
Mixing/synthesis		
N, N-Dimethylformamide:		
Scenario DUT-4(DMF)	65.2	mL
Scenario DUT-4(DCM)	103	mL

Scenario DUT-4(H)	111	mL
Scenario DUT-4(W)	162	mL

2,6-Naphthalene dicarboxylic acid:

Scenario DUT-4(DMF)	0.56	g
Scenario DUT-4(DCM)	0.90	g
Scenario DUT-4(H)	0.96	g
Scenario DUT-4(W)	1.41	g

Nonahydrate aluminum nitrate:

Scenario DUT-4(DMF)	1.13	g
Scenario DUT-4(DCM)	1.79	g
Scenario DUT-4(H)	1.93	g
Scenario DUT-4(W)	2.81	g

Cleaning

N, N-Dimethylformamide:

Scenario DUT-4(DMF)	130	mL
Scenario DUT-4(DCM)	207	mL
Scenario DUT-4(H)	222	mL
Deionized water-Scenario DUT-4(W)	325	mL

Solvent exchange

Dichloromethane:

Scenario DUT-4(DCM)	207	mL
Scenario DUT-4(H)	222	mL
Hexane-Scenario DUT-4(H)	222	mL
Outputs		
Emissions (Drying stage)		
Scenario DUT-4 (DMF), dimethylformamide	2.7	g
Scenario DUT-4(DCM), dichloromethane	9.8	g
Scenario DUT-4(H), hexane	4.5	g
Scenario DUT-4(W), H_2O	4.03	g

FU: functional unit

Environmental impacts of DUT-4 production. All environmental impact results are related to FU. Figure 24 presents the environmental impact assessment results for each Scenario of DUT-4 production through the ReCiPe 2016 endpoint method. The Scenario DUT-4(H) has the highest single score of 269 mPt, due to the environmental impact in the cleaning and solvent exchange stages, where three types of solvents are used: DMF, DCM, and hexane. The use of these solvents also increases the cleaning stage's energy demand (Table 5), because the use of each solvent requires centrifugation. Altogether, the solvent production contributes to 244 mPt in the Scenario DUT-4(H), 61.5 %, 33.3 %, and 5.2 % to DMF, DCM, and hexane, respectively.

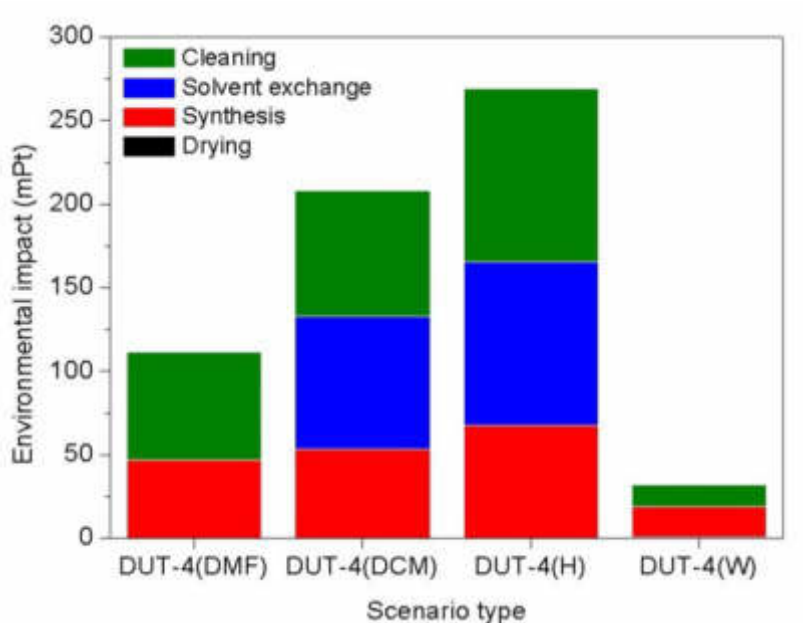

Figure 24: Environmental impact of each Scenario of DUT-4 production through ReCiPe 2016 endpoint method.

The use of these three solvents in the Scenario DUT-4(H) led it to be the leader in all the environmental impact indicators (Figure 25).

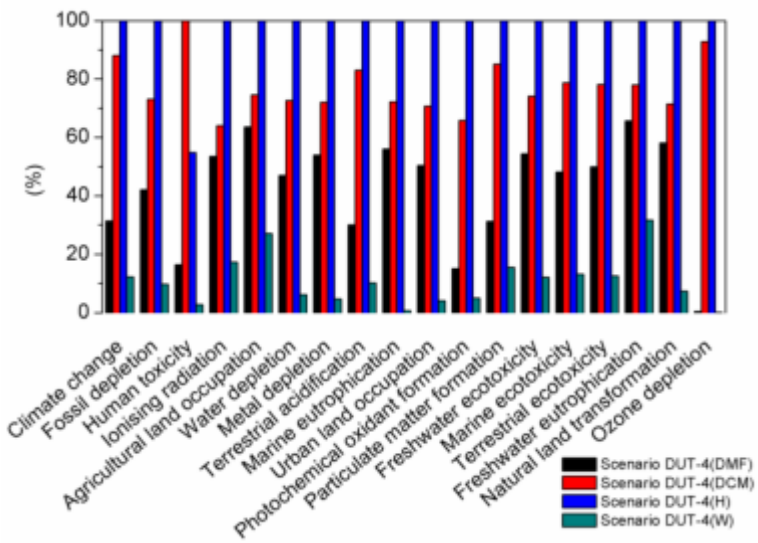

Figure 25: Characterization of the indicators of environmental impact for scenario DUT-4(DMF), scenario DUT-4(DCM), scenario DUT-4(H), and scenario DUT-4(W), using the endpoint ReCiPe.

The Scenario DUT-4(DCM) has similar behavior to the Scenario DUT-4(H), but a lower environmental impact (211.07 mPt) since it uses 29 % and 7 % less DMF and DCM, respectively, and hexane is not used (Table 5). The production of DUT-4 only uses DMF as the solvent, and its environmental impact is 112 mPt (less than half of Scenario DUT-4(H)). The solvents used determine the environmental impact profile of these adsorbents.

In Scenario DUT-4(W), deionized water as the solvent, cause minimum environmental damage, 32 mPt. In this Scenario, the electricity used in the synthesis and cleaning stages (Table 5) accounts for 97 % of the environmental indicator. México's energy primary source for electricity production is 87 % fossil sources (62 % crude oil, 20 % natural gas, 4 % coal, and the remaining condensates) [95].

As shown in Figure 26, the main environmental impact category indicator in all Scenarios of DUT-4 production is fossil depletion (10.71–109.14 mPt); this is mainly due to solvent production. In terms of fossil depletion midpoint indicator, the solvent used in each Scenario have impacts of 1.86×10^{-4}, 0.28, 0.53, and 0.75 kg oil eq for scenarios DUT-4(W), DUT-4(DMF), DUT-4(DCM), and DUT-4(H), respectively; and an electricity consumption <0.08 kg oil eq for all scenarios (Table 6).

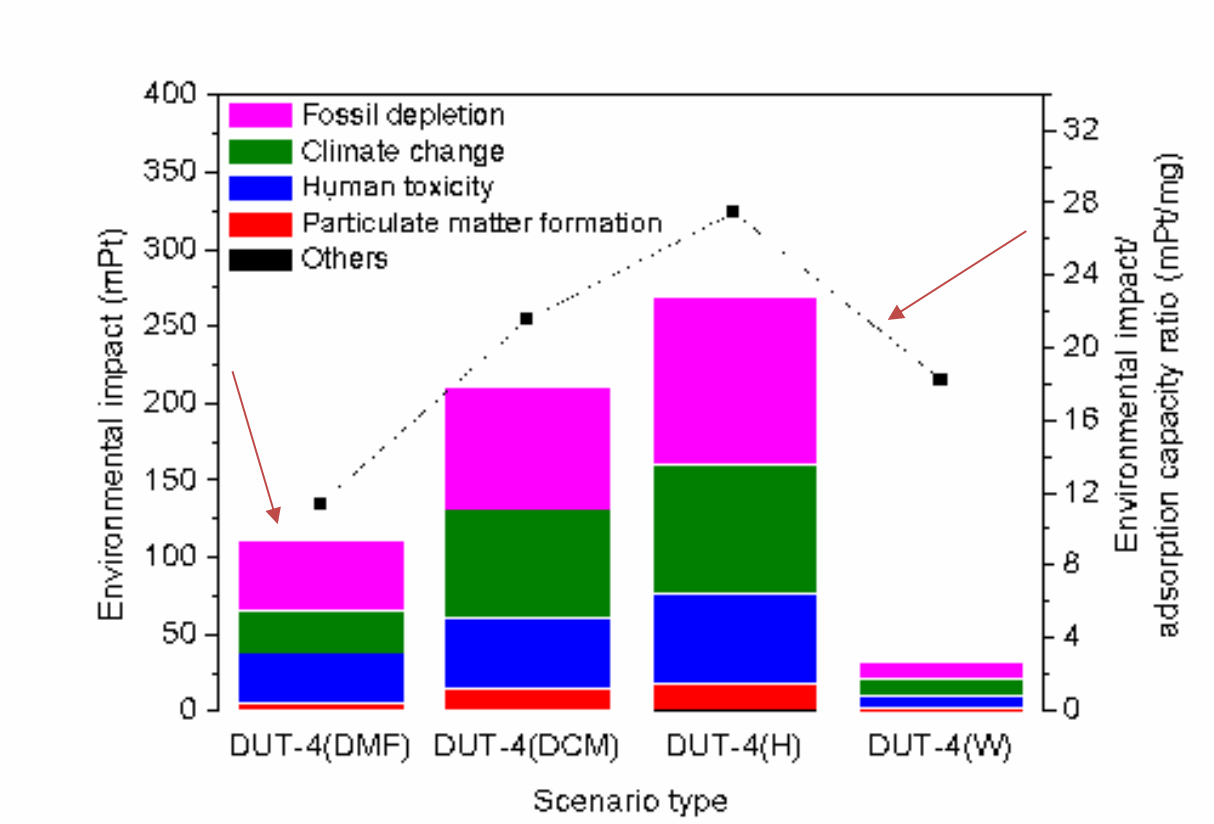

Figure 26: LCA for different DUT-4 production scenarios through endpoint using SimaPro software.

The second most representative indicator is climate change (11.34–83.10 mPt) (Figure 26). Regarding the midpoint indicator, the GHG emissions account for 0.25–2.02 kg CO_2 eq (Table 7), mostly associated with carbon dioxide and methane emission. As in the case of fossil depletion indicator, solvents production is the activity with the most incidence in GHG emissions, 7.23×10^{-4}, 0.45, 1.50, and 1.83 kg CO_2 eq for Scenarios DUT-4(W), DUT-4(DMF), DUT-4(DCM), and DUT-4(H), respectively, while electricity consumption generated <0.24 kg CO_2 eq (Table 6).

Table 6: Contribution solvent and electricity in fossil depletion and climate change indicators by ReCiPe midpoint.

Input	Scenario DUT-4(DMF)	Scenario DUT-4(DCM)	Scenario DUT-4(H)	Scenario DUT-4(W)
Fossil depletion (kg oil eq)				
DMF	0.28	0.34	0.48	-
Dichloromethane	-	0.19	0.20	-
Hexane	-	-	0.07	-
Water	-	-	-	-
Electricity	0.06	0.06	0.06	0.08
Climate change (kg CO_2 eq)				
DMF	0.45	0.55	0.77	-
Dichloromethane	-	0.95	1.02	-
Hexane	-	-	0.04	-
Water	-	-	-	7.23E-04
Electricity	0.18	0.19	0.19	0.24

Table 7: Units of the midpoint indicators for the DUT-4 production scenarios.

Indicator	Unit	Scenario DUT-4(DMF)	Scenario DUT-4(DCM)	Scenario DUT-4(H)	Scenario DUT-4(W)
Climate change	kg CO_2 eq	0.6317	1.7752	2.0164	0.2483
Fossil depletion	kg oil eq	0.3400	0.5912	0.8092	0.0794

Human toxicity	kg 1,4-DB eq	0.0689	0.4209	0.2306	0.0116
Ionising radiation	kBq U235 eq	0.0394	0.0471	0.0736	0.0127
Agricultural land occupation	m^2a	0.0217	0.0255	0.0342	0.0093
Water depletion	m^3	0.0085	0.0132	0.0182	0.0011
Metal depletion	kg Fe eq	0.0052	0.0070	0.0097	0.0005
Terrestrial acidification	kg SO_2 eq	0.0037	0.0101	0.0122	0.0012
Marine eutrophication	kg N eq	0.0019	0.0025	0.0035	0.0000
Urban land occupation	m^2a	0.0019	0.0026	0.0037	0.0002
Photochemical oxidant formation	kg NMVOC	0.0018	0.0080	0.0121	0.0006
Particulate matter formation	kg PM10 eq	0.0016	0.0044	0.0052	0.0008
Freshwater ecotoxicity	kg 1,4-DB eq	0.0016	0.0022	0.0030	0.0004
Marine ecotoxicity	kg 1,4-DB eq	0.0008	0.0013	0.0017	0.0002
Terrestrial ecotoxicity	kg 1,4-DB eq	6.12E-05	9.56E-05	1.22E-04	1.53E-05
Freshwater eutrophication	kg P eq	2.87E-05	3.41E-05	4.37E-05	1.39E-05
Natural land transformation	m^2	9.01E-06	1.11E-05	1.55E-05	1.14E-06
Ozone depletion	kg CFC-11 eq	1.07E-07	2.42E-05	2.61E-05	1.98E-08

The human toxicity indicator in Figure 26 ranges between 7.48–58.70 mPt, equivalent to 0.01–0.42 kg 1,4-DB eq. Similarly, solvents use is the main activity of this environmental damage. For the solvent production, pour barium into water represents 81.4–84.7 % of this indicator, and emitting selenium into the air accounts for 3.1–4.4 %, while the electricity consumption generates <2.6 % in each Scenario. The particulate matter formation indicator (2.59–16.72 mPt) comes mainly from the air emissions in solvent production: $PM_{2.5}$ (1.44–4.20 mPt), sulfur dioxide (0.64–5.41 mPt), and nitrogen oxides (0.32–4.30 mPt).

It is possible to observe that the substitution of solvent for water, during the synthesis of DUT-4(DMF), diminishes environmental damage—Scenario DUT-4(W)—but this substitution changed the physicochemical properties of the original MOF, having consequently a low siloxane adsorption capacity in the biogas purification. This matter deserves to be analyzed from an environmental perspective.

The environmental impact/adsorption capacity ratio was calculated for the four different DUT-4 production scenarios (right axis in Figure 26). The DUT-4(H) adsorbent production has the highest significant environmental impact/adsorption capacity ratio among all four DUT-4 scenarios. In contrast, the DUT-4(DMF) production scenario has the lowest environmental impact/adsorption capacity ratio. These results can be explained by taking into account that DUT-4(DMF) and DUT-4(H) have the same adsorption capacity, but the latter has a higher environmental impact caused by the two solvent exchange stages. Instead, the DUT-4(W) production scenario with a green solvent has a higher environmental impact/adsorption capacity ratio than DUT-4(DMF) production. This result can be

explained considering that DUT-4(W) has the lowest siloxane adsorption capacity; thus, to achieve similar adsorption than the rest (around 9.80 mg/g), it is necessary to produce five times more of this material. This fact could lead to economic savings to foster greater sustainability in removing siloxanes from biogas. From an environmental and technical point of view, DUT-4(DMF) is the best Scenario to produce the siloxane adsorbent since the ratio obtained was 53, 42, and 63% lower than DUT-4(DCM), DUT-4(H), and DUT-4(W), respectively (Figure 26).

7.3 Characterization of DUT-4 powders

7.3.1 FT-IR spectra

The FTIR spectrum of DUT-4(DMF), DUT-4(DCM), DUT-4(H), and DUT-4(W) showed similar adsorption bands (Figure 27). The band in the range 1693–1668 cm^{-1} in each of the spectra corresponded to the stretching vibration of (n(C=O)) of the carbonyl group, which is indicative of the coordination of linker to the metal ion [64]. The band in each spectrum, at 1614–1598 $cm^{-1,}$ corresponded to asymmetric stretching vibrations of carboxylate group (ν_{as}(C-O))[96]; the bands in the range of 1434–1415 cm^{-1} can be associated to symmetric stretching vibrations of carboxylate group (ν_{s}(C-O)), and the peaks observed at 989–985 cm^{-1} can be related to the bending of the bridging groups δ(O-H) [97]; the bands between 792 and 783 cm^{-1} in each of the spectra corresponded to flexions into the aromatic plane, [98], [99] and the bands between 586–561 cm^{-1} in the four spectra were associated with the stretching vibrations of the aluminum atom with oxygen atoms (ν(Al-O)) [100]. Additionally, in the DUT-4(W) spectrum, the band at 1294 cm^{-1} was associated with

the (ν(C-O)) stretch vibration, and the bands at 921–914 cm^{-1} were related to the (δ(O-H)) bend [101].

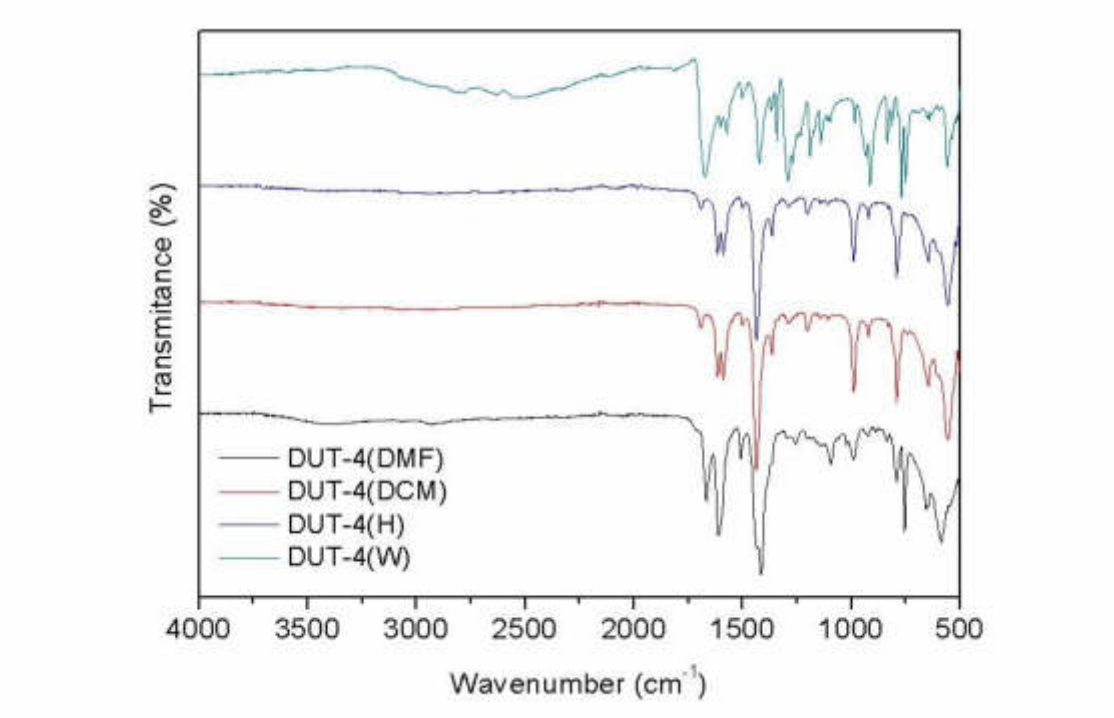

Figure 27: FTIR spectra for DUT-4(DMF), DUT-4(DCM), DUT-4(H), and DUT-4.

7.3.2 Solid State Al MAS NMR

Solid-state ^{27}Al MAS NMR spectroscopy can be used for MOF characterization to determine the local chemical environment and the coordination state of the metal sites. Here, the ^{27}Al MAS NMR spectra for DUT-4(DMF), DUT-4(DCM), DUT-4(H), and DUT-4(W) were obtained (Figure 28). The primary resonating signal of all the materials studied corresponded to 6-fold coordinated aluminum sites ($Al^{[6]}$),[102], [103] with three overlapped signals in the chemical shift range between -20 to 10 ppm, as reported by Volkringer et al. [104], for the Al-MIL-100 structure. According to Vyalikh et al., [105] differences in aluminum sites are due to coordination with distinct types of OH groups. That is, each aluminum site is coordinated to different

OH-groups that participate in intralayer and interlayer hydrogen bonds, causing changes in the chemical environment. Altogether, the NMR spectra for DUT-4 demonstrate the presence of octahedral aluminum sites in the MOF structure.

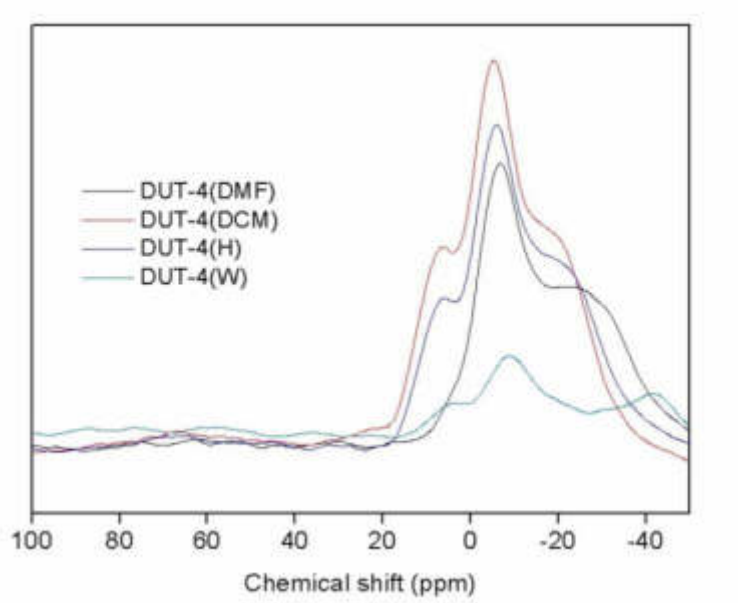

Figure 28: ^{27}Al MAS NMR Spectra for DUT-4(DMF), DUT-4(DCM), DUT-4(H), and DUT-4(W).

7.3.3 X-ray diffraction

The diffraction patterns of as-synthesized samples of DUT-4 by solvothermal synthesis shown characteristic peaks at 6.95º, 13.91º, and 21.04º corresponding to (101), (110), and (113) Miller indices, respectively, and an orthorhombic symmetry according to Senkovska et al. [89]. A significant increase in the relative intensity of the diffraction Bragg peaks was observed on the XRD pattern of DUT-4(DCM) and DUT-4(H) compared to DUT-4(DMF). The calculated crystallinity percentages were 70.82 %, 89.26 %, and 88.74 % for DUT-4(DMF), DUT-4(DCM), and DUT-4(H), respectively. These results suggest that the use of low surface tension solvents instead of DMF improves the crystallinity of the MOF and prevents structural collapse

[54]. To continue, the hydrothermal synthesis of DUT-4(W) allowed to obtain a structure with 89.89 % crystallinity but non-isostructural to DUT-4 (Figure 29). The higher intensity peaks of the DUT-4(W) phase were 16.39º and 27.74º, which are similar to the organic linker 2,6-naphthalene dicarboxylic acid [106]. In this sense, it has been reported that water molecules can prevent the coordination between the organic linkers and the ion atoms by hydrogen bonding interactions with the organic linkers [49].

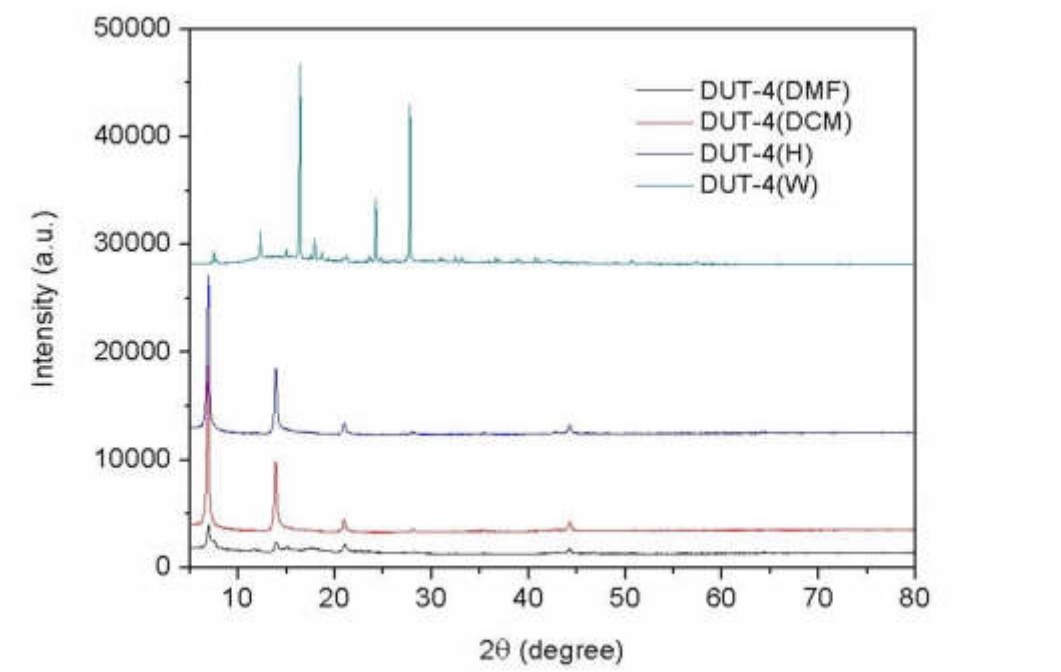

Figure 29: XRD pattern obtained from DUT-4(DMF), DUT-4(DCM), DUT-4(H), and DUT-4(W) powders.

7.3.4 Textural properties

The specific surface area (Table 8) of the synthesized DUT-4(DMF) had a similar value (1348 m^2/g) to that reported by Senkovska et al. [89] (1308 m^2/g). According to Howarth et al., [107] the solvent exchange with low surface tension solvents helps to achieve the highest possible surface area and porosity. Accordingly, a solvent exchange of DMF for CH_2Cl_2 was carried out to obtain the DUT-4(DCM) material,

although a slight reduction of 12 % of the A_s was observed (1184 m^2/g). To overcome this reduction on the A_s, DUT-4(DCM) was subjected to a second solvent exchange process where DCM was exchanged for C_6H_{14}, and the as-synthesized material was named DUT-4(H). The specific surface area of DUT-4(H) (1335 m^2/g) was very similar to that obtained for DUT-4(DMF). Thus, by solvothermal synthesis, irrespective of the solvent exchange, high specific surface areas were obtained. The total pore volume for DUT-4(DMF), DUT-4(DCM), and DUT-4(H) were 1.71, 1.48, and 1.46 cm^3/g, respectively. Differently, a hydrothermal synthesis was carried out to use a greener solvent such as water instead of the toxic DMF solvent, however, very low specific surface area was obtained (2 m^2/g) as well as low total pore volume (0.003 cm^3/g). Usually, water-based MOF has low porosity in comparison with MOF obtained by solvothermal synthesis [108].

Table 8: Textural properties for DUT-4 adsorbents.

Adsorbent	**A_{BET} (m^2/g)**	**V_{Total} (cm^3/g)**	**Pore diameter (nm)**
DUT-4(DMF)	1350	1.71	5.07
DUT-4(DCM)	1180	1.48	5.00
DUT-4(DH)	1330	1.47	4.38
DUT-4(W)	2	0.003	5.99
DUT-4 reported	1300	-	-

7.3.5 Scanning electron microscopy

The particle size of the materials obtained by solvothermal synthesis was dependent on the solvent used in the drying stage. When low surface tension solvents were used, a small particle size was obtained. For instance, DUT-4(DCM) and DUT-4(H)

particle size was lower than 500 nm. Conversely, when a high surface tension solvent such as DMF was used, the particle size of DUT-4(DMF) was greater than 1 µm (Figure 30). Similar results were obtained for the hydrothermal synthesis, where particles of different sizes exceeding 3.25 µm were found. The formation of larger agglomerates during drying of the DUT-4(DMF) and DUT-4(W) was due to the capillary forces overcoming the repulsive forces between the particles; therefore, the particles came closer to each other [109], [110].

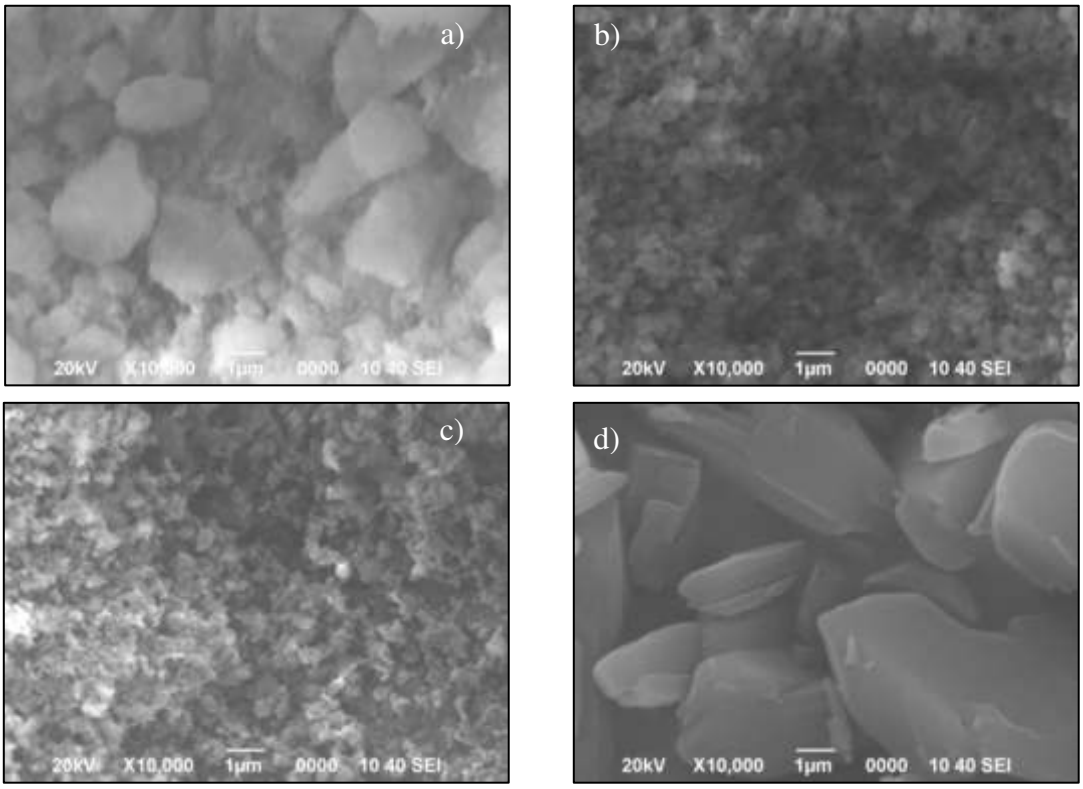

Figure 30: SEM images for a) DUT-4(DMF), b) DUT-4(DCM), c) DUT-4(H), and d) DUT-4(W).

7.4 Synthesis of DUT-4 fibers

Metal-organic frameworks supported on electrospun fibers were produced with the DUT-4(DMF) (Figure 31), since regardless of the synthesis route, DUT-4(DMF),

DUT-4(DCM), and DUT-4(H) had the same adsorption capacity of D4 (q = 10.9 mg/g, at C_0 = 400 mg/m^3 of D4).

DUT-4 particles smaller than 100 nm were obtained with sonification for four hours of electrospinning solutions. Therefore, a better distribution of DUT-4 was obtained on the surface of electrospun fibers. The solution in the shell (solution B, electrospinning coaxial), which contained the DUT-4, had to carry PAN to give it greater viscosity and prevent the particles from being projected towards the collector. Milliliter by milliliter was also spun to prevent the particles from precipitating into the syringe.

Figure 31: Fiber obtained by electrospinning.

Used solvents were other than DMF. It should be mentioned that dimethyl sulfoxide (DMSO) was used as the solvent instead of DMF, but the DUT-4 particles did not adhere to the fiber surface. For this reason, its use was ruled out. Ethanol was then used instead of DMF, but it was not compatible with PAN, and its use was also ruled out.

The characterization of the fibers with DUT-4 began with scanning electron microscopy and nitrogen adsorption-desorption tests to select the type of fibers that

presented the best distribution of DUT-4 on the fiber surface and therefore represented an area of considerable specific surface area.

7.5 Characterization of DUT-4 nanofibers

7.5.1 Scanning electron microscopy

In Figure 32, it can be observed that the diameters for the fibers PD, 20DD, 20ED1, and 20ED13 were from 0.5 μm to 1.0 μm; the fibers showed lumps of different shapes and sizes except for PD fibers. These lumps were evidence of DUT-4 incorporated in the 20DD, 20ED1, and 20ED13 fibers. SEM images for fibers obtained by coaxial electrospinning showed smaller diameters than fibers obtained by uniaxial electrospinning. The diameters for 20CD, 70PD, 100PD, and 140PD fibers were from 0.125 μm to 0.5 μm. In this type of fibers, it shows, as the amount of DUT-4 increased in the spinnable solution (DUT-4 quantity: 20CD<70PD<100PD<140PD), more particles were seen on the surface of the fiber. In addition, on 100PD and 140PD fibers, the DUT-4 particles exceeded one micrometer in diameter, so they were trapped between a set of fibers.

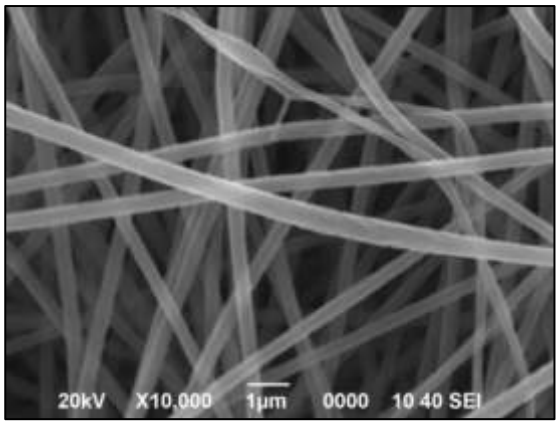

PD

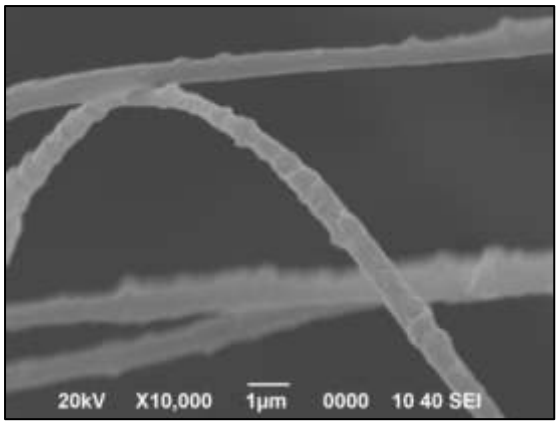

20DD

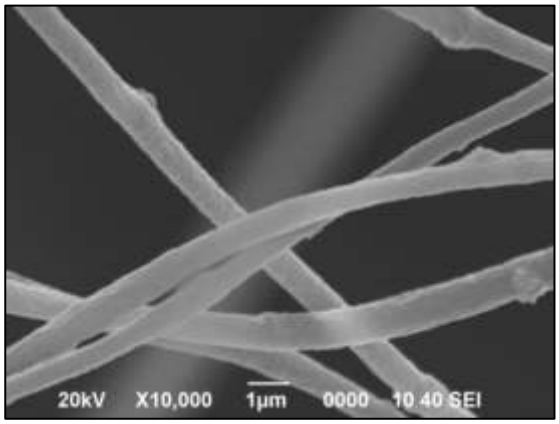

20ED1

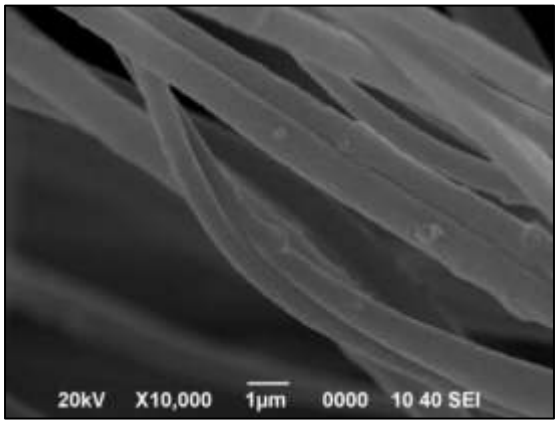

20ED13

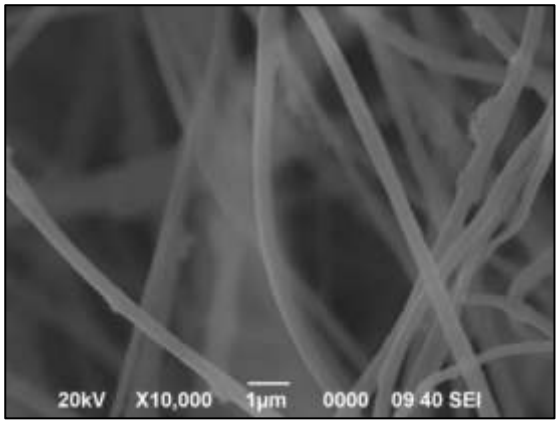

20CD

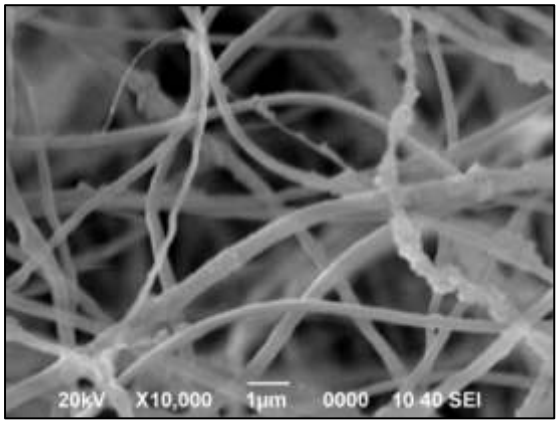

70PD

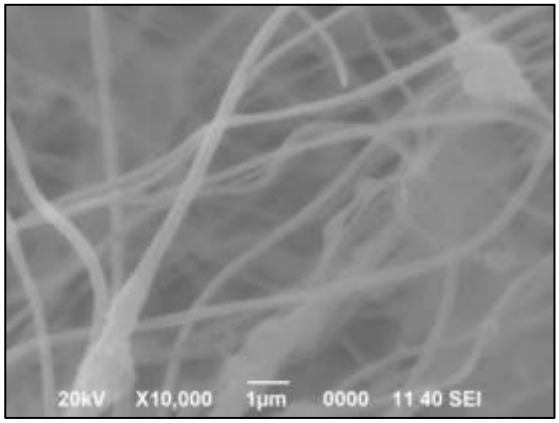

100PD

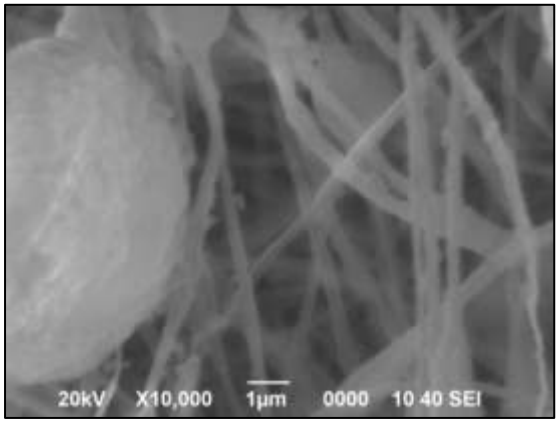

140PD

Figure 32: SEM images for fibers with DUT-4.

7.5.2 Textural properties

The percentage of DUT-4 in the solutions for coaxial electrospinning showed that the specific surface area increases, but there are DUT-4 particles of sizes > 1 mm on the surface of the fibers; for this reason, fibers were prepared with 70% of DUT-4 (70PD fibers), regarding the weight of the polymer PAN.

Specific surface areas were calculated using the Brunauer-Emmett-Teller (BET) method (A_{BET}), the total volume of pores (V_t) was reported at less than 401.113 Å diameter at P/P_0 = 0.949613561, the micropores volume (V_{mic}) was calculated by t-Plot method, and the adsorption average pore width (W_p) was calculated by the BET method.

Table 9: Textural properties of the DUT-4 fibers.

Name fiber	A_{BET} (m^2/g)	V_t P/Po = 0.945 (cm^3/g)	V_{mic} (cm^3/g)	W_p (Å)
PD	11	0.013	0.002	50.72
20DD	20	0.026	0.004	53.11
20ED1	30	0.036	0.008	49.13
20ED13	56	0.053	0.015	37.78
20CD	37	0.038	0.010	41.64
70PD	113	0.100	0.033	35.21

100PD	131	0.105	0.034	31.94
140PD	293	0.193	0.100	26.3815

According to Table 9, the A_{BET} of fibers by uniaxial electrospinning decreased proportionally with the reduction of the particle size of DUT-4 (from 56 to 20 m^2/g). A_{BET} increased as the ratio of DUT-4 to PAN augmented (from 37 to 293 m^2/g), in the case of electrospun coaxial fibers. The V_t and V_{mic} had an upward growth pattern as DUT-4 particle sizes were reduced for uniaxial electrospinning and as the ratio of DUT-4 to PAN for coaxial electrospinning increased. Smaller particle size of DUT-4 led to a higher W_p than the rest of the uniaxial fibers (from 37.78 to 53.11 Å), while a greater amount of DUT-4 in the coaxial fibers reduced the value of W_p (from 41.64 to 26.38 Å).

The use of other solvents different than DMF was also analyzed. The calculated A_{BET} was lower for the fibers prepared with DMSO. Specifically, ABET was halved with uniaxial electrospinning, while in coaxial electrospinning, A_{BET} was reduced up to four times, using DMSO (Figure 33).

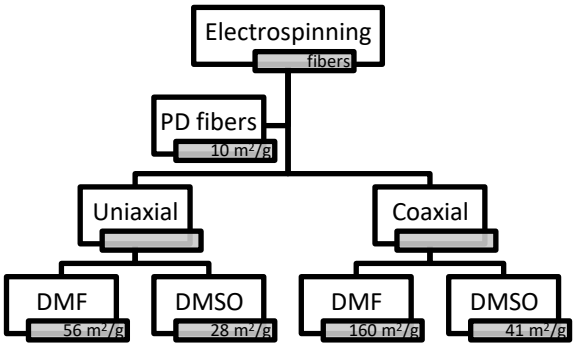

Figure 33: Comparison of ABET of fibers with DUT-4 obtained by uniaxial and coaxial electrospinning, using DMF and DMSO solvents.

The best dispersion of the DUT-4 particles on the surface fibers and the specific surface area obtained were two strategies contemplated to determine the type of fibers used for the rest of the physicochemical analysis adsorption experiments of siloxane D4. The fibers selected were 70PD (113 m^2/g).

7.5.3 FT-IR spectra

In Figure 34, the spectra of 70PD and PD fibers and DUT-4 powder are shown. The bands that were common between the 70PD fibers and the DUT-4 dust were those located at 1617.33 cm^{-1}, corresponded to asymmetric stretching vibrations of the group (ν_{as}(C-O)) [96]; 991.40 cm^{-1} corresponding to the bending of the bridging groups δ(O-H) [97]; 792.08 cm^{-1}, related to flexions into the aromatic plane [98], [99] and the band at 570.48 cm^{-1} associated with the stretching vibrations of the group (ν(Al-O)) [100]. The bands located at 2243.22, 1440.69, 1364.55, 545.43, 522.78, and 507.26 cm^{-1} were between the spectra of 70PD fibers and PD fibers. Similar FTIR spectra for PD fibers were reported by Peres et al. (2019) [111].

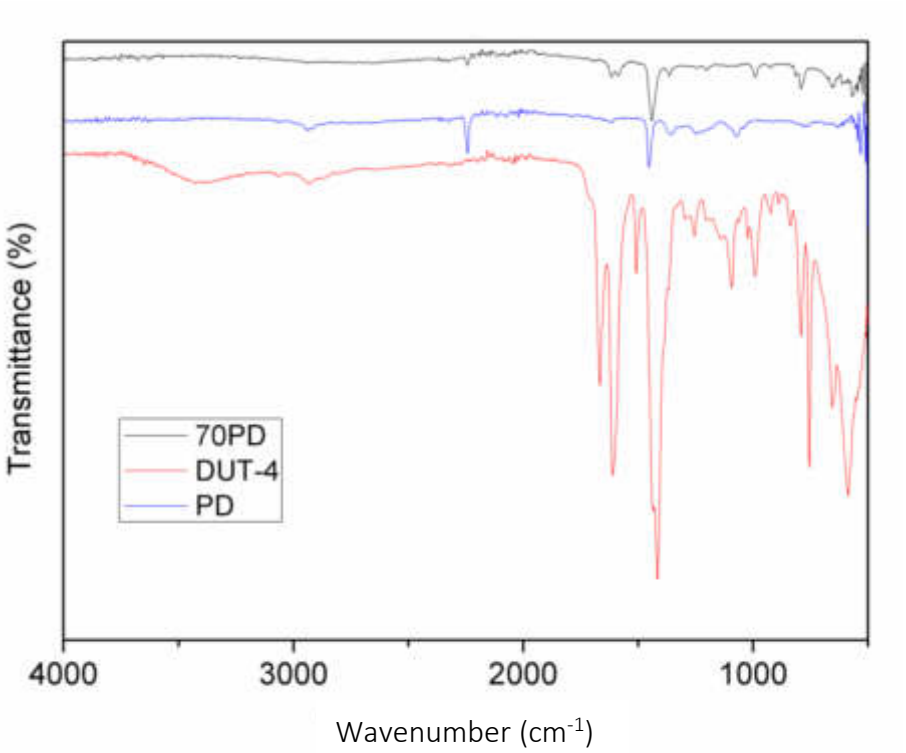

Figure 34: FTIR/ATR spectra for DUT-4 powder, PD and 70PD fibers.

7.5.4 X-ray diffraction

In the XRD patterns shown in Figure 35, 70PD fibers have characteristic peaks of PD and DUT-4 fibers. Peaks at 6.90º and 14º, are common between the 70PD and DUT-4 fibers, and peaks at 17.08º, 33.41º, and 43.06º were familiar between 70PD and PD fibers. The fibers patterns correspond to amorphous structures with a percentage of crystallinity of the PD and 70PD fibers of 46.06 % and 31.35 %, respectively, while the percentage of crystallinity of the DUT-4 was 70.82 %.

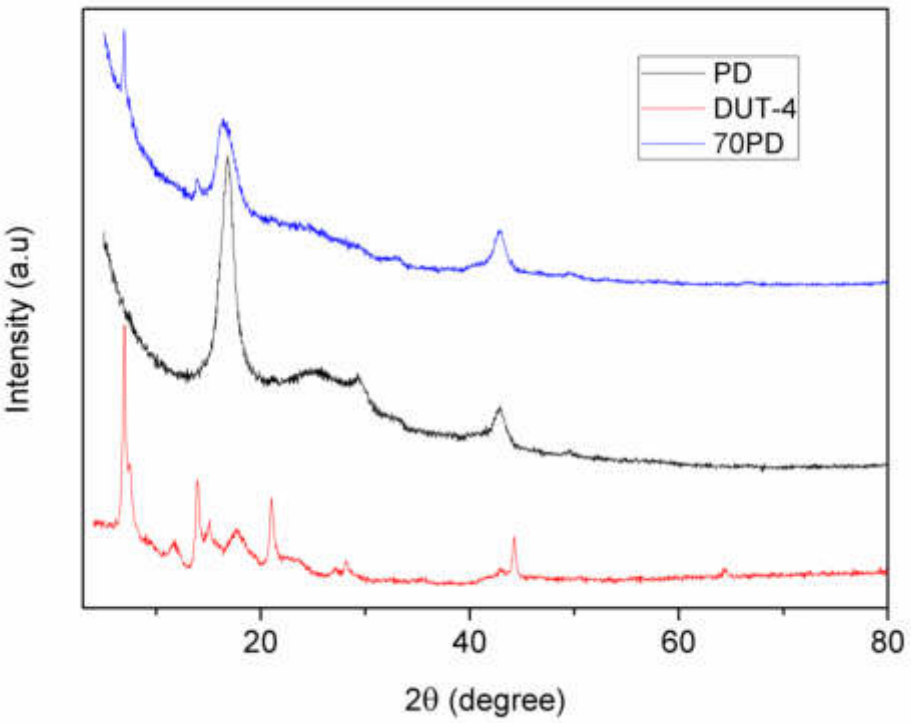

Figure 35: XRD pattern obtained from DUT-4 powder, PD and 70PD fibers.

7.6 Batch Adsorption test with DUT-4 powders

The adsorption experiments were carried out at an initial concentration of 450 mg/Nm^3 of siloxane D4 at room temperature. The kinetic adsorption of the DUT-four materials was rapid, reaching the equilibrium concentration about 4 h (Figure 36). The equilibrium adsorption capacity for DUT-4(DMF), DUT-4(DCM), and DUT-4(H) was 9.80 mg/g, which is 1.4 times greater than the adsorption capacity of AC (A_s 1240 m^2/g), reported in our previous work under the same experimental conditions [10]. The siloxane adsorption during the first hour was higher for DUT-4(DCM) than for DUT-4(H), which is related to the faster adsorption kinetics rate. Thus, a simple approach was made to quantify the adsorption kinetics rate by calculating the slope

of the first experimental points (from zero to one hour). According to the experimental data, the adsorption rate followed the trend of DUT-4(DCM) <DUT-4(DMF) <DUT-4(H) with values of 7.09, 6.54, and 5.08 mg/g·h, respectively. On the other hand, the adsorption capacity of DUT-4(W) was 1.80 mg/g, reaching equilibrium in 2 h and was five times less than the adsorption capacity of the rest of DUT-4 adsorbents associated with its low specific surface area (2 m^2/g).

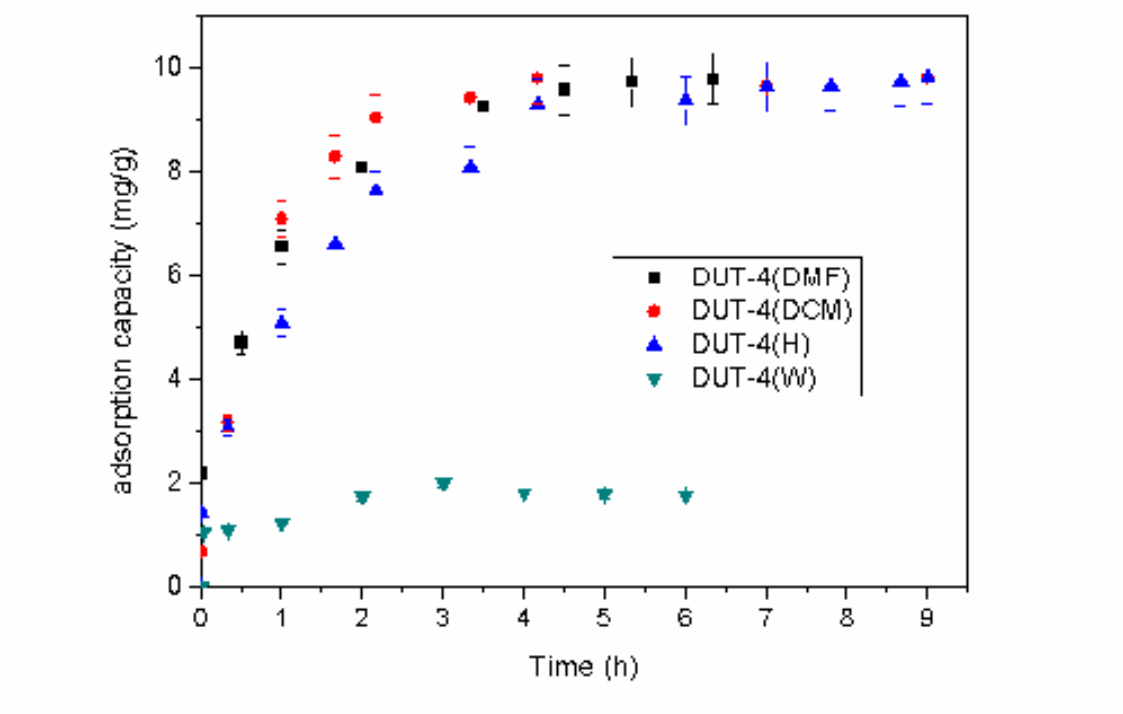

Figure 36: Kinetics adsorption for DUT-4(DMF), DUT-4(DCM), DUT-4(H), and DUT-4(W) at the initial concentration of D4 of 450 mg/Nm^3 and room temperature.

7.7 Batch Adsorption test with DUT-4 fibers

The adsorption experiments were carried out at an initial concentration of 450 mg/Nm^3 of siloxane D4 at room temperature. The kinetics adsorption of the PD, 20DD, 20ED1, and 20ED13 fibers were rapid, reaching equilibrium about two h (Figure 37). The kinetics adsorption of the 20CD, 70PD, 100PD, and 140PD fibers

achieved equilibrium in 3-3.5 h. The equilibrium adsorption capacity for the fibers made by uniaxial electrospinning was 3.88 to 4.13 mg/g at the equilibrium concentrations of 264.78 to 256.85 mg/m^3, respectively, while the adsorption capacity of the fibers without DUT-4 was tiny, 0.86 mg/g at the equilibrium concentration of 403.27 mg/m^3. The adsorption capacity for the coaxial electrospinning was increased from 4.13 to 8.42 mg/g at an equilibrium concentration of 256.85 to 61.26 mg/m^3, respectively.

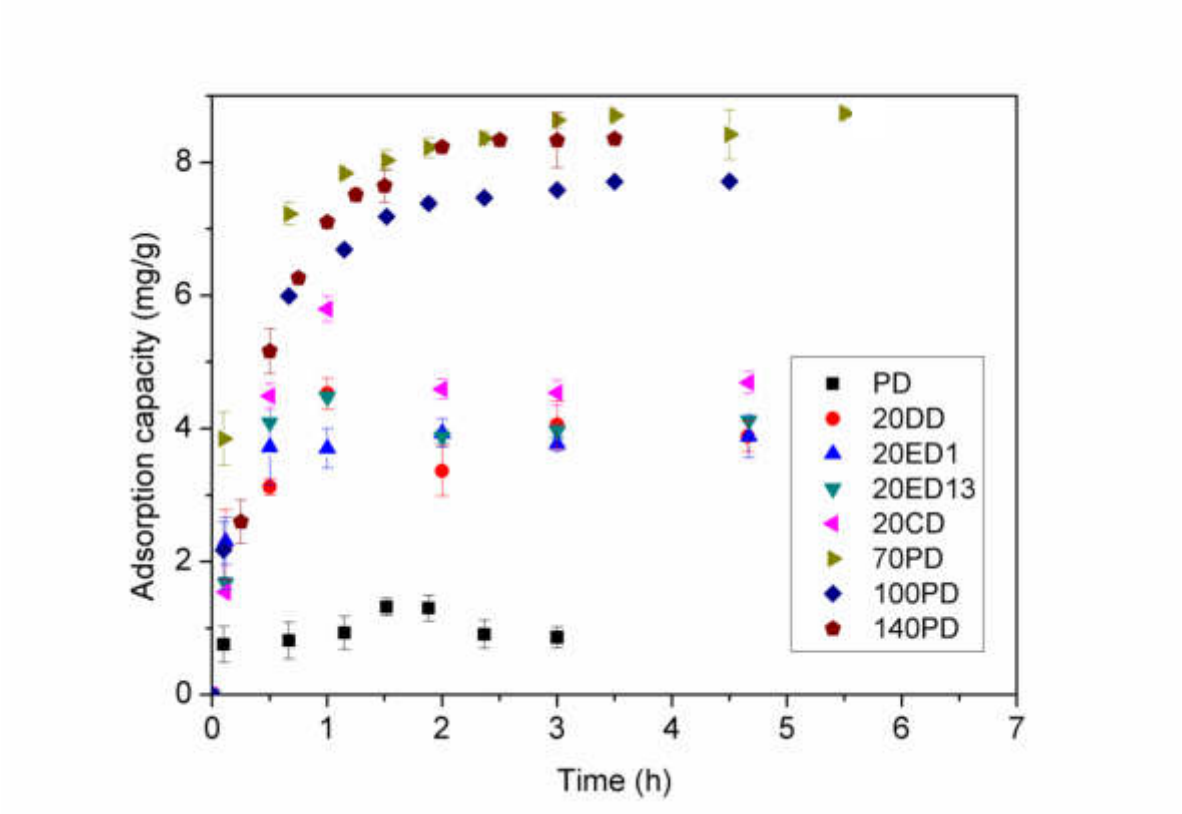

Figure 37: Kinetics adsorption of PD, 20DD, 20ED1, 20ED13, 20CD, 70PD, 100PD and 140PD fibers at initial concentration of D4 of 450 mg/Nm^3 and room temperature.

The siloxane adsorption capacity increased by 20%, when fibers prepared by coaxial electrospinning were compared to those obtained by uniaxial electrospinning (20DD and 20CD fibers). An increase in A_{BET} of 80% was also reflected (Table 10). In this sense, the fibers with the highest siloxane adsorption capacity were those spun

coaxially, which are the fibers with the highest DUT-4 powder load and, therefore, the highest A_{BET}.

Table 10: Specific surface area and adsorption capacity of D4 onto fibers.

Name fiber	A_{BET} (m^2/g)	C_e (mg/m^3)	Q_e (mg/g)	t_e (h)
PD	11	403.27	0.86	2.0
20DD	20	264.78	3.88	2.0
20ED1	30	267.19	3.88	2.0
20ED13	56	256.85	4.13	2.0
20CD	37	226.37	4.69	3.0
70PD	113	61.26	8.42	3.5
100PD	131	94.10	7.71	3.5
140PD	293	65.3	8.35	3.5

7.8 Continuos adsorption test

The continuous adsorption experiments were carried out according to the conditions described in section 6.6. The fibers were dried at 120 ºC for four h; then, the threads were rolled up to an approximate diameter of 1 cm (diameter of the column) and placed in the column vertically. The experimental results had high deviations (average absolute deviations of 128.92), indicating no reproducibility. It could be attributed to the formation of preferential paths favored by the packing; therefore, we got different experimental curves at the same experimental conditions. Another reason why the experiment probably failed is that we used a minimal flow rate for

such a significant bed height, so for future work, we will use a flow rate of at least 100 mL/min.

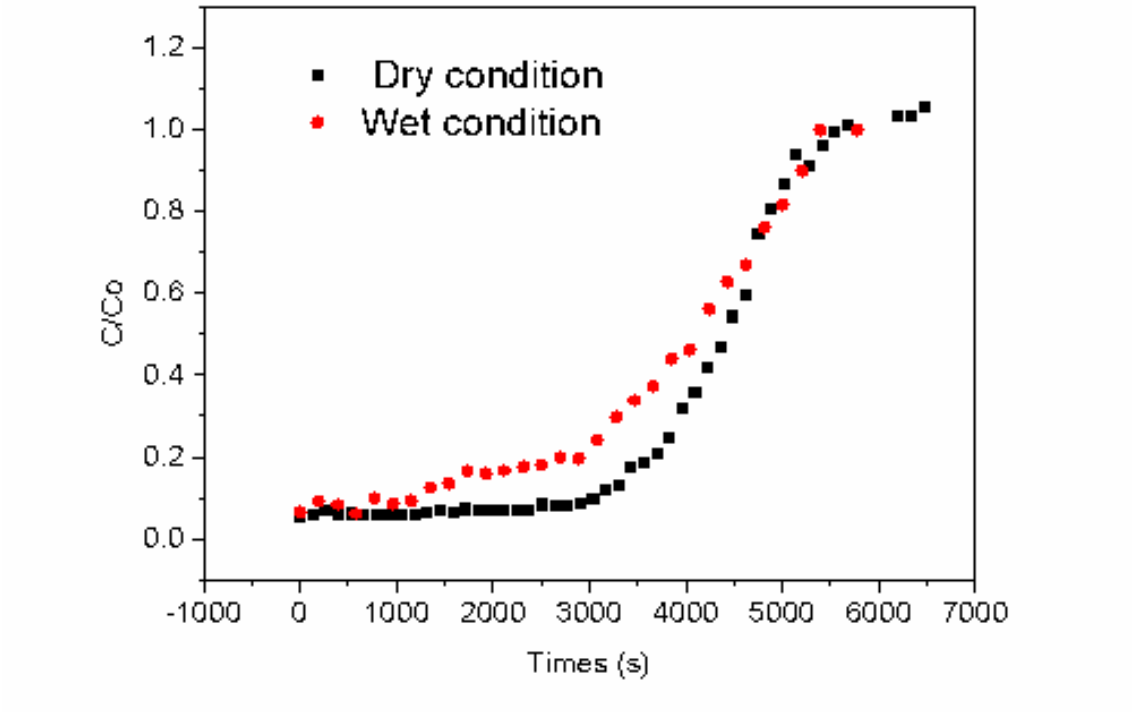

Figure 38: Experimental curves of column test run.

In Figure 38, breakthrough curves of D4 onto 100DP fibers at dry and humid conditions are presented. However, a discussion of the experimental results is prevented due to the low reproducibility of the data.

8 Conclusions

In this study, the synthesis of DUT-4 was carried out by four different routes to improve its physicochemical characteristics for higher siloxane D4 adsorption. In addition, the environmental impacts of the different routes used were evaluated by the life cycle assessment (LCA) methodology. According to the FTIR and NMR analysis, the materials obtained by both solvothermal and hydrothermal synthesis shown the characteristics absorption bands of the functional groups of the organic linker and the chemical shifts related to the six-fold coordinated Al, respectively. However, only the solvothermal synthesis produced materials isostructural to DUT-4, according to the XRD analysis. The four synthesized materials presented a crystalline structure with values between 70–90%. In another way, the solvothermal synthesis favors high specific surface areas with values higher than 1100 m^2/g. Meanwhile, the hydrothermal synthesis generated a low specific surface area and low total pore volume caused by high surface tension solvent. Similarly, the solvent used on the drying stage affected the particle size of the studied materials. In other words, low surface tension solvent leads to a small particle size. The trend on the particle size was DUT-4(H)» DUT-4(DCM) <DUT-4(DMF) <DUT-4(W), which is similar to the trend of the surface tension of solvents: C_6H_{14} (18.8 dyn/cm) <Cl_2CH_4 (29.5 dyn/cm) <DMF (37.9 dyn/cm) <H_2O (72.8 dyn/cm). The DUT-4 obtained by solvothermal synthesis can be applied as adsorbent material for siloxane removal due to its high adsorption rate and high equilibrium adsorption capacity.

The LCA emphasizes that using DMF, DCM, and hexane increases environmental damage, mainly in the indicators of fossil depletion, climate change, and human

toxicity. By contrast, the synthesis of DUT-4(W) generated the lowest environmental impact of 32 mPt per FU. However, DUT-4(W) presented the lowest siloxane adsorption capacity compared to DUT-4(DMF), DUT-4(DCM), and DUT4(H). Finally, based on the environmental impact/adsorption capacity ratio, the Scenario DUT-4(DMF) production is the most convenient because lower adsorbent mass is required to remove siloxane, which reduces the environmental impacts of the adsorption process.

Likewise, the immobilization of DUT-4 on the fibers was carried out by two routes to favor the minor change in their physicochemical characteristics and to achieve a better adsorption capacity of the D4 siloxane. According to the A_{BET} and SEM surface area analyses, the fibers generated by 70PD coaxial electrospinning were those with the highest A_{BET} (113.0 m^2/g) and the best dispersion on the fiber surface. According to the FTIR analysis, the 70PD fibers showed the characteristic absorption bands of the DUT-4 particles. However, these fibers were shown to be less crystalline than DUT-4 powders, based on XRD analysis. The 70PD fibers presented a crystalline structure with a value of 31.35%, while the fibers without DUT-4 presented a value of 46.06%. 70PD fibers can also be applied as an adsorbent material for siloxane removal due to its high equilibrium adsorption capacity (8.42 mg/g) and its adsorption capacity in both dry and humid conditions.

9 Conclusiones

En el presente trabajo se sintetizó la estructura organometálica DUT-4 mediante cuatro rutas diferentes a fin de mejorar sus características fisicoquímicas para una mayor adsorción de siloxano D4. También fueron evaluados, mediante la metodología de evaluación del ciclo de vida (LCA), los impactos ambientales de las diferentes rutas utilizadas. De acuerdo con el análisis FTIR y NMR, los materiales obtenidos por síntesis solvotérmica e hidrotermal mostraron bandas de absorción características de los grupos funcionales del enlazador orgánico y los desplazamientos químicos relacionados con el aluminio sexta-coordinado, respectivamente. De acuerdo con el análisis de XRD, solo los materiales producidos por síntesis solvotérmica mostraron estructuras iso-DUT-4. Los cuatro materiales sintetizados presentaron una estructura cristalina con valores entre el 70 y el 90%. Por otro lado, la síntesis solvotermal favorece elevadas áreas superficiales con valores superiores a 1100 m^2/g. Mientras tanto, la síntesis hidrotermal generó un área superficial específica baja y un volumen de poro total bajo, causado por el solvente que tenía una alta tensión superficial. Asimismo, el solvente utilizado en la etapa de secado, afectó al tamaño de partícula de los materiales estudiados. En otras palabras, el disolvente de baja tensión superficial conduce a un tamaño de partícula menor. La tendencia en el tamaño de partícula fue DUT-4(H)>>DUT-4(DCM)<DUT-4(DMF)<DUT-4(W), que es similar a la tendencia de la tensión superficial de los solventes: C_6H_{14} (18.8 din/cm)<Cl_2CH_4 (29,5 din/cm)<DMF (37,9 din/cm)<H_2O(72,8 din/cm). El DUT-4 obtenido por síntesis solvotermal se puede aplicar como material adsorbente para la remoción de siloxano debido a su alta tasa de adsorción y alta capacidad de adsorción en equilibrio.

El ACV enfatiza que el uso de DMF, DCM y hexano aumenta el daño ambiental, principalmente en los indicadores de agotamiento de fósiles, cambio climático y toxicidad humana. Por el contrario, la síntesis de DUT-4(W) generó el menor impacto ambiental con 32 mPt por UF. Sin embargo, el DUT-4(W) presentó la capacidad de adsorción de siloxano más baja en comparación con DUT-4(DMF), DUT-4(DCM) y DUT4(H). Finalmente, según la relación impacto ambiental/capacidad de adsorción, la producción del escenario DUT-4 (DMF) es la más conveniente porque se requiere una masa de adsorbente menor, para eliminar la misma cantidad de siloxano, lo que reduce los impactos ambientales del proceso de adsorción.

Asimismo, la inmovilización de DUT-4 sobre las fibras se realizó por dos vías para favorecer el menor cambio en sus características fisicoquímicas y lograr una mayor capacidad de adsorción del siloxano D4. Según los análisis de área de superficie A_{BET} y SEM, las fibras generadas por electrohilado coaxial 70PD fueron las que tenían el A_{BET} más alta (113 m^2/g) y la mejor dispersión en la superficie de la fibra. Según el análisis FTIR, las fibras 70PD mostraron las bandas de adsorción características de las partículas DUT-4. Sin embargo, se demostró que estas fibras eran menos cristalinas que los polvos DUT-4, según el análisis XRD. Las fibras 100PD presentaron una estructura cristalina con un valor de 31,35%, mientras que las fibras sin DUT-4 presentaron un valor de 46,06%. Las fibras 70PD también se pueden aplicar como material adsorbente para la eliminación de siloxano debido a su alta capacidad de adsorción en equilibrio (8,42 mg/g) y su alta estabilidad tanto en condiciones secas como húmedas.

10 References

[1] Energy Information Adminsitration, «Renewable Energy Explained». https://www.eia.gov/energyexplained/?page=renewable_home (accedido ago. 17, 2018).
[2] University of Florida, «Biogas a renewable bíofuel». http://biogas.ifas.ufl.edu/biogasdefs.asp (accedido ago. 20, 2018).
[3] M. T. Varnero Moreno, «Manual de biogás». 2011. [En línea]. Disponible en: http://www.fao.org/family-farming/detail/es/c/342734/
[4] O. D. N. Djao *et al.*, «Complete genome sequence of Syntrophothermus lipocalidus type strain (TGB-C1T)», *Stand. Genomic Sci.*, vol. 3, n.º 3, pp. 268-275, dic. 2010, doi: 10.4056/sigs.1233249.
[5] C. M. Plugge *et al.*, «Complete genome sequence of Syntrophobacter fumaroxidans strain (MPOBT)», *Stand. Genomic Sci.*, vol. 7, n.º 1, pp. 91-106, sep. 2012, doi: 10.4056/sigs.2996379.
[6] F. Ermici, «BIOMASS AND BIOGAS», 2016.
[7] X. Y. Chen, H. Vinh-Thang, A. A. Ramirez, D. Rodrigue, y S. Kaliaguine, «Membrane gas separation technologies for biogas upgrading», *RSC Adv.*, vol. 5, n.º 31, pp. 24399-24448, 2015, doi: 10.1039/C5RA00666J.
[8] «Calorific Value | Glossary | Marquard & Bahls». https://www.marquard-bahls.com/en/news-info/glossary/detail/term/net-calorific-value-gross-calorific-value.html (accedido mar. 18, 2021).
[9] International Energy Agency, «Outlook for biogas and biomethane, Prospects for organic growth», mar. 19, 2020. https://webstore.iea.org/outlook-for-biogas-and-biomethane (accedido nov. 17, 2020).
[10] S. Pioquinto García *et al.*, «Siloxane removal for biogas purification by low cost mineral adsorbent», *J. Clean. Prod.*, p. 124940, nov. 2020, doi: 10.1016/j.jclepro.2020.124940.
[11] G. Wang, Z. Zhang, y Z. Hao, «Recent advances in technologies for the removal of volatile methylsiloxanes: A case in biogas purification process», *Crit. Rev. Environ. Sci. Technol.*, vol. 49, n.º 24, pp. 2257-2313, dic. 2019, doi: 10.1080/10643389.2019.1607443.
[12] G. Soreanu y P. Seto, «Approaches concerning siloxane removal from biogas * A review», *Can. Biosyst. Eng.*, vol. 53, p. 18, 2011.
[13] L. Ghorbel, R. Tatin, y A. Couvert, «Relevance of an organic solvent for absorption of siloxanes», *Environ. Technol.*, vol. 35, n.º 3, pp. 372-382, feb. 2014, doi: 10.1080/09593330.2013.828778.
[14] J. Álvarez-Flórez y E. Egusquiza, «Analysis of damage caused by siloxanes in stationary reciprocating internal combustion engines operating with landfill gas», *Eng. Fail. Anal.*, vol. 50, pp. 29-38, abr. 2015, doi: 10.1016/j.engfailanal.2015.01.010.
[15] J. Álvarez-Flórez y E. Egusquiza, «Analysis of damage caused by siloxanes in stationary reciprocating internal combustion engines operating with landfill gas», *Eng. Fail. Anal.*, vol. 50, pp. 29-38, abr. 2015, doi: 10.1016/J.ENGFAILANAL.2015.01.010.
[16] M. Schweigkofler y R. Niessner, «Removal of siloxanes in biogases», *J. Hazard. Mater.*, vol. 83, n.º 3, pp. 183-196, may 2001, doi: 10.1016/S0304-3894(00)00318-6.
[17] M. Ajhar, M. Travesset, S. Yüce, y T. Melin, «Siloxane removal from landfill and digester gas - A technology overview», *Bioresour. Technol.*, vol. 101, n.º 9, pp. 2913-2923, 2010, doi: 10.1016/j.biortech.2009.12.018.
[18] G. Soreanu *et al.*, «Approaches concerning siloxane removal from biogas * A review», *Can. Biosyst. Eng.*, vol. 53, p. 19, 2011.

[19] K. Gaj, «Applicability of selected methods and sorbents to simultaneous removal of siloxanes and other impurities from biogas», *Clean Technol. Environ. Policy*, vol. 19, n.º 9, pp. 2181-2189, nov. 2017, doi: 10.1007/s10098-017-1422-1.
[20] G. Ruiling, C. Shikun, y L. Zifu, «Research progress of siloxane removal from biogas», *Biol Eng*, vol. 10, p. 10, 2017.
[21] M. Schweigkofler y R. Niessner, «Removal of siloxanes in biogases», *J. Hazard. Mater.*, vol. 83, n.º 3, pp. 183-196, may 2001, doi: 10.1016/S0304-3894(00)00318-6.
[22] E. Wheless y J. Pierce, «Siloxanes in Landfill and Digester Gas Update», 2004, p. 10.
[23] E. Lichtfouse, J. Schwarzbauer, y D. Robert, *Environmental Chemistry for a Sustainable World: Volume 2: Remediation of Air and Water Pollution*. Springer Netherlands, 2011. [En línea]. Disponible en: https://books.google.es/books?id=-M0lRBMuWygC
[24] M. Shen, Y. Zhang, D. Hu, J. Fan, y G. Zeng, «A review on removal of siloxanes from biogas: with a special focus on volatile methylsiloxanes», *Environ. Sci. Pollut. Res.*, vol. 25, n.º 31, pp. 30847-30862, nov. 2018, doi: 10.1007/s11356-018-3000-4.
[25] F. Accettola, G. M. Guebitz, y R. Schoeftner, «Siloxane removal from biogas by biofiltration: biodegradation studies», *Clean Technol. Environ. Policy*, vol. 10, n.º 2, pp. 211-218, may 2008, doi: 10.1007/s10098-007-0141-4.
[26] S. C. Popat y M. A. Deshusses, «Biological Removal of Siloxanes from Landfill and Digester Gases: Opportunities and Challenges», *Environ. Sci. Technol.*, vol. 42, n.º 22, pp. 8510-8515, nov. 2008, doi: 10.1021/es801320w.
[27] E. R. Rene, M. Montes, M. C. Veiga, y C. Kennes, «Novel Bioreactors for Waste Gas Treatment», en *Environmental Chemistry for a Sustainable World: Volume 2: Remediation of Air and Water Pollution*, Dordrecht: Springer Netherlands, 2012. doi: 10.1007/978-94-007-2439-6.
[28] R. Dewil, L. Appels, y J. Baeyens, «Energy use of biogas hampered by the presence of siloxanes», *Energy Convers. Manag.*, vol. 47, n.º 13-14, pp. 1711-1722, 2006, doi: 10.1016/j.enconman.2005.10.016.
[29] G. Piechota, M. Hagmann, y R. Buczkowski, «Removal and determination of trimethylsilanol from the landfill gas», *Bioresour. Technol.*, vol. 103, n.º 1, pp. 16-20, ene. 2012, doi: 10.1016/j.biortech.2011.09.002.
[30] I. D. Charry Prada, R. Rivera-Tinoco, y C. Bouallou, «Biogas industry: Novel acid gas removal technology using a superacid solvent. Process design, unit specification and feasibility study compared with other existing technologies», *Chem. Eng. Res. Des.*, vol. 154, pp. 212-231, feb. 2020, doi: 10.1016/j.cherd.2019.12.007.
[31] E. Słupek, P. Makoś-Chełstowska, y J. Gębicki, «Removal of Siloxanes from Model Biogas by Means of Deep Eutectic Solvents in Absorption Process», *Materials*, vol. 14, n.º 2, p. 241, ene. 2021, doi: 10.3390/ma14020241.
[32] M. Ajhar y T. Melin, «Siloxane removal with gas permeation membranes», *Desalination*, vol. 200, n.º 1-3, pp. 234-235, nov. 2006, doi: 10.1016/j.desal.2006.03.308.
[33] M. Ajhar *et al.*, «Siloxane removal using silicone–rubber membranes», *Sep. Purif. Technol.*, vol. 89, pp. 234-244, mar. 2012, doi: 10.1016/j.seppur.2012.01.003.
[34] E. Santos-Clotas, A. Cabrera-Codony, J. Comas, y M. J. Martín, «Biogas purification through membrane bioreactors: Experimental study on siloxane separation and biodegradation», *Sep. Purif. Technol.*, vol. 238, p. 116440, may 2020, doi: 10.1016/j.seppur.2019.116440.

[35] A. Cabrera-Codony, E. Santos-Clotas, C. O. Ania, y M. J. Martín, «Competitive siloxane adsorption in multicomponent gas streams for biogas upgrading», *Chem. Eng. J.*, vol. 344, pp. 565-573, jul. 2018, doi: 10.1016/J.CEJ.2018.03.131.
[36] V. T. L. Tran *et al.*, «Siloxane adsorption on activated carbons: Role of the surface chemistry on sorption properties in humid atmosphere and regenerability issues», *Chem. Eng. J.*, vol. 371, pp. 821-832, sep. 2019, doi: 10.1016/j.cej.2019.04.087.
[37] P. R. Estupiñan, L. Giraldo, y J. C. Moreno-Piraján, «Modificación de la química superficial de carbones activados. Efecto de la oxidación con soluciones de HNO3 y H2O2 sobre la remoción de Cadmio (II) en solución acuosa», p. 8, 2014.
[38] J. C. Cortés, L. Giraldo, A. A. García, C. García, y J. C. Moreno, «OXIDATION OF AN ACTIVATED CARBON COMMERCIAL AND CHARACTERIZATION OF THE CONTENT OF SUPERFICIAL ACID GROUPS», *Rev. Colomb. Quím.*, n.º 1, p. 11, 2008.
[39] H. Gong, Z. Chen, Y. Fan, M. Zhang, W. Wu, y W. Wang, «Surface modification of activated carbon for siloxane adsorption», *Renew. Energy*, vol. 83, pp. 144-150, nov. 2015, doi: 10.1016/j.renene.2015.04.004.
[40] V. T. L. Tran, P. Gélin, C. Ferronato, J. Chovelon, L. Fine, y G. Postole, «Adsorption of linear and cyclic siloxanes on activated carbons for biogas purification: Sorbents regenerability», *Chem. Eng. J.*, vol. 378, p. 122152, dic. 2019, doi: 10.1016/j.cej.2019.122152.
[41] A. Peluso, N. Gargiulo, P. Aprea, F. Pepe, y D. Caputo, «Nanoporous Materials as H_2S Adsorbents for Biogas Purification: a Review», *Sep. Purif. Rev.*, vol. 48, n.º 1, pp. 78-89, ene. 2019, doi: 10.1080/15422119.2018.1476978.
[42] J. Wang, J. Li, M. Gao, y X. Zhang, «Recent advances in covalent organic frameworks for separation and analysis of complex samples», *TrAC Trends Anal. Chem.*, vol. 108, pp. 98-109, nov. 2018, doi: 10.1016/j.trac.2018.07.013.
[43] T. Saeed *et al.*, «Structure, nomenclature and viable synthesis of micro/nanoscale metal organic frameworks and their remarkable applications in adsorption of organic pollutants», *Microchem. J.*, vol. 159, p. 105579, dic. 2020, doi: 10.1016/j.microc.2020.105579.
[44] O. M. Yaghi, M. J. Kalmutzki, y C. S. Diercks, *Introduction to Reticular Chemistry*. 2019. doi: 10.1002/9783527821099.
[45] F. Gándara, «Metal-organic frameworks: nuevos materiales con espacios llenos de posibilidades», *Quím*, p. 7, 2012.
[46] H. T. D. Nguyen, Y. B. N. Tran, H. N. Nguyen, T. C. Nguyen, F. Gándara, y P. T. K. Nguyen, «A Series of Metal–Organic Frameworks for Selective CO_2 Capture and Catalytic Oxidative Carboxylation of Olefins», *Inorg. Chem.*, vol. 57, n.º 21, pp. 13772-13782, nov. 2018, doi: 10.1021/acs.inorgchem.8b02293.
[47] V. Kumar, S. Kumar, K.-H. Kim, D. C. W. Tsang, y S.-S. Lee, «Metal organic frameworks as potent treatment media for odorants and volatiles in air», *Environ. Res.*, vol. 168, pp. 336-356, ene. 2019, doi: 10.1016/j.envres.2018.10.002.
[48] N. D. Rudd *et al.*, «Highly Efficient Luminescent Metal–Organic Framework for the Simultaneous Detection and Removal of Heavy Metals from Water», *ACS Appl. Mater. Interfaces*, vol. 8, n.º 44, pp. 30294-30303, nov. 2016, doi: 10.1021/acsami.6b10890.
[49] B. Zhang *et al.*, «Solvent determines the formation and properties of metal-organic framework», p. 7, 2012.
[50] S. R. Bajpe *et al.*, «Direct Observation of Molecular-Level Template Action

Leading to Self-Assembly of a Porous Framework», *Chem. - Eur. J.*, vol. 16, n.º 13, pp. 3926-3932, abr. 2010, doi: 10.1002/chem.200903239.
[51] H. Guo, Y. Zhu, S. Wang, S. Su, L. Zhou, y H. Zhang, «Combining Coordination Modulation with Acid–Base Adjustment for the Control over Size of Metal–Organic Frameworks», *Chem. Mater.*, vol. 24, n.º 3, pp. 444-450, feb. 2012, doi: 10.1021/cm202593h.
[52] W.-J. Son, J. Kim, J. Kim, y W.-S. Ahn, «Sonochemical synthesis of MOF-5», *Chem. Commun.*, n.º 47, p. 6336, 2008, doi: 10.1039/b814740j.
[53] B. Zhang *et al.*, «Solvent determines the formation and properties of metal-organic framework», p. 11, 2012.
[54] J. Ma, A. P. Kalenak, A. G. Wong-Foy, y A. J. Matzger, «Rapid Guest Exchange and Ultra-Low Surface Tension Solvents Optimize Metal-Organic Framework Activation», *Angew. Chem. Int. Ed.*, vol. 56, n.º 46, pp. 14618-14621, nov. 2017, doi: 10.1002/anie.201709187.
[55] Y. Mito-oka *et al.*, «Siloxane D4 capture by hydrophobic microporous materials», *J. Mater. Chem. A*, vol. 1, n.º 27, p. 7885, 2013, doi: 10.1039/c3ta11217a.
[56] N. Gargiulo *et al.*, «Chromium-based MIL-101 metal organic framework as a fully regenerable D4 adsorbent for biogas purification», *Renew. Energy*, vol. 138, pp. 230-235, ago. 2019, doi: 10.1016/j.renene.2019.01.096.
[57] E. Haya Leiva, «Análisis de Ciclo de Vida». Creative Commons, 2016.
[58] D. Loya-González *et al.*, «Optimal activated carbon production from corn pericarp: A life cycle assessment approach», *J. Clean. Prod.*, vol. 219, pp. 316-325, may 2019, doi: 10.1016/j.jclepro.2019.02.068.
[59] C. V. Sepúlveda-Cervantes, E. Soto-Regalado, P. Rivas-García, M. Loredo-Cancino, F. dJ Cerino-Córdova, y R. B. García Reyes, «Technical-environmental optimisation of the activated carbon production of an agroindustrial waste by means response surface and life cycle assessment», *Waste Manag. Res.*, vol. 36, n.º 2, pp. 121-130, feb. 2018, doi: 10.1177/0734242X17741680.
[60] C. A. Grande, R. Blom, A. Spjelkavik, V. Moreau, y J. Payet, «Life-cycle assessment as a tool for eco-design of metal-organic frameworks (MOFs)», *Sustain. Mater. Technol.*, vol. 14, pp. 11-18, dic. 2017, doi: 10.1016/j.susmat.2017.10.002.
[61] N. Stock y S. Biswas, «Synthesis of Metal-Organic Frameworks (MOFs): Routes to Various MOF Topologies, Morphologies, and Composites», *Chem. Rev.*, vol. 112, n.º 2, pp. 933-969, feb. 2012, doi: 10.1021/cr200304e.
[62] J. Sánchez-Laínez, I. Gracia-Guillén, B. Zornoza, C. Téllez, y J. Coronas, «Thin supported MOF based mixed matrix membranes of Pebax® 1657 for biogas upgrade», *New J. Chem.*, vol. 43, n.º 1, pp. 312-319, 2019, doi: 10.1039/C8NJ04769C.
[63] A. Sabetghadam *et al.*, «Metal Organic Framework Crystals in Mixed-Matrix Membranes: Impact of the Filler Morphology on the Gas Separation Performance», *Adv. Funct. Mater.*, vol. 26, n.º 18, pp. 3154-3163, may 2016, doi: 10.1002/adfm.201505352.
[64] T. G. Glover y M. Bin, *Gas Adsorption in Metal-Organic Frameworks: Fundamentals and Applications*, First. Boca Raton. Accedido: ene. 18, 2021. [En línea]. Disponible en: https://books.google.com.mx/books?id=HwprDwAAQBAJ&pg=PT522&lpg=PA1&focus=viewport&hl=es#v=onepage&q&f=false
[65] H. Thakkar, S. Eastman, Q. Al-Naddaf, A. A. Rownaghi, y F. Rezaei, «3D-Printed Metal–Organic Framework Monoliths for Gas Adsorption Processes», *ACS Appl Mater*

Interfaces, p. 9, 2017.
[66] I. Majchrzak-Kucęba y A. Ściubidło, «Shaping metal–organic framework (MOF) powder materials for CO2 capture applications—a thermogravimetric study», *J. Therm. Anal. Calorim.*, vol. 138, n.º 6, pp. 4139-4144, dic. 2019, doi: 10.1007/s10973-019-08314-5.
[67] J. Cousin-Saint-Remi, A.-L. Finoulst, C. Jabbour, G. V. Baron, y J. F. M. Denayer, «Selection of binder recipes for the formulation of MOFs into resistant pellets for molecular separations by fixed-bed adsorption», *Microporous Mesoporous Mater.*, vol. 304, p. 109322, sep. 2020, doi: 10.1016/j.micromeso.2019.02.009.
[68] S. Ramakrishna, K. Fujihara, W. Teo, T. Yong, Z. Ma, y R. Ramaseshan, «El e c t r o s p u n n a n o f i b e r s »:, *Mater. Today*, vol. 9, n.º 3, pp. 40-50, 2006, doi: 10.1016/S1369-7021(06)71389-X.
[69] J. Huang y T. You, «Electrospun Nanofibers : From Rational Design , Fabrication to Electrochemical Sensing Applications», *Adv. Nanofibers*, pp. 36-83, 2013, doi: 10.5772/57099.
[70] G. Ungur y J. Hrůza, «Modified polyurethane nanofibers as antibacterial filters for air and water purification», *RSC Adv.*, vol. 7, n.º 78, pp. 49177-49187, 2017, doi: 10.1039/c7ra06317b.
[71] M. Gao, L. Zeng, J. Nie, y G. Ma, «Polymer-metal-organic framework core-shell framework nanofibers: Via electrospinning and their gas adsorption activities», *RSC Adv.*, vol. 6, n.º 9, pp. 7078-7085, 2016, doi: 10.1039/c5ra23147g.
[72] S. Egodawatte *et al.*, «Electrospun hematite nanofiber/mesoporous silica core/shell nanomaterials as an efficient adsorbent for heavy metals», *RSC Adv.*, vol. 6, n.º 93, pp. 90516-90525, 2016, doi: 10.1039/c6ra19876g.
[73] T. Burks, *Application of Nanomaterials for the Removal of Hexavalent Chromium and their Biological Implications*. 2016.
[74] Y. Dou, W. Zhang, y A. Kaiser, «Electrospinning of Metal–Organic Frameworks for Energy and Environmental Applications», *Adv. Sci.*, vol. 7, n.º 3, p. 1902590, feb. 2020, doi: 10.1002/advs.201902590.
[75] D. Ricaurte Ortega y a Subrenat, «Siloxane treatment by adsorption into porous materials.», *Environ. Technol.*, vol. 30, n.º 10, pp. 1073-1083, 2009, doi: 10.1080/09593330903057540.
[76] E. Finocchio *et al.*, «Purification of biogases from siloxanes by adsorption: On the regenerability of activated carbon sorbents», *Energy Fuels*, vol. 23, n.º 8, pp. 4156-4159, 2009, doi: 10.1021/ef900356n.
[77] L. Sigot, G. Ducom, y P. Germain, «Adsorption of octamethylcyclotetrasiloxane (D4) on silica gel (SG): Retention mechanism», *Microporous Mesoporous Mater.*, vol. 213, pp. 118-124, 2015, doi: 10.1016/j.micromeso.2015.04.016.
[78] M. Schweigkofler y R. Niessner, «Removal of siloxanes in biogases», *J. Hazard. Mater.*, vol. 83, n.º 3, pp. 183-196, 2001, doi: 10.1016/S0304-3894(00)00318-6.
[79] L. Sigot, G. Ducom, B. Benadda, y C. Labouré, «Adsorption of octamethylcyclotetrasiloxane on silica gel for biogas purification», *Fuel*, vol. 135, pp. 205-209, nov. 2014, doi: 10.1016/j.fuel.2014.06.058.
[80] F. Gándara, «Metal-organic frameworks : nuevos materiales con espacios llenos de posibilidades», vol. 108, pp. 190-196, 2012.
[81] S. Pioquinto-García, N. Tiempos-Flores, A. A. Rico-Barragan, y N. E. Dávila-Guzmán, «Metal-organic frameworks as adsorbents for impurities of biogas», *Mater. Today*

Proc., p. S2214785321018460, abr. 2021, doi: 10.1016/j.matpr.2021.02.693.
[82] K. Fan, Z. Jin, G. Wang, H. Yang, y D. Liu, «Catalysis Science & Technology», pp. 2352-2363, 2018, doi: 10.1039/c8cy00380g.
[83] X. Dong, J. Li, Z. Han, P. Duan, L. Li, y S. Zang, «of metal – organic frameworks in hybrid membranes», pp. 3464-3474, 2017, doi: 10.1039/c6ta07761g.
[84] I. Senkovska, F. Hoffmann, M. Fröba, J. Getzschmann, W. Böhlmann, y S. Kaskel, «New highly porous aluminium based metal-organic frameworks: Al(OH)(ndc) (ndc = 2,6-naphthalene dicarboxylate) and Al(OH)(bpdc) (bpdc = 4,4′-biphenyl dicarboxylate)», *Microporous Mesoporous Mater.*, vol. 122, n.º 1-3, pp. 93-98, 2009, doi: 10.1016/j.micromeso.2009.02.020.
[85] J. E. Efome, D. Rana, T. Matsuura, y C. Q. Lan, «Insight Studies on Metal-Organic Framework Nanofibrous Membrane Adsorption and Activation for Heavy Metal Ions Removal from Aqueous Solution», *ACS Appl. Mater. Interfaces*, vol. 10, n.º 22, pp. 18619-18629, 2018, doi: 10.1021/acsami.8b01454.
[86] R. Xue *et al.*, «Preparation and energy storage application of a long-life and high rate performance pseudocapacitive COF material linked with –NH– bonds», *New J. Chem.*, vol. 42, n.º 16, pp. 13726-13731, 2018, doi: 10.1039/C8NJ01942H.
[87] E. D. Dikio, «Modified Electro-spun Polyvinyl Alcohol Nanofibers Used as Super Adsorbing Material for Lead Ions in Aqueous Solution», vol. 13, n.º 3, 2016, doi: 10.12783/issn.1544-8053/13/3/7.
[88] J. Ren, N. M. Musyoka, P. Annamalai, H. W. Langmi, B. C. North, y M. Mathe, «Electrospun MOF nanofibers as hydrogen storage media», *Int. J. Hydrog. Energy*, vol. 40, n.º 30, pp. 9382-9387, 2015, doi: 10.1016/j.ijhydene.2015.05.088.
[89] I. Senkovska, F. Hoffmann, M. Fröba, J. Getzschmann, W. Böhlmann, y S. Kaskel, «New highly porous aluminium based metal-organic frameworks: Al(OH)(ndc) (ndc=2,6-naphthalene dicarboxylate) and Al(OH)(bpdc) (bpdc=4,4′-biphenyl dicarboxylate)», *Microporous Mesoporous Mater.*, vol. 122, n.º 1-3, pp. 93-98, jun. 2009, doi: 10.1016/j.micromeso.2009.02.020.
[90] «ISO 14044:2006(es), Gestión ambiental — Análisis del ciclo de vida — Requisitos y directrices». https://www.iso.org/obp/ui/#iso:std:iso:14044:ed-1:v1:es (accedido abr. 16, 2020).
[91] «ecoQuery - Login». https://ecoquery.ecoinvent.org/Account/LogOn?ReturnUrl=%2fFile%2fReports (accedido may 23, 2020).
[92] E. Ramírez Lara *et al.*, «A comprehensive hazardous waste management program in a Chemistry School at a Mexican university», *J. Clean. Prod.*, vol. 142, pp. 1486-1491, 2017, doi: 10.1016/j.jclepro.2016.11.158.
[93] M. Z. Hauschild, R. K. Rosenbaum, y S. I. Olsen, Eds., *Life Cycle Assessment*. Cham: Springer International Publishing, 2018. doi: 10.1007/978-3-319-56475-3.
[94] M. A. J. Huijbregts *et al.*, «ReCiPe2016: a harmonised life cycle impact assessment method at midpoint and endpoint level», *Int. J. Life Cycle Assess.*, vol. 22, n.º 2, pp. 138-147, feb. 2017, doi: 10.1007/s11367-016-1246-y.
[95] «SENER | Sistema de Información Energética | Producción de energía primaria». http://sie.energia.gob.mx/bdiController.do?action=cuadro&cvecua=IE11C01 (accedido sep. 23, 2020).
[96] J. F. Kurisingal *et al.*, «Porous aluminum-based DUT metal-organic frameworks for the transformation of CO2 into cyclic carbonates: A computationally supported study»,

Catal. Today, vol. 352, pp. 227-236, ago. 2020, doi: 10.1016/j.cattod.2019.12.038.
[97] H. Embrechts, M. Kriesten, M. Ermer, W. Peukert, M. Hartmann, y M. Distaso, «*In situ* Raman and FTIR spectroscopic study on the formation of the isomers MIL-68(Al) and MIL-53(Al)», *RSC Adv.*, vol. 10, n.º 13, pp. 7336-7348, 2020, doi: 10.1039/C9RA09968A.
[98] «11.5: Infrared Spectra of Some Common Functional Groups», *Chemistry LibreTexts*, feb. 09, 2016. https://chem.libretexts.org/Bookshelves/Organic_Chemistry/Map%3A_Organic_Chemistry_(Wade)/11%3A_Infrared_Spectroscopy_and_Mass_Spectrometry/11.05%3A_Infrared_Spectra_of_Some_Common_Functional_Groups (accedido ago. 18, 2020).
[99] F. Rojo Callejas, «Tablas de Espectroscopía Infrarroja». http://depa.fquim.unam.mx/amyd/archivero/TablasIR_34338.pdf (accedido ago. 18, 2020).
[100] A. E. J. Hoffman *et al.*, «Elucidating the Vibrational Fingerprint of the Flexible Metal–Organic Framework MIL-53(Al) Using a Combined Experimental/Computational Approach», *J. Phys. Chem. C*, vol. 122, n.º 5, pp. 2734-2746, feb. 2018, doi: 10.1021/acs.jpcc.7b11031.
[101] «IR: carboxylic acids». https://orgchemboulder.com/Spectroscopy/irtutor/carbacidsir.shtml (accedido ago. 18, 2020).
[102] G. A. Rosales-Sosa *et al.*, «High Elastic Moduli of a 54Al2O3-46Ta2O5 Glass Fabricated via Containerless Processing», *Sci. Rep.*, vol. 5, n.º 1, dic. 2015, doi: 10.1038/srep15233.
[103] P. Benito, F. M. Labajos, L. Mafra, J. Rocha, y V. Rives, «Carboxylate-intercalated layered double hydroxides aged under microwave–hydrothermal treatment», *J. Solid State Chem.*, vol. 182, n.º 1, pp. 18-26, ene. 2009, doi: 10.1016/j.jssc.2008.09.015.
[104] C. Volkringer *et al.*, «The use of aluminium and others p elements (gallium, indium) for the generation of MOF-type materials», en *Studies in Surface Science and Catalysis*, vol. 174, Elsevier, 2008, pp. 447-450. doi: 10.1016/S0167-2991(08)80237-6.
[105] A. Vyalikh, K. Zesewitz, y U. Scheler, «Hydrogen bonds and local symmetry in the crystal structure of gibbsite: Hydrogen bonds and local symmetry in structure of gibbsite», *Magn. Reson. Chem.*, vol. 48, n.º 11, pp. 877-881, nov. 2010, doi: 10.1002/mrc.2682.
[106] J. A. Kaduk y J. T. Golab, «Structures of 2,6-disubstituted naphthalenes», *Acta Crystallogr. B*, vol. 55, n.º 1, pp. 85-94, feb. 1999, doi: 10.1107/S0108768198008945.
[107] A. J. Howarth, A. W. Peters, N. A. Vermeulen, T. C. Wang, J. T. Hupp, y O. K. Farha, «Best Practices for the Synthesis, Activation, and Characterization of Metal–Organic Frameworks», *Chem. Mater.*, vol. 29, n.º 1, pp. 26-39, ene. 2017, doi: 10.1021/acs.chemmater.6b02626.
[108] C. Duan *et al.*, «Water-based routes for synthesis of metal-organic frameworks: A review», *Sci. China Mater.*, vol. 63, n.º 5, pp. 667-685, may 2020, doi: 10.1007/s40843-019-1264-x.
[109] A. Maskara y D. M. Smith, «Agglomeration during the Drying of Fine Silica Powders, Part II: The Role of Particle Solubility», *J. Am. Ceram. Soc.*, vol. 80, n.º 7, pp. 1715-1722, ene. 2005, doi: 10.1111/j.1151-2916.1997.tb03044.x.
[110] H. L. Lim, K. P. Hapgood, y B. Haig, «Understanding and preventing agglomeration in a filter drying process», *Powder Technol.*, vol. 300, pp. 146-156, oct. 2016, doi: 10.1016/j.powtec.2016.03.003.
[111] B. U. Peres *et al.*, «Experimental composites of polyacrilonitrile-electrospun nanofibers containing nanocrystal cellulose», *Dent. Mater.*, vol. 35, n.º 11, pp. e286-e297,

nov. 2019, doi: 10.1016/j.dental.2019.08.107.

11 Biographical summary

Sandra Pioquinto García

Candidate for the Degree of Doctor of Science with Orientation in Sustainable Processes

Thesis: Adsorption studies of octamethylcyclotetrasiloxane onto electrospun nanofibers for biogas purification

Field of study: Engineering, Chemical Sciences

Personal information:
Born in Huamantla, Tlaxcala, August 29, 1992, daughter of Esperanza García Rosales and Miguel Pioquinto Bautista.
Married, Husband: Jorge Luis Robledo Hernández.
Daughter: Valentina Robledo Pioquinto.

Education:

- Degree in Environmental Engineering (2010-2015) Benemérita Universidad Autónoma de Puebla.
- Master of Science with Orientation in Sustainable Processes (2016-2018) Universidad Autónoma de Nuevo León.

Research Experience:

- Consejo Nacional de Ciencia y Tecnología - PROINNOVA 2018. Development of a new process and product of particles of vermiculite, for its application in polymeric nanocomposites retardant to the flame and as adsorbent of pollutants in biogas, (2018).
- Internship: École Nationale Supérieure de Chimie de Rennes, France. Batch system adsorption studies for siloxane removal experiments using commercial adsorbents, (September to December 2017).
- Internship: Instituto Tecnológico Superior de Conkal, Yuc., Mexico.- Research in the soil area in the state of Yucatán in order to characterize and classify them according to the corresponding regulations, (July to August 2013).